

PL-TR-91-2064

AD-A237 622



2

Propagation of Regional Seismic Phases in Western Europe

M. Bouchon
M. Campillo
St. Gaffet
B. Massinon
P. Mechler
F. Riviere

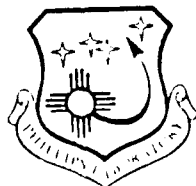
Radiomana - Societe Civile
27 rue Claude Bernard
75005 Paris, FRANCE

8 March 1991

Final Report
15 July 1987-14 July 1990

DTIC
ELECTE
JUL 08 1991
S B D

Approved for public release; distribution unlimited



PHILLIPS LABORATORY
AIR FORCE SYSTEMS COMMAND
HANSOM AIR FORCE BASE, MASSACHUSETTS 01731-5000

91-03929




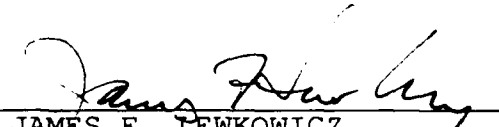
SPONSORED BY
Defense Advanced Research Projects Agency
Nuclear Monitoring Research Office
ARPA ORDER NO. 5299

MONITORED BY
Phillips Laboratory
AFOSR Grant 87-0331

The views and conclusions contained in this document are those of the authors and should not be interpreted as representing the official policies, either expressed or implied, of the Defense Advanced Research Projects Agency or the U.S. Government.

This technical report has been reviewed and is approved for publication.


JAMES F. LEWKOWICZ
Contract Manager
Solid Earth Geophysics Branch
Earth Sciences Division


JAMES F. LEWKOWICZ
Branch Chief
Solid Earth Geophysics Branch
Earth Sciences Division

FOR THE COMMANDER


DONALD H. ECKHARDT, Director
Earth Sciences Division

This report has been reviewed by the ESD Public Affairs Office (PA) and is releasable to the National Technical Information Service (NTIS).

Qualified requestors may obtain additional copies from the Defense Technical Information Center. All others should apply to the National Technical Information Service.

If your address has changed, or if you wish to be removed from the mailing list, or if the addressee is no longer employed by your organization, please notify PL/IMA, Hanscom AFB, MA 01731-5000. This will assist us in maintaining a current mailing list.

Do not return copies of this report unless contractual obligations or notices on a specific document requires that it be returned.

REPORT DOCUMENTATION PAGE				Form Approved OMB No. 0704-0188	
1a. REPORT SECURITY CLASSIFICATION Unclassified			1b. RESTRICTIVE MARKINGS		
2a. SECURITY CLASSIFICATION AUTHORITY			3. DISTRIBUTION/AVAILABILITY OF REPORT Approved for public release Distribution unlimited		
2b. DECLASSIFICATION/DOWNGRADING SCHEDULE			5. MONITORING ORGANIZATION REPORT NUMBER(S) PL-TR-91-2064		
4. PERFORMING ORGANIZATION REPORT NUMBER(S)		6a. NAME OF PERFORMING ORGANIZATION Radiomana - Société Civile		6b. OFFICE SYMBOL (if applicable)	
6c. ADDRESS (City, State, and ZIP Code) 27 Rue Claude Bernard 75005 Paris France		7a. NAME OF MONITORING ORGANIZATION European Office of Aerospace and Development			
7b. ADDRESS (City, State, and ZIP Code) Box 14 FPO New York 09510 - 0200		8a. NAME OF FUNDING/SPONSORING ORGANIZATION Phillips Laboratory			
8b. OFFICE SYMBOL (if applicable)		9. PROCUREMENT INSTRUMENT IDENTIFICATION NUMBER AFOSR 87 0331 A			
8c. ADDRESS (City, State, and ZIP Code) Hanscom AFB MA 01731 - 5000		10. SOURCE OF FUNDING NUMBERS			
		PROGRAM ELEMENT NO 61101 E	PROJECT NO 7 A 10	TASK NO D A	WORK UNIT ACCESSION NC C Z
11. TITLE (Include Security Classification) (U) Propagation of Regional Seismic Phases in Western Europe					
12. PERSONAL AUTHOR(S) M. Bouchon- M. Campillo- St Gaffet- B. Massinon- P. Mechler and F. Rivière					
13a. TYPE OF REPORT Final		13b. TIME COVERED FROM 87/07/15 TO 90/07/14		14. DATE OF REPORT (Year, Month, Day) 91/03/08	
				15. PAGE COUNT 76	
16. SUPPLEMENTARY NOTATION					
17. COSATI CODES			18. SUBJECT TERMS (Continue on reverse if necessary and identify by block number)		
FIELD	GROUP	SUB-GROUP	Keys words: tomography, high frequency Q, Q coda, explosion, Eastern Kazakh, magnitude, site effect, source function, wavenumber, boundary integral method, diffraction, heterogeneous media, defocusing.		
19. ABSTRACT (Continue on reverse if necessary and identify by block number)					
<p>This report describes the main results achieved during the period July 1987 thru July 1990 for the following researches.</p> <ul style="list-style-type: none"> - Propagation of regional phases in Western Europe. - Determination of QLg and Q coda in the 1 to 15 Hz frequency band. <p>Geographical variations of Q are strongly correlated to the tectonical features and to other geophysical anomalies. This result corresponds to the attenuation of Lg phases propagating through the positive Bouguer anomaly in the Western Alp. Those variations in Q were, not only observed, but also modeled.</p> <ul style="list-style-type: none"> - Far field effects due to the structure near the joint sources: numerical computations show variation of mb up to 0.25 at teleseismic distances induced by variations in the shape of the basement beneath a seismic event. - Source evaluation at teleseismic distance: we observed limitations in the relative magnitude determination of Eastern Kazakh events in using the French Seismic Network. The source functions computed with this network are definitively different for events originating in the NE or in the SW of Shagan River. 					
20. DISTRIBUTION/AVAILABILITY OF ABSTRACT <input checked="" type="checkbox"/> UNCLASSIFIED, UNLIMITED <input type="checkbox"/> SAME AS RPT <input type="checkbox"/> DTIC USERS			21. ABSTRACT SECURITY CLASSIFICATION Unclassified		
22a. NAME OF RESPONSIBLE INDIVIDUAL James Lewkowicz			22b. TELEPHONE (Include Area Code) (617) 377 - 3028		22c. OFFICE SYMBOL PL/IWH

INTRODUCTION

This report is the final scientific report covering the period 15 July 1987 thru 14 July 1990.

In the last research Progress and Forecast report we have developed three main subjects:

- 1 - Propagation of regional phases in western Europe
- 2 - Far field effects due to complex geological structures vicinity of point sources.
- 3 - Source evaluation at teleseismic distance.

1- The main purposes of the subject n° 1 have been achieved and we present a complete report on that subject including our results on QLg and Q coda evaluations for a set of regional events recorded on an homogeneous seismic network. We found very similar results in the evaluation of both Q factors in the studied frequency zone (1 to 15 Hz) consistent with other studies, (e.g.: Singh and Herrmann 1983) and suggesting that both QLg and Q coda measure the total Q factor resulting from intrinsic and scattering attenuations.

Concerning the interpretation of Q-values, their correlation with the tectonic activity has been established in France (Chapter 1). As a complementary study, we have developed a research programm on the attenuation of Lg phases propagating through the western Alps (Chapter 2). We have collected a set of records from short period seismic stations in France and Italy for earthquakes which occurred within and around the Alps. Lg to Pn amplitudes have been computed for different frequency ranges to characterize the relative efficiency of wave propagation in the crust and in the upper mantle. Along some paths the extinction of Lg waves is almost complete.

From this computation, we have built up a map showing a very sharp zone of anomaly of propagation located on the positive Bouguer anomaly which extends along a narrow band in the western Alps.

At a frequency of 2Hz the value of the mean ratio between Lg and Pn amplitudes is larger than 4 in the western Alps and in central France, but decreases to less than 0.3 in the Bouguer anomaly zone or to the east of this zone.

In a second part, we have modeled the propagation of Lg waves through the Alps. For that purpose we built up a simplified cross section of the western Alps including the most important features likely to severely affect the crustal wave propagation (geometry of the Moho; deep sedimentary basin on both sides of the range).

The computed sismograms obtained by the discrete wavenumber boundary integral method for irregularly layered medium (Bouchon 1989) limited to the case of Sh waves, show a large decrease of Lg amplitude in the central part of the mountain range. The amplitudes strongly increase when the waves reach the molassic sedimentary basin to the west of the Alps.

Two causes might account for the results : the curvature of the Moho in its deepest part tending to focus reflecting shear waves which make up the Lg wavetrain: the diffraction of the crustal waves near the edge of the molassic basin will result in the excitation of waves trapped in the sediments associated with high amplitudes (Campillo 1987).

2- The subject n° 2 concerns the evaluation of farfield effects due to complex geological structures in the vicinity of point sources (Chapter 3).

Using synthetic models, we investigate and try to separate the relative effects of the structure heterogeneities and of the source medium which contribute to the teleseismic ground motion recorded by a thin aperture network. The numerical simulation are carried out using the discrete wavenumber - boundary integral equation formulation. The computed seismograms correspond to the P-wave displacement component recorded at a distance of 80° . In the calculation the source region is heterogeneous, the travel in the mantle is assumed to be governed by the Futterman inelastic attenuation law, and the receiver transfer function is assumed to be flat. We show that the shape of the basement has a large influence on the magnitude estimates. The magnitude variations related to the explosion locations can get as large as $m_b = 0.25$, and the frequency corresponding to the maximum observed amplitude is correlated to the thickness of the alluvium deposit.

This study shows the importance, at teleseismic distances, of the structure heterogeneities surrounding the source region, and describes the evolution of the seismogram shapes with the complexity of the source model.

3- The subject n°3 deals with an evaluation of seismic sources at teleseismic distances (chap. 4).

The main results were already presented in a "research progress and forecast report" (11-02-1989) but we think worthwhile, for completeness, to summarize the results in this final scientific report.

The records obtained by the French Seismic Network on about twenty Eastern Kazakh events were studied.

The first goal of this work was to improve the magnitude determination. Of course, the relatively small aperture of the seismic array used, limits this determination. The only hope was to improve the relative magnitude between the events, as all sources are in the same small geographic area.

We definitively improve the magnitudes of those events, but only slightly. The main advantage of our proposition is that this determination is independant of the seismologist and the main disadvantage is that it has to be calibrated, so is only possible to apply for a known "seismic" area.

To explain the observed limitations, we look at the time history of each sources, as seen from the French Seismic Network. The already known division of the Shagan River Test Site in a SW and a NE sub Test sites was found again.

We interprete the variation in the seismic sources as the crossing by seismic rays originated in the N.E. part of Shagar River of a low velocity zone in the vicinity of the Test Site.

Certainly we are close from the limits of seismic sources interpretations using a small aperture seismic array at teleseismic distances.

Accession For	
NTIS GRA&I	<input checked="checked" type="checkbox"/>
DTIC TAB	<input type="checkbox"/>
Unannounced	<input type="checkbox"/>
Justification	
By	
Distribution/	
Availability Codes	
Dist	Avail and/or Special
A-1	

Regional seismic phases attenuation and seismic source evaluation

J.L. Plantet

Laboratoire de Détection et de Géophysique Commissariat à l'Energie Atomique BP 12, 91680 Bruyères-le-Châtel, France

Y. Cansi

Laboratoire de Détection et de Géophysique Commissariat à l'Energie Atomique BP 12, 91680 Bruyères-le-Châtel, France

M. Campillo

Laboratoire de Géophysique Interne et Tectonophysique Université Joseph Fourier and Observatoire de Grenoble IRIGM, BP 53X, 38041 Grenoble, France

1-7.1 INTRODUCTION

The main parameters of seismic signals are related to both earthquake sources and propagation medium : arrival times to location and velocity structure, amplitude to source energy and attenuation within the earth.

If, as soon as the beginning of the century, the study of seismic travel time is tackled in a theoretical way by Herglotz and Wiechert (1909) to obtain the variation of the velocity with the depth from readings of seismograms and by Geiger (1910) to localize earthquake, the study of the amplitude was for a long time neglected.

It is only since Richter's work in 1935, that numbers (i.e.: magnitudes) are assigned to quantify the size of earthquakes. The magnitude is based on amplitude measurements on instrumental recordings. The original purpose was to facilitate cataloging of earthquakes without depending exclusively on felt intensities to compare one event to another. Richter's work introduced the so-called local magnitude scale based on the trace amplitude recorded on the Wood-Anderson seismograph. This amplitude is a function of the 'size' of the earthquake (magnitude) and of the attenuation which is only represented by an empirical formula relating amplitude and distance. Gutenberg and Richter, during the 1940's, extended the empirical tables, (i) to use observations made at distant stations and on seismographs of other than the standard type, (ii) to cover earthquakes of significant focal depth and (iii) to enable independent magnitude estimates to be made from body and surface waves.

It is necessary to wait for the 1960's to have a new impulse in the amplitude studies, with the modelization of the far-field displacement spectrum produced by a propagating fault (Ben-Menahem et al. 1963, Haskell 1966, Brune 1970, Madariaga 1976) depending on the source parameters (seismic moment, fault length, stress drop).

The end of the 1980's shows a real burst of the number of attenuation studies at regional distances in various regions of world (for references see Herraiz et al. 1986) following the increase of numerical seismic signal recordings.

The attenuation can be defined by the wave amplitude decay that occurs when a wave propagates through a real medium. This decay has two very different origins: (i) the geometrical spreading which is independent of the frequency in numerous cases, and (ii) the anelastic attenuation which acts generally as a low-pass filter.

The anelastic attenuation is usually parameterized by the quality factor Q . The observed Q is thought to be a combination of two different loss mechanisms: a frequency-independent intrinsic quality factor Q_i and loss due to scattering process.

The intrinsic Q is given by $1/Q_i = -\Delta E/(2\pi E)$, where $\Delta E/E$ is the fraction of energy lost in a wave cycle due to imperfection in the elasticity of the material.

The effect of the scattering is not exactly energy loss, but rather a redistribution of energy in the medium. The amount of scattered energy is very dependent on the ratio between obstacle and wavelength sizes, and the resulting effect is strongly frequency dependent. The scattering can be also parameterized by a quality factor given by $1/Q_s = f/gv$ (Dainty 1981) where g is the turbidity (i.e. the inverse of mean free path), v is the wave velocity, and f is the frequency.

The attenuation is the sum of these two contributions and the observed Q can be written as

$$\frac{1}{Q} = \frac{1}{Q_i} + \frac{1}{Q_s}$$

The knowledge of the attenuation can have three different purposes: (i) the computation of the source parameters, (ii) the estimation of the tectonic activity of the area and, (iii) perhaps, the earthquake prediction.

-The seismic signals emitted by the earthquake are strongly affected by the attenuation and then the adequate knowledge of the attenuation of high-frequency seismic energy within the earth is very important in order to study the seismic source (seismic moment, source radius and stress drop) and to predict ground motion from theoretical sources with application to seismic hazard analysis.

-It is now generally accepted that observed Q increases with frequencies between 1 and 30Hz (Mitchell 1981). This frequency dependence, which usually is expressed by the relation $Q(f) = Q_0 f^a$, is often found to be stronger with increasing tectonic activity and is often explained as being related to the decrease of homogeneity in crust (Aki 1981). On a very large chinese data set Jin and Aki (1988) found a remarkably linear relation between the logarithm of the coda Q_0 and the maximum earthquake within the area sampled by coda waves. Then the knowledge of the attenuation could be used to evaluate the maximum earthquake in a region and would be very useful for siting critical facilities such as nuclear power plants.

-Attenuation is a good indicator of the heterogeneous state and of the dissipative property of the lithosphere; and it is expected that these conditions in and around the seismic source volume change before an earthquake. Then it is reasonable to search for temporal variation of the attenuation and probe the possibility of using this variation for earthquake prediction (Gusev et al., 1984, Jin et al., 1986). But some authors have found no precursory change in attenuation (Scherbaum 1985, Huang 1988) and this use of the attenuation is not now operational.

In this paper, after a quick review on the two main methods to evaluate the quality factor, we present, as examples, a number of studies of attenuation in France.

1-7.2 METHODS

- The most common way to estimate the anelastic attenuation in the earth consists in studying the decay of the seismic energy of a wave with distance. The quality factor obtained by this method will be written as Q_w where w represents the name of the studied wave (i.e., P_g , L_g , etc.) This method needs several stations in order to have a good sampling of the epicentral distances.

- It is also possible to measure the attenuation with only one station. The tail of a wavetrain, which contains the energy recorded after the direct wave is named its coda. Two points of view are necessary to explain the amplitudes of these two wave types (direct and coda):

- For direct waves, a deterministic point of view associates without ambiguity one effect to one well-known heterogeneity.

- On the other hand, a stochastic approach considers coda-waves as diffracted primary waves by a uniform distribution of heterogeneities. In this case the medium can be described by a set of statistical parameters (e.g.: mean free path, density of scatterers) which depend on the physical theory used to explain the diffraction. In all the cases the energy loss of a primary wave can be summarized by the use of a quality factor Q_s representing all the scattering effects, which is surimposed to the intrinsic quality factor Q_i .

In a given region, the relative importance of the absorption and the scattering determines the shape of seismograms of local earthquakes. High Q_i and strong scattering is associated with very long time duration seismograms. This is the case for lunar seismograms. On the other hand, a low Q_i (i.e., strong absorption) diminishes the time duration on the recordings. Hence the coda of seismograms is affected by attenuation and therefore the coda recordings can be used to evaluate attenuation. The quality factor obtained by coda measurements will be identified as Q_c .

7.2.1 Q_w EVALUATION

As the source and path effects are separated, the spectral amplitude of the wave w recorded at station i produced by earthquake j is :

$$A_{wij}(f, \Delta) = S_{wij}(f) P_{wij}(f, \Delta)$$

where Δ denotes the epicentral distance, f the frequency, $S_{wij}(f)$ the source contribution of the j th earthquake and $P_{wij}(f, \Delta)$ the propagation effect. Each factor can be modeled (Campillo et al., 1985) as:

- The source effect :

$$S_{wij}(f) = \Omega_j(f) R_{ij}$$

- $\Omega_j(f)$ is the source amplitude spectrum of the j th earthquake. Following Brune (1970), this spectrum is characterized by 3 parameters: $\Omega(0)$ the low-frequency level, which is proportional to the seismic moment M_0 ; f_c the corner frequency related to the fault length; and m the power of the high-frequency asymptote. The spectrum is described by the relation:

$$\Omega(f) = \frac{\Omega(0)}{[1 + (\frac{f}{f_c})^{2m}]^{1/2}} \quad \text{I-7.1}$$

- R_{ij} is the radiation pattern of the j th earthquake to the i th station, function of the source geometry for a given wave type.

- The propagation effect :

$$P_{wij}(f, \Delta) = E_w(\Delta) AA_w(f, \Delta) ST_{wi}(f)$$

- $E_w(\Delta)$ is the geometrical spreading. Since epicentral distance range is small ($< 10^\circ$) this factor can be written in the approximative form

$$E_w(\Delta) = \Delta^{-\gamma} \quad \text{I-7.2}$$

- $AA_w(f, \Delta)$ is the anelastic attenuation factor. It can be written as:

$$AA_w(f, \Delta) = e^{-\frac{\pi f \Delta}{Q_w(f) v}} \quad \text{I-7.3}$$

with $Q_w(f) = Q_{w0} f^a$ the quality factor and v the group velocity of the wave.

- $ST_{wi}(f)$ is the station response and represents the particular characteristics of the station which are not included in the instrumental response. In many attenuation studies this factor is neglected but our experience convinces us of its great importance. This factor is mainly the frequency response of the superficial structures beneath the station. Generally these structures are not known with sufficient accuracy and then this factor must be deduced from observations. In this case it is necessary to assume for each frequency f :

$$\prod_{i=1}^N ST_{wi}(f) = 1 \quad \text{I-7.4}$$

where N is the number of stations.

After linearization by taking logarithms, the spectral amplitude A of the wave is:

$$\log(A_{wij}(f)) = \log(S_{wij}(f)) - \gamma \log(\Delta) - \frac{\pi f \Delta}{Q_w(f) v} + \log(ST_{wi}(f)) \quad \text{I-7.5}$$

This equation can be solved by an iterative process using the least squares.

7.2.2 Q_c EVALUATION

Many models have been used by the investigators in coda-wave analysis. A cornerstone of these models is the relation:

$$\Phi(f, t) = \Psi(f) C(f, t) \quad \text{I-7.6}$$

It relates the power spectrum Φ of the coda for frequency f at lapse-time t , with a function Ψ which includes only source parameters and a function C which represents the effects of a large geographical area and is independent of distance and details of path connecting source to station. This relation is based on experimental evidences (Aki and Chouet, 1975).

It also indicates the two steps which must be accomplished in a coda-wave study:

- finding a mathematical expression (model) for both $\Psi(f)$ and $C(f, t)$,
- relating $\Phi(f, t)$ and the coda amplitudes.

• Among the different models which have been suggested to explain the formation of coda-waves (e.g.: surface-waves scattering, diffusion model, multiple scattering, etc.), the "Single Backscattering Model" (Aki and Chouet, 1975, Rautian and Khalturin, 1978) seems to be the most common. It describes the coda-waves as a superposition of backscattering body-waves from discrete scatterers.

Under these assumptions, the function describing the medium effects can be written:

$$C(f, t) = t^{-2\gamma} e^{-2\pi f t / Q_c} \quad \text{I-7.7}$$

The first term of this function is the geometrical spreading factor and the exponential term represents both intrinsic and scattering attenuation effects.

• The second step is the relation between the power spectrum $\Phi(f, t)$ and the amplitudes $A_c(f, t)$ of the coda for a given frequency f and a given lapse-time t . As for other problems of time-frequency analysis, two approaches can be followed that proceeds in the time and frequency domain respectively.

• In the time domain, the method consists of an evaluation of the mean amplitude over a little moving window of signal filtered around a given frequency.

• In the frequency domain, the amplitude is obtained by an averaged value around the given frequency f of the Fourier spectrum of a moving time-window centered at time t .

In both cases the amplitudes are related to the power spectrum by the relation:

$$A_c(f, t) = \sqrt{2\Phi(f, t)\Delta f} \quad \text{I-7.8}$$

where Δf is the bandwidth of the filter in the time-domain method, and the bandwidth of frequency averaging in the frequency method.

Combining relations [I-7.6], [I-7.7] and [I-7.8] we get the classical formula:

$$A_c(f, t) = \sqrt{2\Psi(f)\Delta f} t^{-\gamma} e^{-\pi f t / Q_c}$$

Then, the Q -factor can be obtained by a least-squares fit of the logarithm of this formula.

I-7.3 DATA

It results from the preceding section that both Q_c and Q_w evaluations can be carried out after spectral computations of part of signals. Though some studies have been carried out using analog signals, numerical records are more useful because they allow the investigators to compute the amplitude spectra using the Fast Fourier Transform algorithm.

Concerning the data set, Q_w studies imply the use of a network in order to have a good sampling of distance for each event. On the other hand, though a coda- Q_c value can be obtained for each station-earthquake couple, the use of a network allows us to get a statistical value for the studied region including stations and earthquakes.

In France, to study the attenuation, we use the waves recorded by the short-period vertical seismic stations of the seismic network run by the *Laboratoire de Détection et Géophysique* (L.D.G.) of the French *Commissariat à l'Energie atomique* (C.E.A.) (fig. I-7.1). Each station is mainly composed of a 1 Hz high-gain vertical-component seismometer. Numerical data are digitized with a 50 Hz sampling frequency and telemetered to the recording center where they are recorded on paper and magnetic tape for digital processing.

The spatial distribution and the magnitude range of the western Europe seismicity (see figure I-6.10 of this book) allow us to have accurate evaluation for both Q_w and Q_c . For Q_w measurements, the area is controlled by the station repartition and then its evaluation will be made only for Central France. A better spatial repartition on France will be obtained by the coda measurements.

I-7.4 RESULTS

7.4.1 Q_w STUDY

For intermediate distances (150-1500km) along continental propagation, seismograms are mostly dominated by crustal phases and especially by L_g , as far as amplitudes and durations are concerned (fig. I-7.2). Interpreted as a complex composition of multi-reflected S waves within the crust (Bouchon 1982), the L_g wavetrain is particularly well-adapted for attenuation measurement.

We present here the main results obtained by Campillo et al. (1985) on the attenuation in the crust beneath central France. In this work the equation [I-7.5] is solved for a set of 18 earthquakes (fig. I-7.2) recorded by 22 stations of the permanent L.D.G. network. In order to increase the stability in the inversion process, the geometrical spreading factor (equation [I-7.1]) must be fixed. Using numerical simulations of L_g -wave propagation in an elastic homogeneous layered crust, where only geometrical attenuation is considered, we have found $\gamma = 0.83$ (Campillo et al. 1984).

7.4.1.1 STATION RESPONSE

The transfer functions obtained are not absolute but relative to the mean of the station set (equation [I-7.4]). They are essentially representative of any attenuation or magnification for high frequencies by factors up to 3 and as shown by figure I-7.3 they are quite the same for P_g and L_g waves. They are also rather well correlated with seismic noise spectrum variation (fig. I-7.3). This result is important because it means, that for a quick evaluation of a site effect, it is possible to compare only noise spectrum between the site and a close reference point.

7.4.1.2 QUALITY FACTOR

The quality factor is computed for three parts of the L_g wavetrain defined by the group velocity windows:

$$\begin{aligned} 3.1 \text{ km/s} < v < 3.6 \text{ km/s} & L_{g1} \quad (\text{maximum amplitude of } L_g) \\ 2.6 \text{ km/s} < v < 3.1 \text{ km/s} & L_{g2} \quad (\text{early part of the coda}) \\ 2.3 \text{ km/s} < v < 2.6 \text{ km/s} & L_{g3} \end{aligned} \quad \text{I-7.9}$$

Assuming the same geometrical spreading ($\gamma = 0.83$) and the same frequency dependence, the Q_{w0} obtained for these three parts are very close with only a slight increase from L_{g1} to L_{g3} :

$$\begin{aligned} Q_{Lg1} &= 290 * f^{0.52} \\ Q_{Lg2} &= 310 * f^{0.52} \\ Q_{Lg3} &= 330 * f^{0.52} \end{aligned}$$

These relations mean that the L_g waves and their early coda have the same apparent attenuation and confirm the similarity of the Q factors computed from S waves and from their coda.

7.4.1.3 SOURCE SPECTRUM

The knowledge of the spectral energy decay and of the station responses can be used to compute the source excitation of each earthquake. The source spectrum presents a dispersion (Fig. I-7.4) probably due to a rough modeling of propagation which does not take into account lateral variations of the crustal structures. Nevertheless, the spectra pointed out the main features of the source amplitude spectrum (equation [I-7.1]), and can be used to evaluate the seismic source parameters (seismic moment, fault length and stress drop). Usually this estimation is made only with sufficiently close stations to avoid attenuation corrections, or for large earthquake with measurements on surface waves recorded at distant stations. The use of L_g wave allows to extend this calculation to the regional distance ranges. The three parts of the L_g wavetrain lead to similar source spectra (figure I-7.4), and in the case of saturated records the early parts of the coda can be used to compute the source parameters.

7.4.2 Q_c STUDY

This section presents the results obtained on the frequency dependence of Q_c measured from the coda of regional earthquakes. Its high frequency behaviour is investigated up to 100 Hz. The frequency dependence exhibits clearly regional variations. Q_c will be compared with the previous Q_{Lg} determination.

7.4.2.1 Q_c as a function of frequency

To study the high frequency behaviour of the Q_c -factor in a wide frequency band, we use a broadband recording system at station Lormes (LOR) of the French L.D.G. network. The output signal from the seismograph is separated into 3 channels after filtering in different frequency bands and with amplification and digitalization rate adapted to each frequency band. This system presents a dynamic range large enough to study Q_c in a wide frequency band ranging from 1 to 100 Hz.

A typical record of this system is shown on the figure I-7.5. It is an $m_L=3.6$ earthquake which occurred in the southern part of the Rhinegraben at 270 km from station LOR. On the 3 filtered traces one can see the 4 classical phases of a regional earthquake. The crustal wavetrains Pg and Lg are clearly seen on the low frequency channel. But, for frequencies greater than 40 Hz, only the refracted waves Pn and Sn are well developed, so that for these frequencies the coda is the coda of Sn waves.

Despite this observation, the frequency variations of the quality factor follow a very regular power-law function (Fig. I-7.6):

$$Q_c = 133f^{0.81} \quad \text{I-7.10}$$

which leads to a low value for the quality factor at 1 Hz Q_{c0} . This result, rather different than the network averaged value obtained for Q_{Lg} , suggests a more complete study of the regional variations of coda- Q_c .

7.4.2.2 Regional variations of Q_c

In order to study the regional variations of the Q_c factor, we have processed automatically a set of earthquakes having a local magnitude ranging from 3.8 to 5.0. The earthquake set is separated into three parts according to their locations. For each set Q_c is computed (fig. I-7.7 for eastern part). We found the following results:

$$Q_c = (210 \pm 40)f^{(0.60 \pm 0.10)} \quad \text{Eastern part} \quad \text{I-7.11}$$

$$Q_c = (290 \pm 50)f^{(0.54 \pm 0.08)} \quad \text{Central part} \quad \text{I-7.12}$$

$$Q_c = (320 \pm 50)f^{(0.52 \pm 0.06)} \quad \text{Western part} \quad \text{I-7.13}$$

7.4.3 Q_{Lg} AND Q_c COMPARISON

We have obtained estimations of S-wave attenuation within the crust beneath France with two different methods and for different regions.

- In the common studied zone (i.e.: Central France), the results are very similar (see equations I-7.9 and I-7.12). Another similar value is obtained for the Western part of France (equation I-7.13). This confirms the hypothesis of Aki et al. [1986], which indicates that Q_c and Q_{Lg} agree very well as soon as $Q_{Lg} > 150$.

These values suggest that the central part of France is situated between active and stable zones (Figure I-7.8). Following Jin's relation [1988], the maximum magnitude corresponding to $Q_{c0} = 300$ is roughly 6.

- For the Eastern part of France, both Q_{c0} and the frequency dependence suggest that this region is more tectonically active (see equations I-7.10 and I-7.11). The maximum magnitude estimation is 6.7 (with $Q_c = 210$) or 7.5 (with $Q_c = 133$) which is reasonable according to the size of the greatest earthquakes suffered in this region (Basel, 1356 and Swabian Jura, 1911).

In summary this study shows the importance of the regionalized measurement of the Q -factor and suggests a more detailed approach using a discrete model of attenuation and a tomographic inversion.

7.4.4 TOMOGRAPHY OF THE QUALITY FACTOR

The attenuation measurements made from L_g amplitudes are suitable for tomographic studies because the mean value of Q deduced from one record concerns a slice of crust around the source-receiver path. The tomographic approach is more difficult to apply when considering Q_c measurements because the volume of lithosphere concerned is large.

We have computed the distribution of Q_c in the crust from a large set of L_g records in different frequency ranges (Campillo and Plantet, 1990). We use raw data from 430 earthquakes. Our results confirm that the eastern part of France, namely the Alps region, is associated with low apparent Q -values (figure I-7.8).

On the other hand, we found in the western part of France, a zone where a stronger attenuation is associated with a high reflectivity of the lower crust, as shown by a wide angle reflection profile.

The tomography reveals clearly the heterogeneity of the distribution of attenuation and shows that some anomalies are difficult to predict from the analysis of surface geological structures.

I-7.5 CONCLUSION

The quality factor of both coda-waves and L_g -waves has been studied using a set of regional events recorded on a seismic homogeneous network.

- Using coda- Q method, the frequency dependence of the Q -factor has been clearly shown in a wide frequency band (1 to 100 Hz).

- The two methods lead to very similar results in the common studied zone (see equations I-7.9 and I-7.12) for the studied frequency band (1 to 15 Hz). This is consistent with other studies (e.g.: Singh and Herrmann, 1983), and suggests that both Q_{Lg} and coda- Q measure the total Q , resulting from intrinsic and scattering attenuations.

- Then these attenuation functions have been used to compute source spectra which are the basic elements for the evaluation of physical seismic parameters such as seismic moment, stress drop and fault length. This has been done by an inversion technique using a model including source spectrum pattern and station responses. We have shown that this last factor plays a prominent part and cannot be neglected.

- Concerning the interpretation of Q -values, their correlation with the tectonic activity has been established in France. This confirms, at a regional scale, the result pointed out by Jin et al. (1986), concerning the ability of Q -factor to be a useful parameter to characterize the tectonic activity.

Further studies might investigate the possibility of temporal changes in Q -values. If this fact is proved, Q -factor will be also a worthy parameter for earthquake prediction, which is one of the most important goals of present-day seismology.

REFERENCES

- Aki, K. and B. Chouet (1975). Origin of coda waves: source, attenuation, and scattering effects, *J. Geophys. Res.* **80**, 3322-3342.
- Aki, K. (1981). Source and scattering effects on the spectra of small local earthquakes, *Bull. Seism. Soc. Am.* **71**, 1687-1700.
- Ben-Menahem, A. and M. N. Toksöz (1963). Source mechanism from spectra of long period surface waves, *J. Geophys. Res.* **68**, 5207-5222.
- Bouchon, M. (1982). The complete synthesis of seismic crustal phases at regional distances, *J. Geophys. Res.* **87**, 1735-1741.
- Brune, J. N. (1970). Tectonic stress and the spectra of seismic shear waves from earthquakes, *J. Geophys. Res.* **75**, 4997-5009.
- Campillo, M., M. Bouchon, and B. Massinon (1984). Theoretical study of the excitation, spectral characteristics and geometrical attenuation of regional seismic phases, *Bull. Seism. Soc. Am.* **74**, 79-90.
- Campillo, M., J. L. Plantet, and M. Bouchon (1985). Frequency-dependent attenuation in the crust beneath Central France from L_g waves: data analysis and numerical modeling, *Bull. Seism. Soc. Am.* **75**, 1395-1411.
- Campillo, M. and J. L. Plantet (1990). Frequency dependence and spatial distribution of seismic attenuation in France: experimental results and possible interpretations, *submitted to Phys. Earth. Planet. Interiors*.
- Dainty, A. M. (1981). A scattering model to explain seismic Q observations in the lithosphere between 1 and 30Hz, *Geophys. Res. Lett.* **8**, 1126-1128.
- Geiger, L. (1910). Herdbestimmung bei Erdbeben aus den Ankunftszeiten, *K. Gesell. Wiss. Gott.* **4**, 331-349.
- Gusev, A. A. and V. K. Lemzikov (1985). Properties of scattered elastic waves in the lithosphere of Kamchatka: parameters and temporal variations, *Tectonophysics* **112**, 137-153.
- Haskell, N. A. (1966). Total energy and energy spectral density of elastic wave radiation from propagating faults. II, *Bull. Seism. Soc. Am.* **56**, 125-140.
- Herglotz, G. (1907). Über das Benndorfsche Problem der Fortpflanzungsgeschwindigkeit der Erdbebenstrahlen, *Phys. Z.* **8**, 145-7.
- Herraz, M. and A. F. Espinosa (1986). Scattering and attenuation of high-frequency seismic waves: development of the theory of coda waves, *USGS Open-File Report* **86-455**.
- Huang, Z. X. and M. Wyss (1988). Coda Q before the 1983 Hawaii ($M_S = 6.6$) earthquake, *Bull. Seism. Soc. Am.* **78**, 1279-1296.
- Jin, A. and K. Aki (1986). Temporal change in coda Q before the Tangshan earthquake of 1976 and the Haicheng earthquake of 1975, *J. Geophys. Res.* **91**, 665-673.
- Jin, A. and K. Aki (1988). Spatial and temporal correlation between coda Q and seismicity in China, *Bull. Seism. Soc. Am.* **78**, 741-769.
- Madariaga, R. (1976). Dynamics of an expanding circular fault, *Bull. Seism. Soc. Am.* **66**, 639-666.
- Mitchell, B. (1981). Regional variation and frequency dependence of Q_β in the crust of the United States, *Bull. Seism. Soc. Am.* **71**, 1531-1538.
- Rautian, T. G., and V. I. Khalturin (1978). The use of the coda for determination of the earthquake source spectrum, *Bull. Seism. Soc. Am.* **68**, 923-943.
- Richter, C. F. (1935). An instrumental earthquake magnitude scale, *Bull. Seism. Soc. Am.* **43**, 95-102.
- Sherbaum, F. and C. Kisslinger (1985). Coda Q in the Adak seismic zone, *Bull. Seism. Soc. Am.* **75**, 615-620.
- Singh, S. and R. B. Herrmann (1983). Regionalization of crustal coda Q in the continental United States, *J. Geophys. Res.* **88**, 527-538.

FIGURE CAPTIONS

Figure I-7.1: Map of stations (triangles) and earthquakes used for the attenuation estimations. Circles refer to the Q_{Lg} evaluation and crosses to the Q_c study. The star shows the position of the event used in the wide frequency-band study.

Figure I-7.2: Examples of regional earthquake seismograms. The epicenter is located in the Pyrenees (France). The seismograms are delayed on the P_g arrival-time. For clarity,

only 4 stations are displayed among the 16 which have recorded this event.

Figure I-7.3: Examples of station responses. The responses are calculated from L_g waves (solid line), P_g waves (thin line) and from noise (dashed line). This figure shows the importance of this factor (magnification up to 3). Note that the different evaluations (L_g , P_g and noise) lead to similar results.

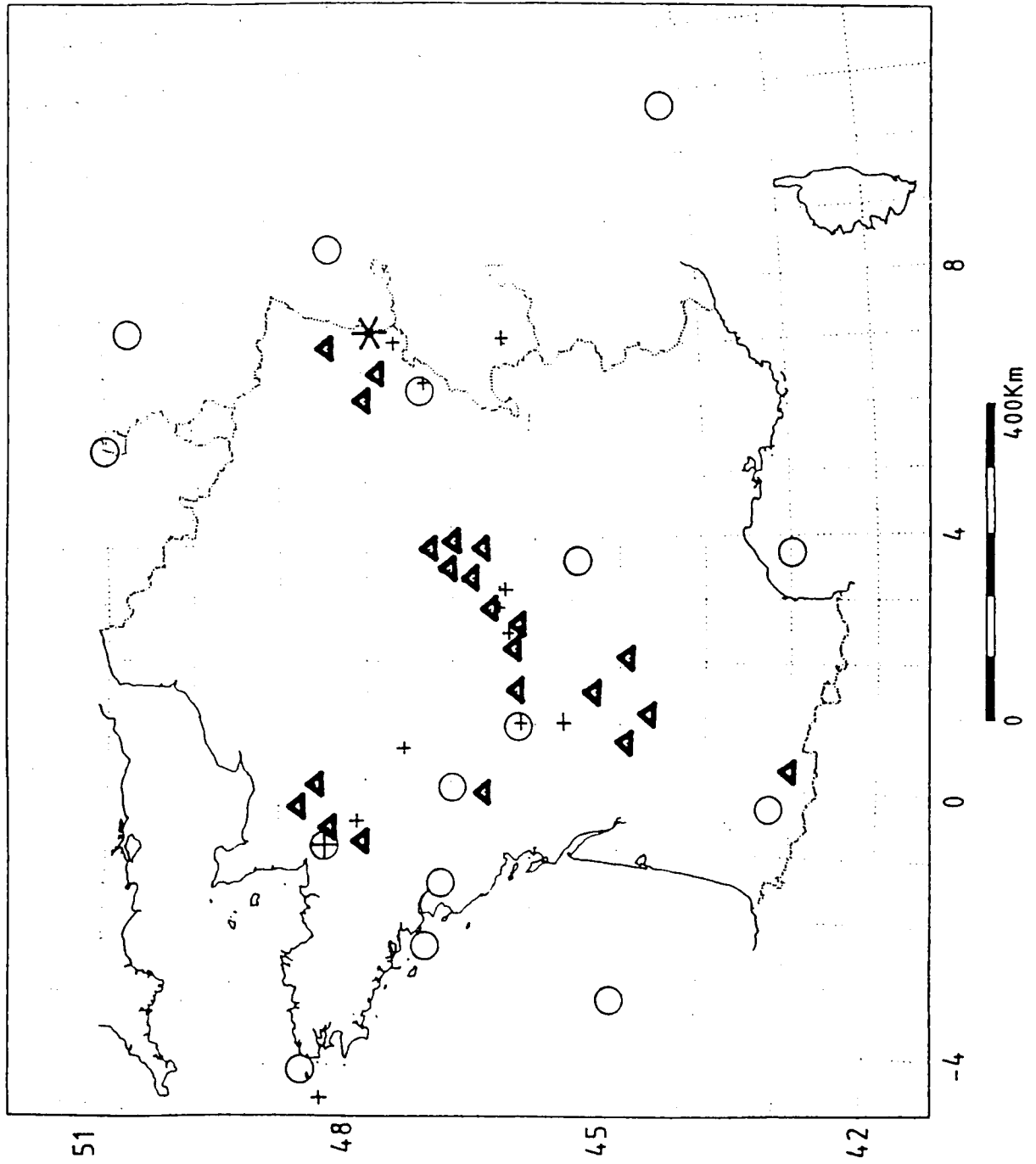
Figure I-7.4: Source excitation spectra obtained from L_{g1} , L_{g2} and L_{g3} waves. Each solid line represents the spectrum at each station after propagation and station response corrections. Heavy lines figure the best fit and the deduced corner frequencies are shown.

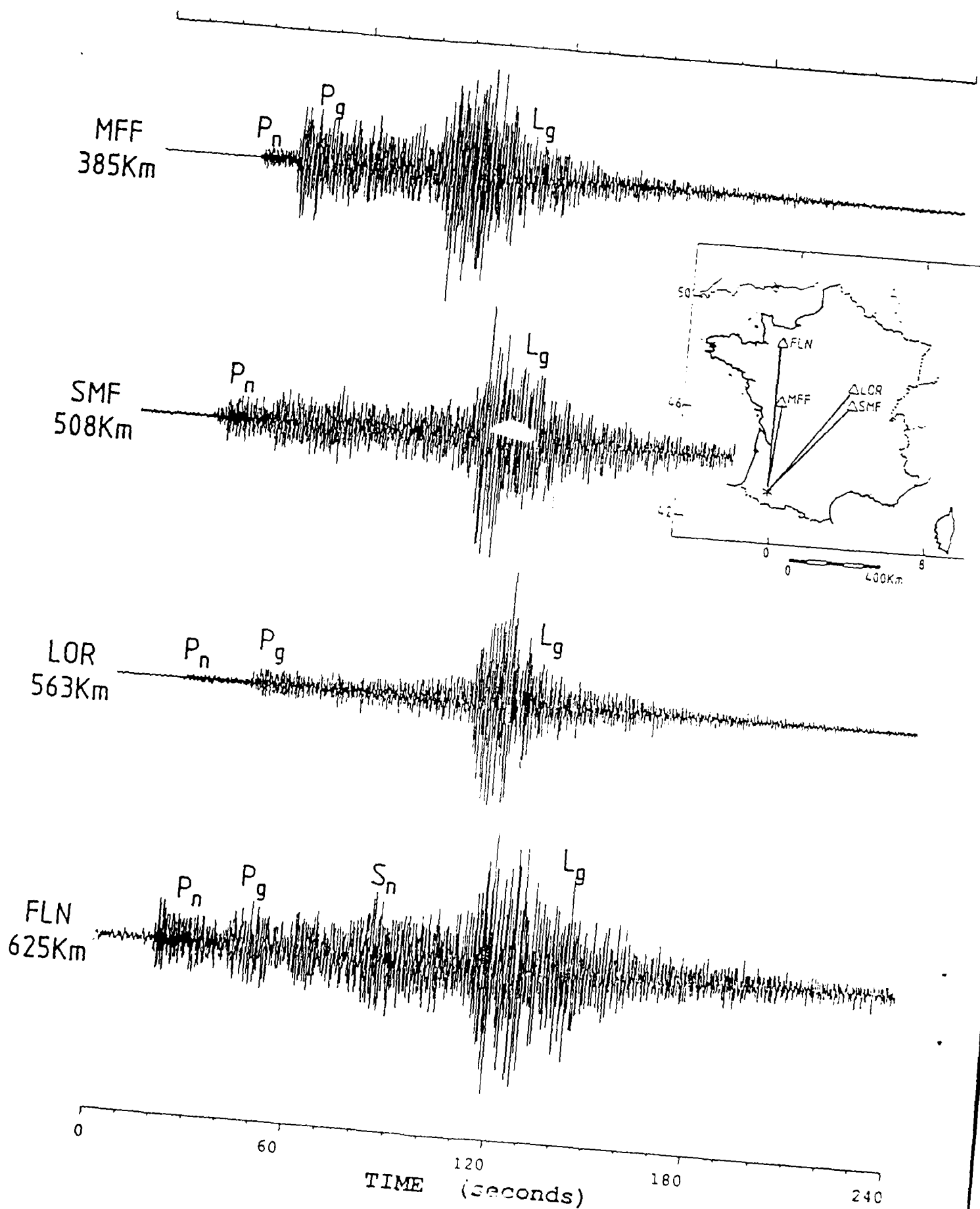
Figure I-7.5: Example of seismic vertical signal for a $m_L = 3.6$ earthquake recorded with the temporarily implemented broad-band system in station LOR. The distance of this event is 270 km. Each trace is the same signal filtered with the bandwidth displayed on the left of each trace.

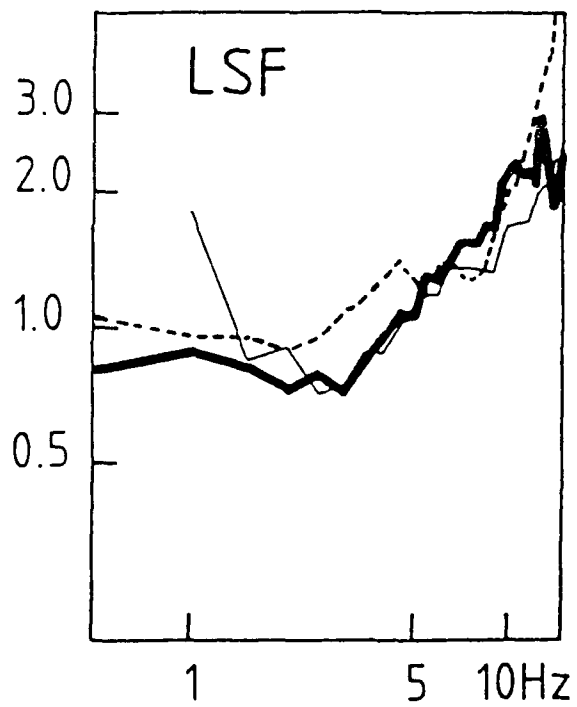
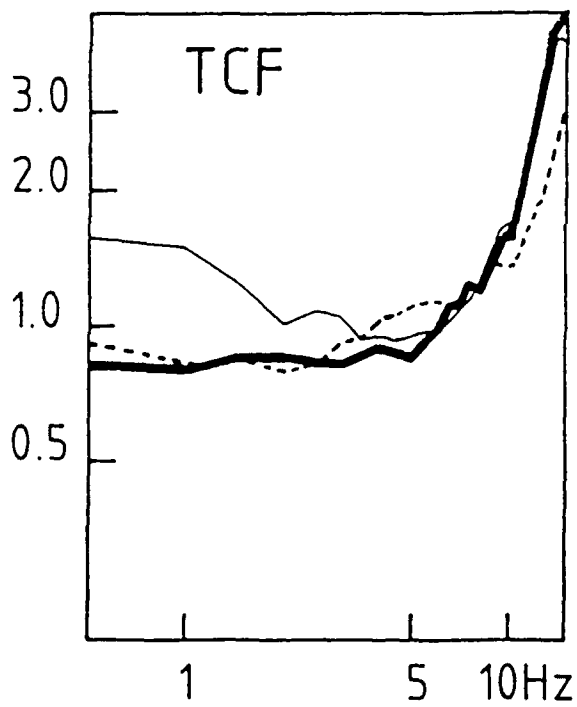
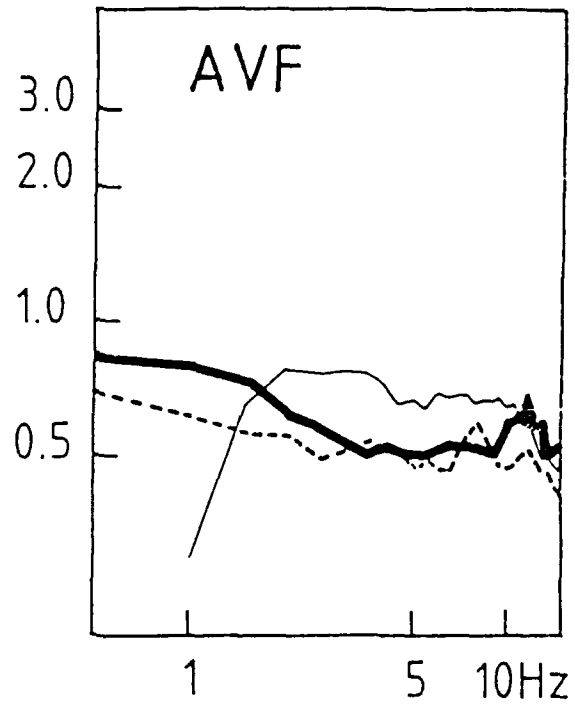
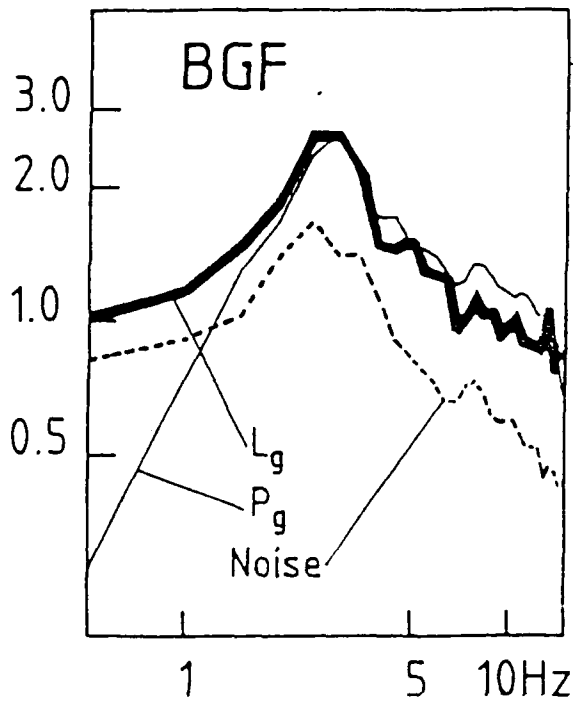
Figure I-7.6: The left part of the figure shows the envelopes of the coda for different frequencies referenced on the right. The lines are the results of the least-squares fit of the studied part of the coda which yields to Q_c -values also referenced on the right. The flat level connected to each curve by a dotted line shows the noise level in the corresponding frequency band. The right part of the figure shows the frequency variations of the Q_c values and the corresponding least-squares fit by a power law function.

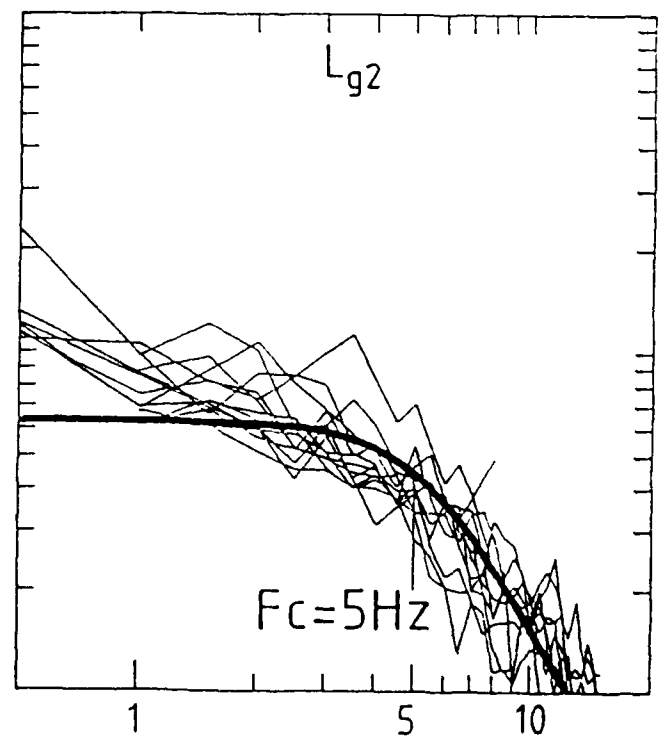
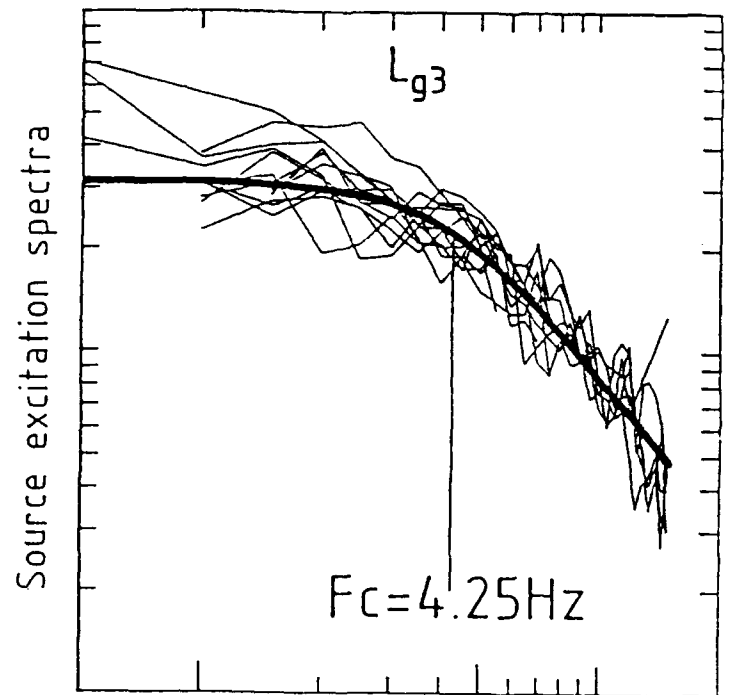
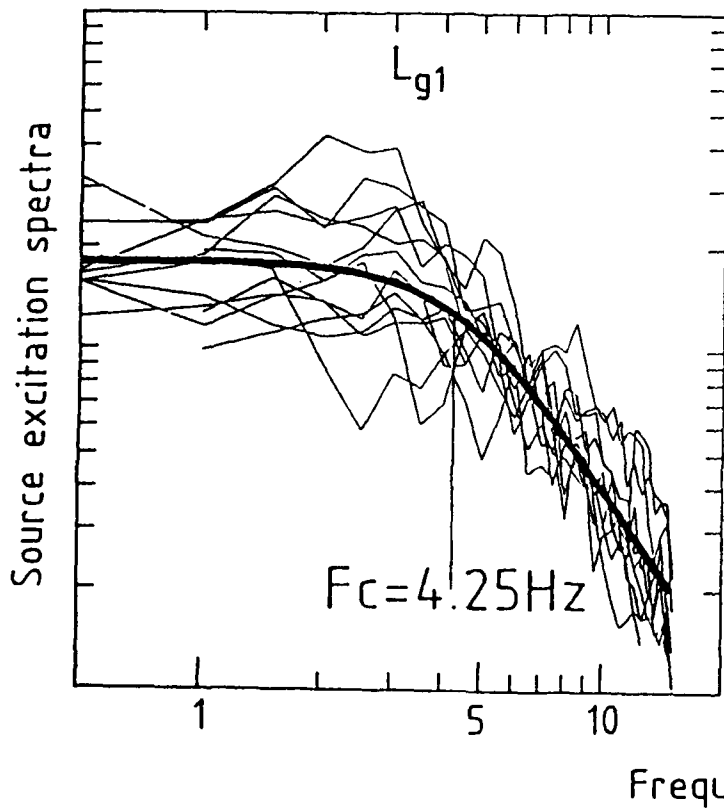
Figure I-7.7: The top part of the figure shows the coefficients of the power-law function $Q_c(f) = Q_0 f^a$ resulting from the least-squared fit of the data set represented on the map below. Each trace connects a station (triangle) to an earthquake (dot).

Figure I-7.8: Tomographic map of Q_{Lg} at 3 Hz obtained by a global inversion of attenuation, station responses and source spectra from a 430 earthquakes set recorded on the L.D.G. network. The strong variations of Q at a regional scale is clearly shown, and indicate that they must be taken into account for strong motion decay evaluation.



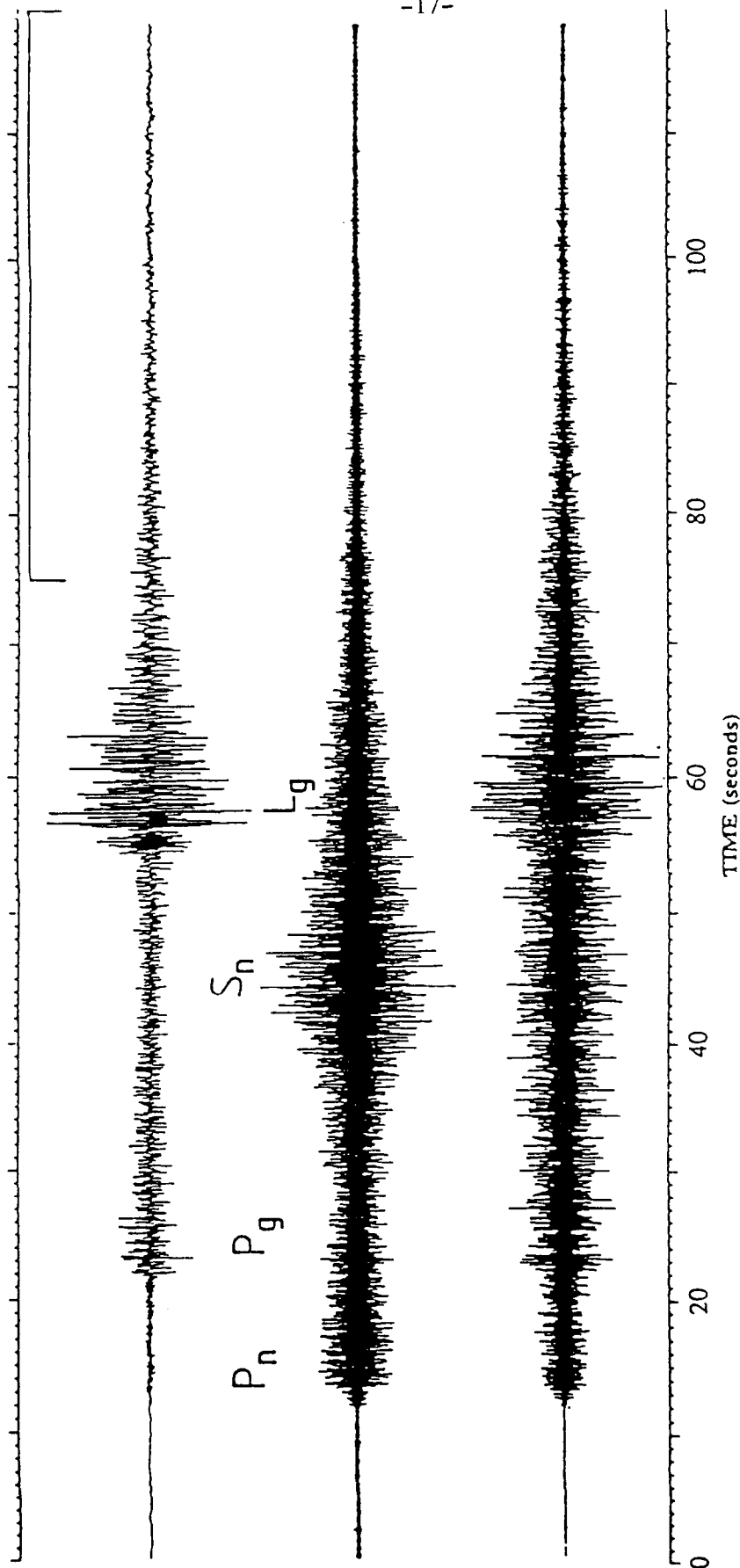
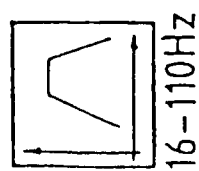
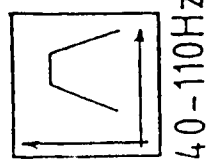
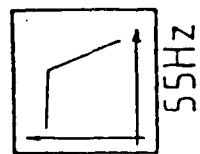




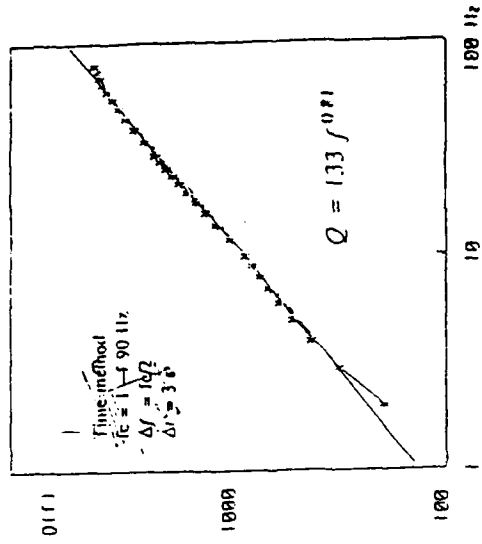
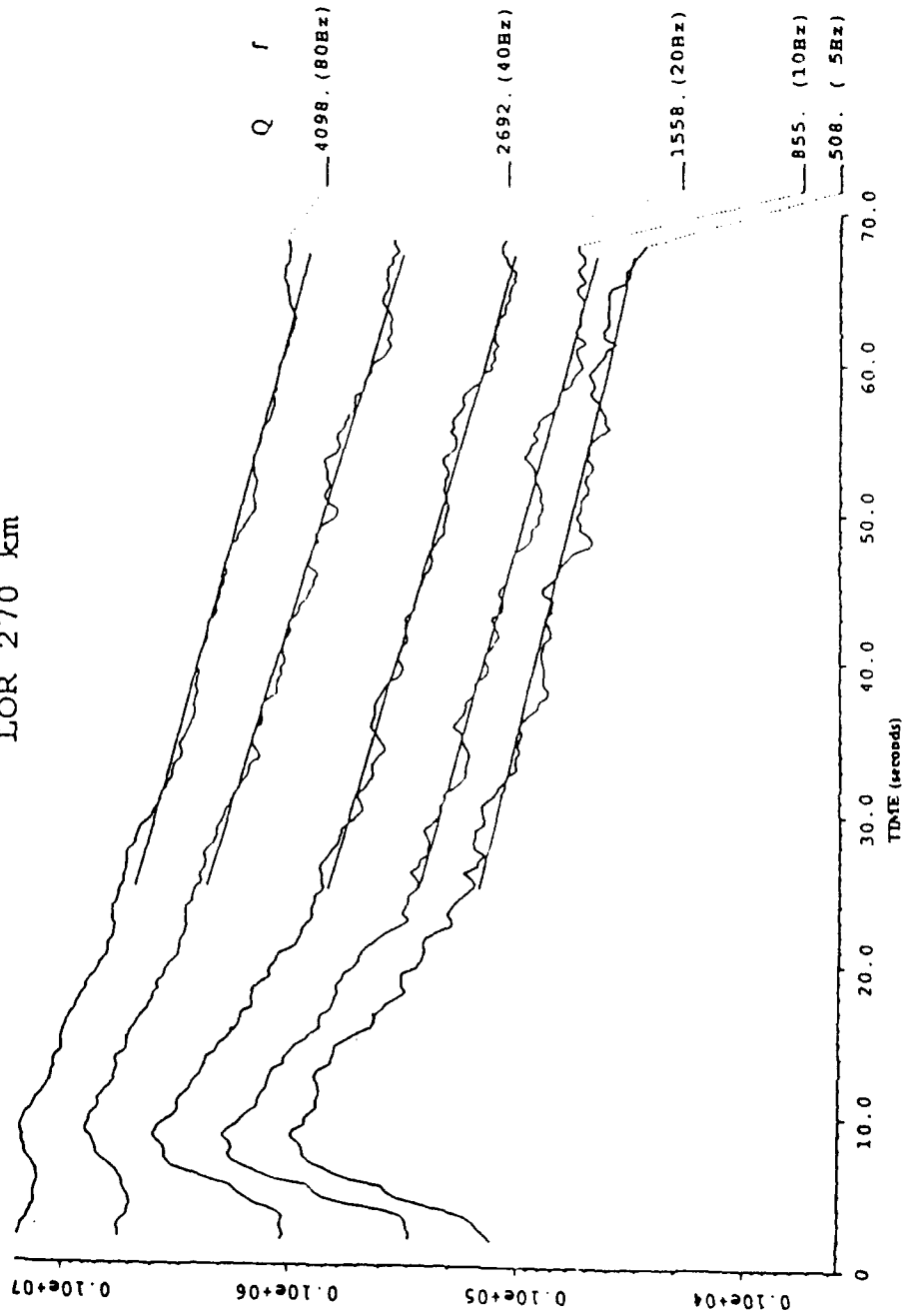


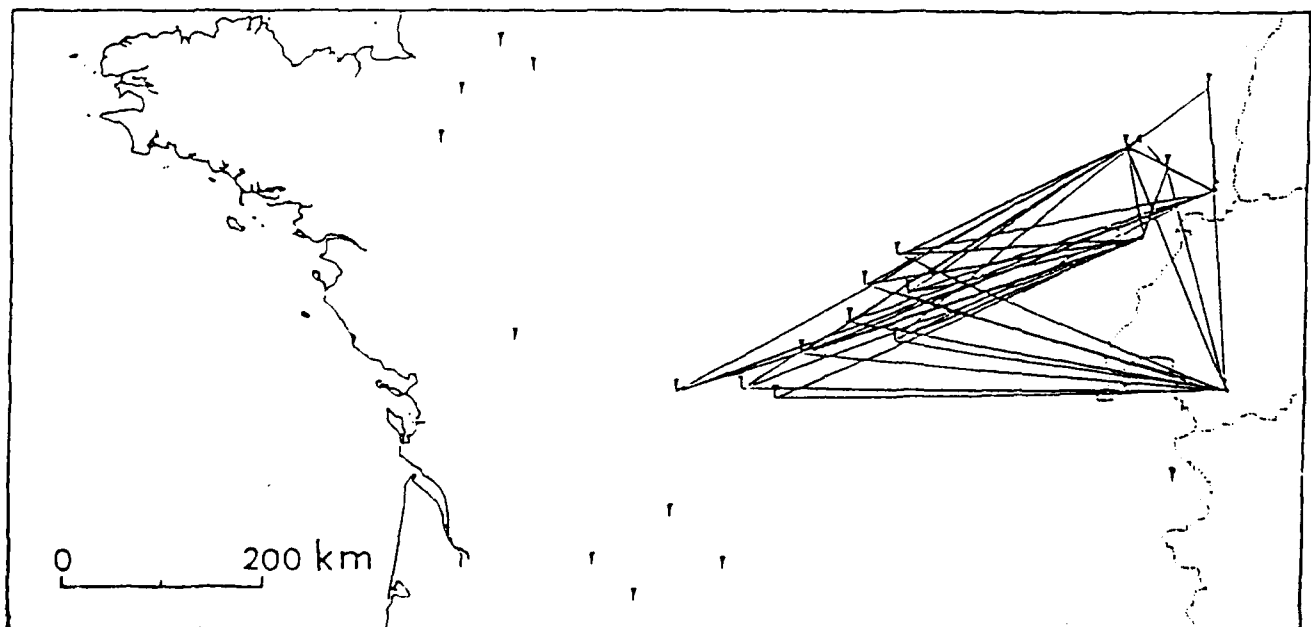
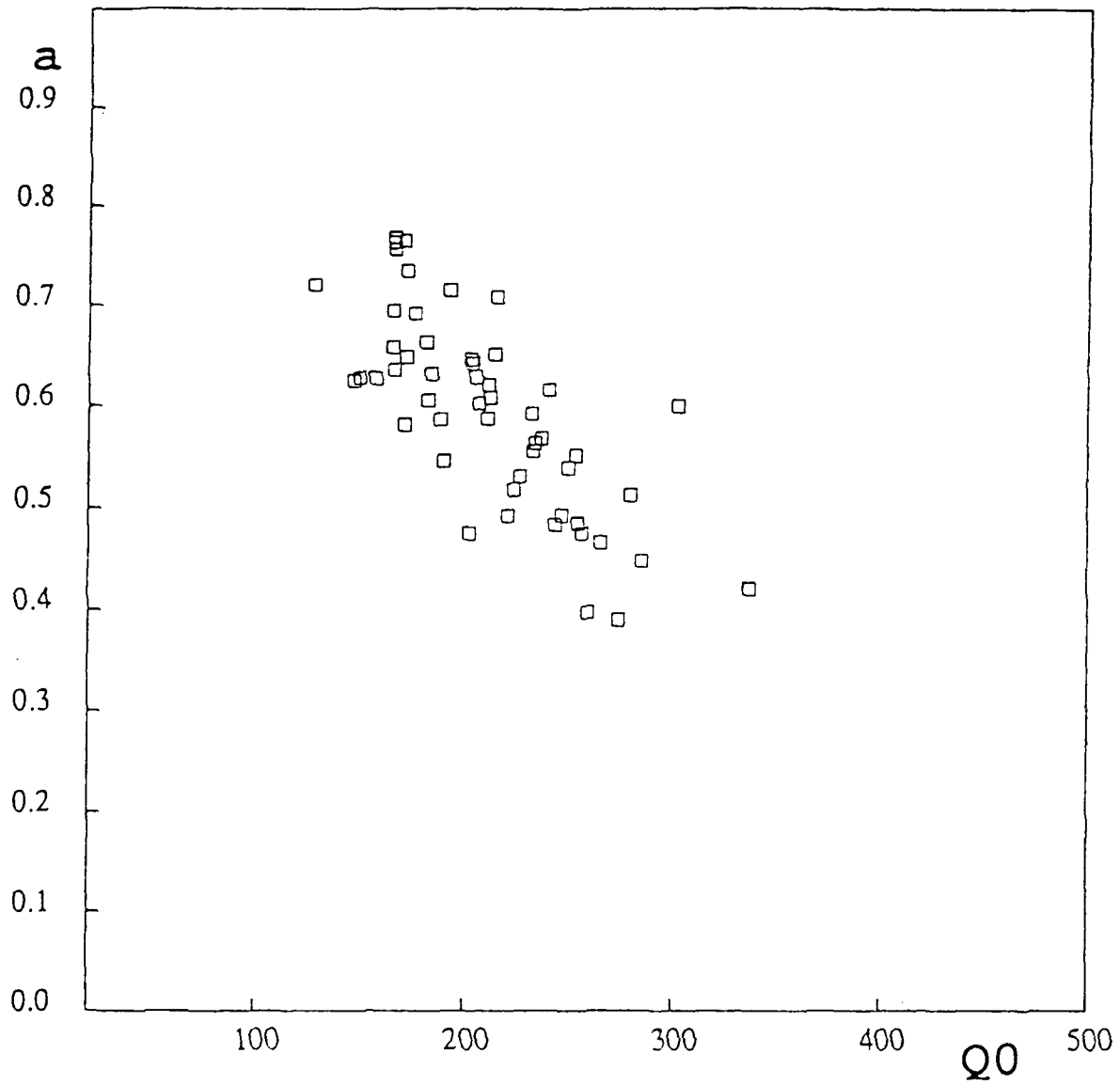
LOR 270Km

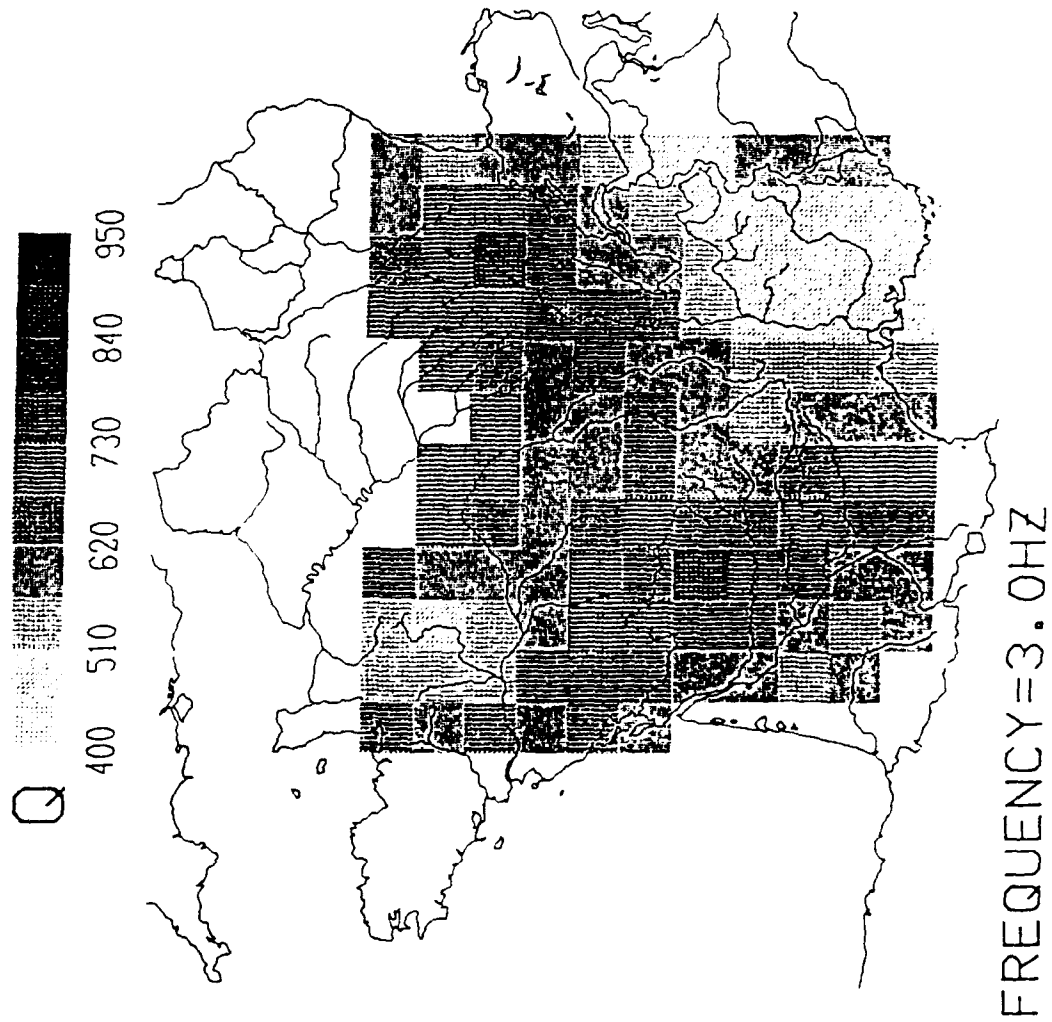
STUDIED TIME WINDOW



LOR 270 km







II

ATTENUATION OF CRUSTAL WAVES ACROSS THE ALPINE RANGE.

Michel Campillo^(*), Bruno Feigner^(**) Michel Bouchon^(*)
and Nicole Béthoux^(**)

^(*)LGIT, Université Joseph Fourier, Grenoble, France.

^(**)Centre Scientifique de Monaco, Monaco.

Although structural boundaries are known to affect the propagation of short period regional phases, our understanding of the phenomenon remains poor. Several reasons may be invoked to explain this gap. The first one is the extreme variability of the situations encountered in the Earth and our poor knowledge of the geometries of the deep crustal structures. A second reason is the small number of detailed seismological studies of regional phases across a structural boundary, particularly with regard to the quantitative analysis of amplitude variations. Finally, our modeling capabilities have lagged behind the medium complexity revealed by geophysical investigations and structural interpretations.

On the other hand several zones of anomaly in continental areas have been reported for Lg waves such as in the Himalyan Belt (Ruzaikin et al., 1972) or in the North Sea (Kennett and Mykkeltveit, 1984). As we will show in this study, a zone of strong weakening of Lg also exists in the western Alps. This

region, comprising part of France, Italy and Switzerland has been extensively studied by geologists and geophysicists (for a review see Vialon and Thouvenot). Following numerous refraction and wide angle seismic experiments, a deep reflection profile was recently conducted through the range (Ecors Project). The deep structure along a East-West cross section is therefore known in its gross features.

Seismological evidences

The existence of an anomaly of propagation of the crustal phase Lg in the Western Alps is directly revealed by the analysis of the seismological bulletin of the french LDG network. For a set of earthquakes in this region, we have drawn on Figure 1a the ray paths for which Pn phases were read and picked while in Figure 1b are plotted the ray paths for which Lg arrivals were picked. These two maps allow us to compare grossly the characteristics of propagation in the upper mantle and in the crust. They suggest that a strong anomaly of propagation of the crustal phase Lg exists in the region. On the maps is also represented, by a thick dotted line, the axis of the strong Bouguer gravity anomaly corresponding to the Ivrea Zone. This simple comparison suggests that the same deep structure is responsible for the extinction of Lg and for the positive gravity anomaly.

In order to confirm the presence of a zone of extinction of Lg in the Alps, and obtain quantitative information about this phenomenon, we selected a series of earthquakes occurring in the region and we computed the density of spectral amplitude for Pn and Lg. The Pn amplitude is measured in the group velocity window 8.2-7.9 km/sec while the Lg amplitude corresponds to the window 3.6-2.9 km/sec. Examples of records used in this study are presented in Figure 2. Figure 2a shows a record obtained at station LOR (Central France: 47.16N 3.51E) for an earthquake in the region of Gap (44.0N 6.22E), in the western part of the Alpine range. The path does not cross the Alps. The Lg wavetrain is clearly visible and presents a serie of peaks much larger than the coda of earlier arrivals. A spectral analysis of this record indicates that, in the spectral domain Lg dominates Pn for frequencies up to 8 Hz. On the contrary, we present in Figure 2b a record from an earthquake near Genova (44.52N 9.51E) obtained at station BGF in Central France (46.33N 02.50E). In this case the travel path crosses the zone of positive Bouguer anomaly. The Lg wavetrain is no longer visible on the seismogram. In this case, the spectral amplitude of the signal in the Lg group velocity window is about the same as the one in the Pn window for frequencies below 3 Hz, while at higher frequencies the Pn amplitude is larger.

We selected a set of earthquakes in Switzerland, Northern

Italy and Southeastern France recorded at short period stations of the LDG (Laboratoire de Detection Geophysique, France) and IGG (Istituto Geofisico di Genova, Italy) networks. The location of these events is presented in Figure 3. For each record we computed the ratio of Lg to Pn spectral amplitudes. To present the results in a convenient way, we defined a regular grid with a mesh of 20 km that covers the region of interest. We simply affected to each cell a value equal to the mean value of the ratio of amplitude Lg/Pn computed for all the paths that cross the cell. This operation was performed in different frequency ranges. The results obtained at 2 Hz and 3 Hz are presented in Figure 4. These images indicate the presence of the anomaly of propagation east of the Alpine range. We cannot resolve the extension to the east of the zone where Lg are sharply attenuated because all the Italian stations of the IGG network are located west or south of the positive Bouguer anomaly, that seems to correspond to the eastern limit of "normal" propagation of Lg. It is important to note that this zone of anomaly does not correspond neither to the region of the highest topographies nor to the one of the deepest Moho, that are clearly located west of the region characterized by the anomaly of crustal propagation. One may also notice the existence of a zone of strong weakening of amplitude ratio in the gulf of Genova. This is probably an effect of the well known vanishing of Lg in oceanic areas (Press and Ewing, 1952). However the propagation is efficient in the

coastal region, suggesting that the structures responsible for the extinction of Lg do not extent in the Southern part of the chain.

At a frequency of 2 Hz the value of the mean ratio between Lg and Pn amplitudes is larger than 4 in the Western Alps and in central France, but decreases to less than 0.3 in or east of the zone of positive Bouguer anomaly. This gives a rough indication of the order of magnitude of the sharp decay of amplitude occuring along paths crossing the range in the East West direction: the amplitudes are divided by more than 10.

A simple structural model.

In order to be able to model the propagation of Lg through the Alps we need to make some simplifying assumptions. We shall only consider paths in the East-West direction that cross the central part of the range. In this region the structures are elongated mostly in the North-South direction which allows us to reduce the study of the effects of these structures to a two-dimensional problem. Following the model of lithospheric overthrusting established by Menard and Thouvenot (1984) , we built up a simplified cross section of the Western Alps (Figure 5) that includes the most important features likely to severely affect crustal wave propagation: the geometry of the Moho and the presence of deep sedimentary basins on both sides of the range. To compute synthetic seismograms, we used the discrete wavenumber

boundary integral method proposed for irregularly layered medium by Bouchon et al. (1989). We limited our computations to the case of SH waves. We assumed the source to be located 15 km beneath the Po basin, as indicated by a star on Figure 5. The values of shear wave velocity and density are the following: 2.8 km/sec and 2.8 in the sediments, 3.5 km/sec and 3.1 in the crust and 4.7 km/sec and 3.3 in the upper mantle. We assumed the quality factor to be 100 in the sediments and 400 elsewhere. Because of limitations in computation time, we considered only frequencies lower than 1 Hz. We calculated time series of 80 sec duration at equally spaced receivers located at epicentral distances ranging from 100 to 400 km. To get a view of what should be "normal" propagation we also present in Figure 6 a seismic section corresponding to the case of a flat layered medium. Both sets of seismograms are plotted with a reduction velocity of 3.5 km/sec. As indicated in Figure 5, point (A) denotes the Western limit of the Po sedimentary basin while point (B) gives the location of the eastern edge of the Rhone and molassic basin. The seismograms computed for the Alps model show a spectacular decrease of Lg amplitude in the central part of the mountain range. However, the amplitude strongly increases when the waves reach the molassic sedimentary basin to the west of the Alps. Two causes can account for this result. First the curvature of the Moho in its deepest part will tend to focus the reflecting shear waves which make up the Lg wavetrain. Secondly,

the diffraction of the crustal waves near the edge of the molassic basin will result in the excitation of waves trapped in the sediments that are associated with high amplitudes as shown in Campillo (1987). The importance of this last phenomenon in our simulation is shown by the apparent velocity of the late arrivals. In the case of a flat layered model, the arrivals at locations farther away than (B) have apparent velocities higher than the reduction velocity of 3.5 km/sec, in accordance with their nature of multiply reflected waves. For the Alpine crustal model, the arrivals in the same distance range are characterized by apparent velocities lower than the reduction velocity, indicating that they correspond to waves trapped in the low velocity sediments. The increase in amplitude and duration of the wavetrain when penetrating in the zone of sediments may be due to the well known effect of amplification by a soft superficial layer. Because the attenuation in sediments is large, one may argue that these waves will rapidly decrease.

In order to identify the part corresponding to waves that sample the entire crust (the Lg waves), we repeated the computation using similar models where the sedimentary layers were replaced with crustal materials. The seismograms obtained are presented in Figure 7. They indicate that multiply reflected waves continue to exist after the crossing of the range, in spite of the very complex geometry of the crust-mantle boundary. This result means that the structural model proposed does not produce

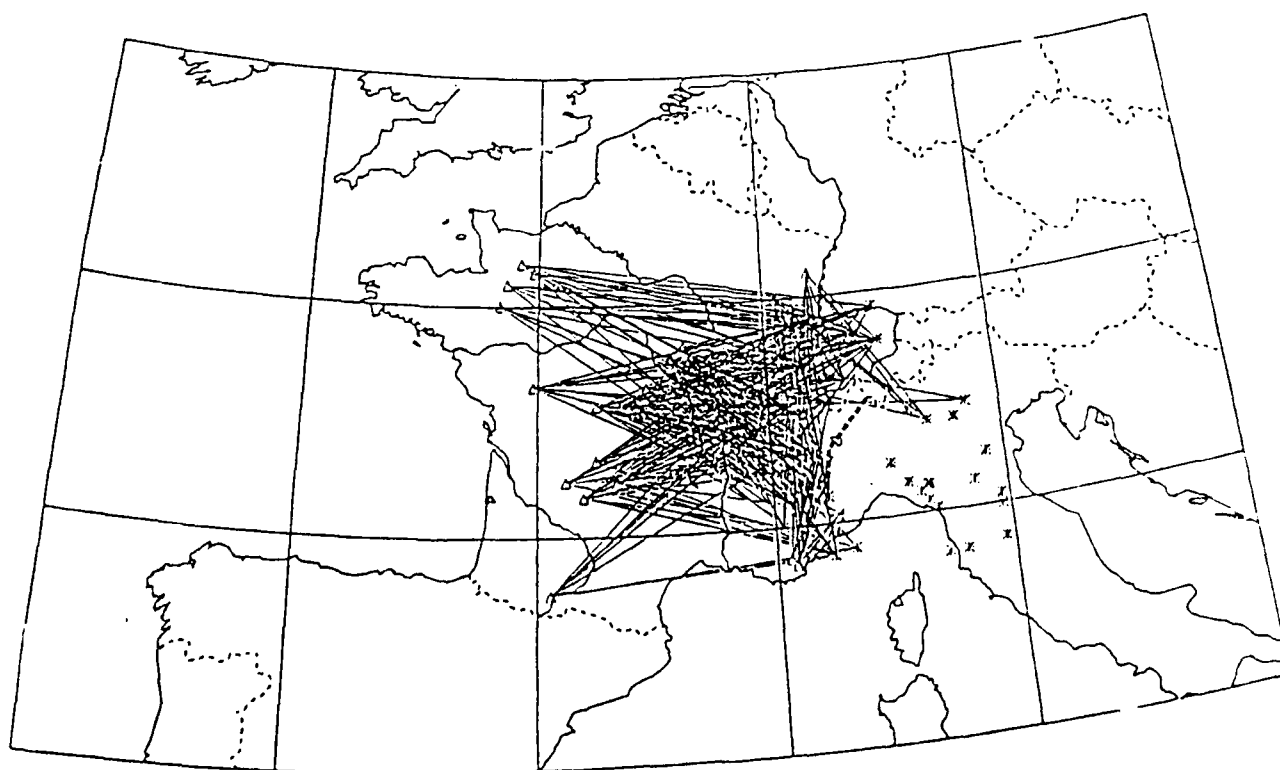
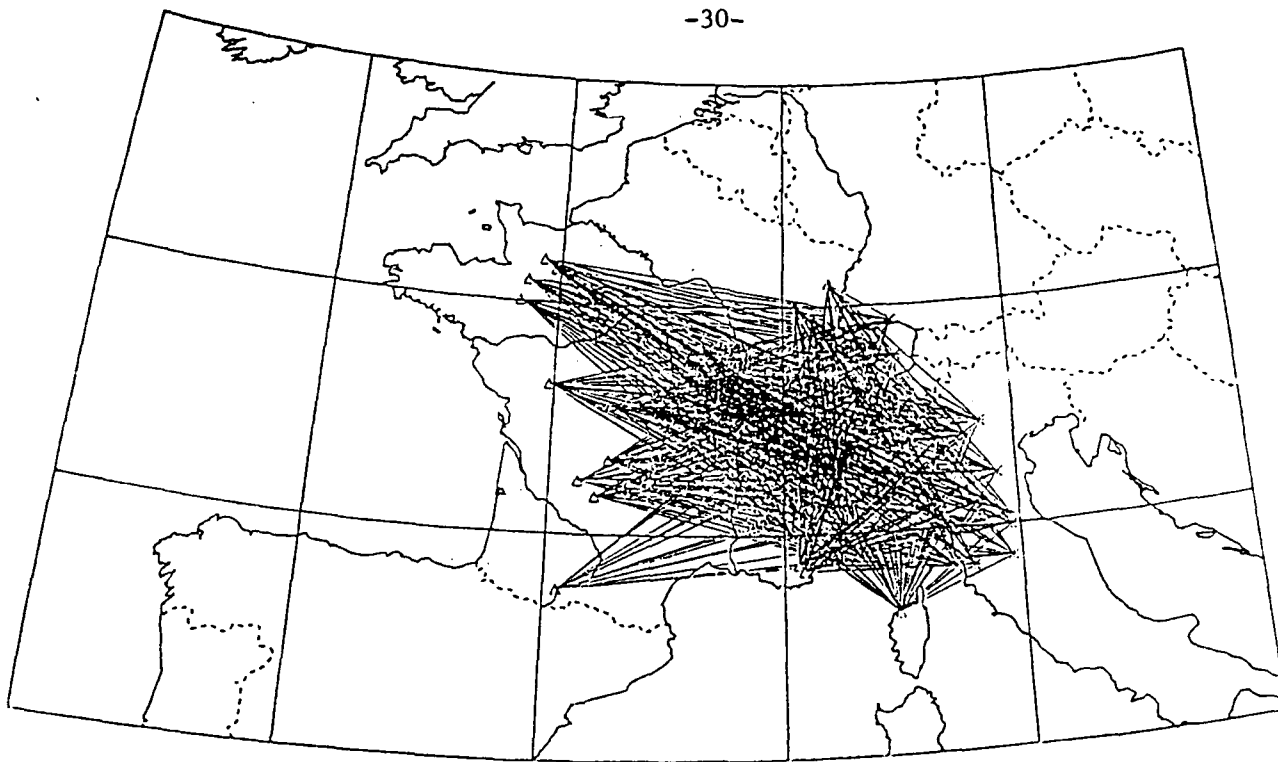
a complete extinction of Lg.

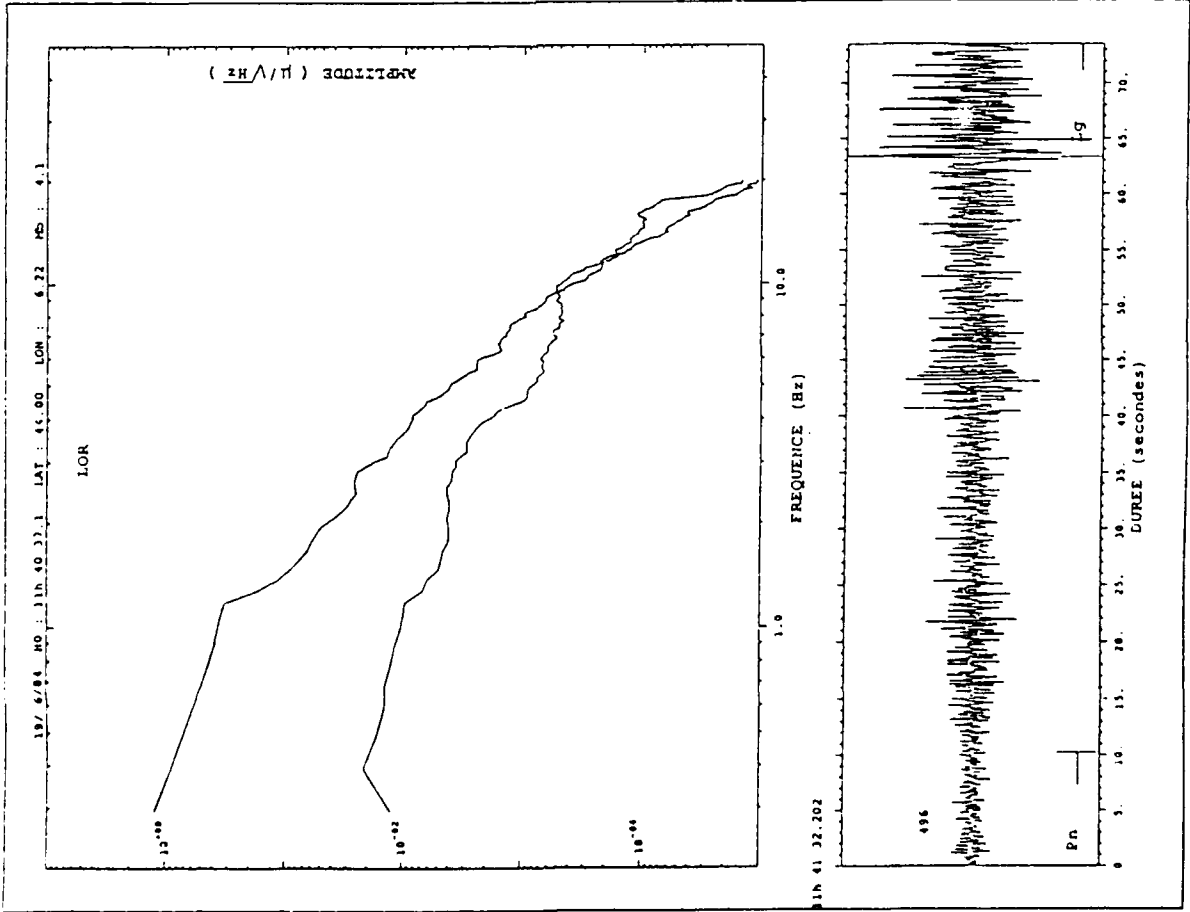
To measure the effective decay of amplitude due to the crossing of our simplified Alps model, we present in Figure 8, the spectral amplitude at frequencies around 0.75 Hz as a function of distance. The curves are plotted both for the flat model and for the model of the Alps including the sedimentary basins. The comparison between the two curves indicates that the complex geometry of the structure is responsible for a decrease by a factor of at least 2 of the amplitude, in spite of the presence of the sediments. On the other hand, this effect is not sufficient to account for the observed extinction of Lg.

If one accepts the fact that the main features of the crustal structures beneath the Western alps are known, the existence of a zone of extinction of Lg can be explained only partially by the effect of large scale lateral structural variations. To explain the observed extinction, we need to invoke causes which were not taken into account in our simplified model. Obviously, the existence in the crust of a zone of intense attenuation of body waves, due either to anelasticity or to scattering on small scale inhomogeneities, could be sufficient. Quantitatively, the attenuation required corresponds to a 100 km wide zone with a mean Q of 100.

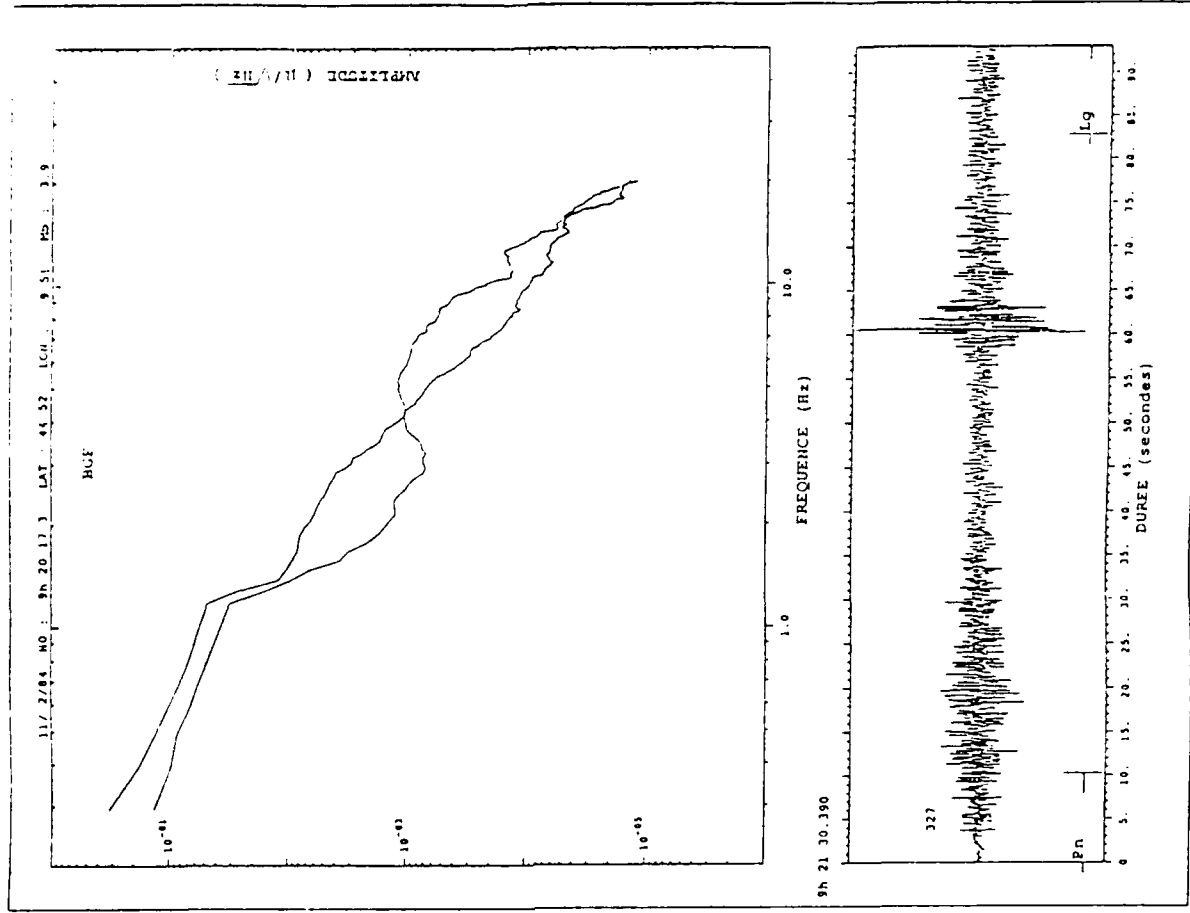
Another simplification introduced in our model is the assumption that the crust mantle boundary is smooth. The potential effect of the roughness cannot be addressed at this

stage since we are not able to quantify the most likely cause of vanishing i.e. the intrinsic attenuation of the crustal materials.

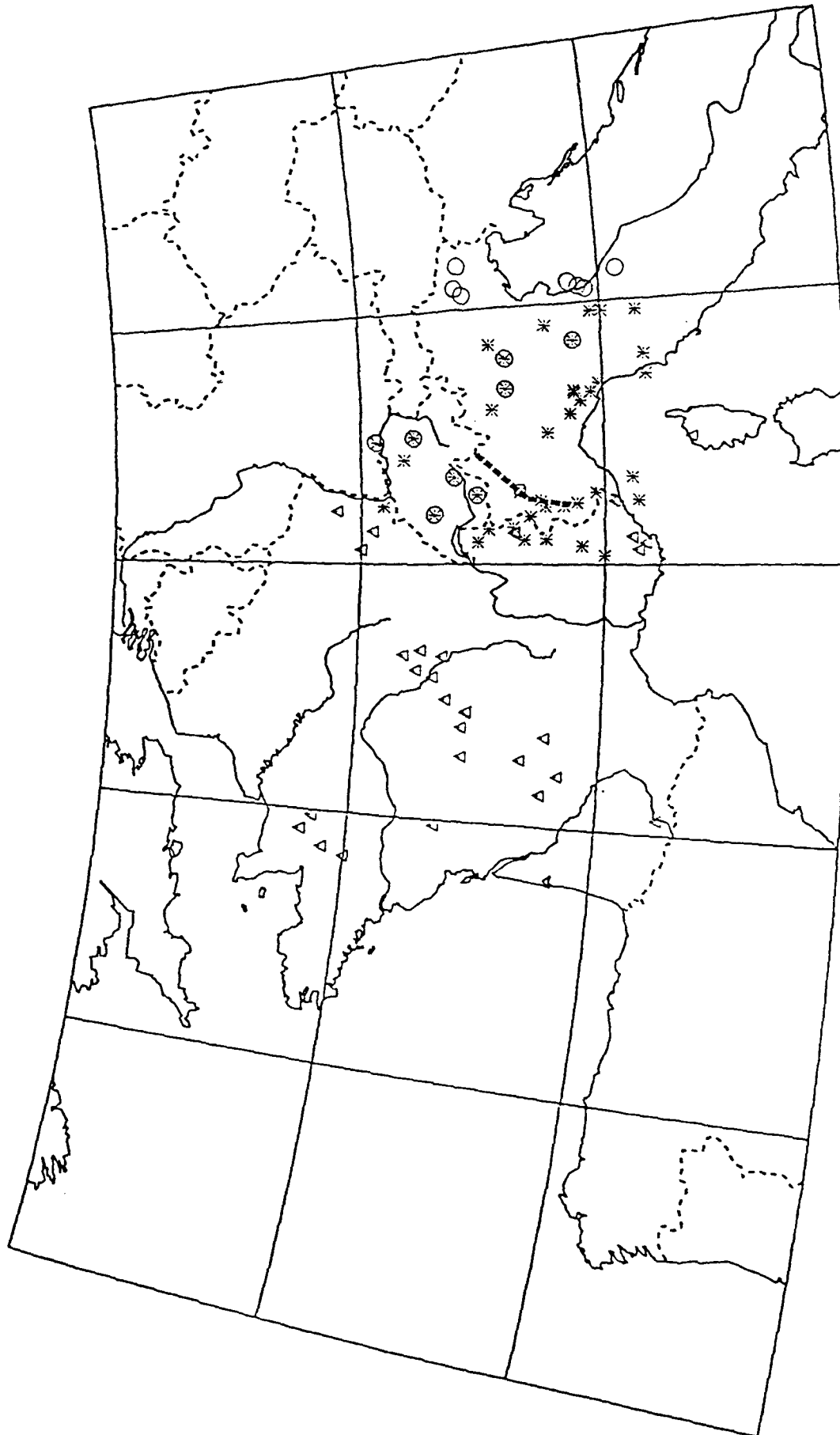




2 a



2 b



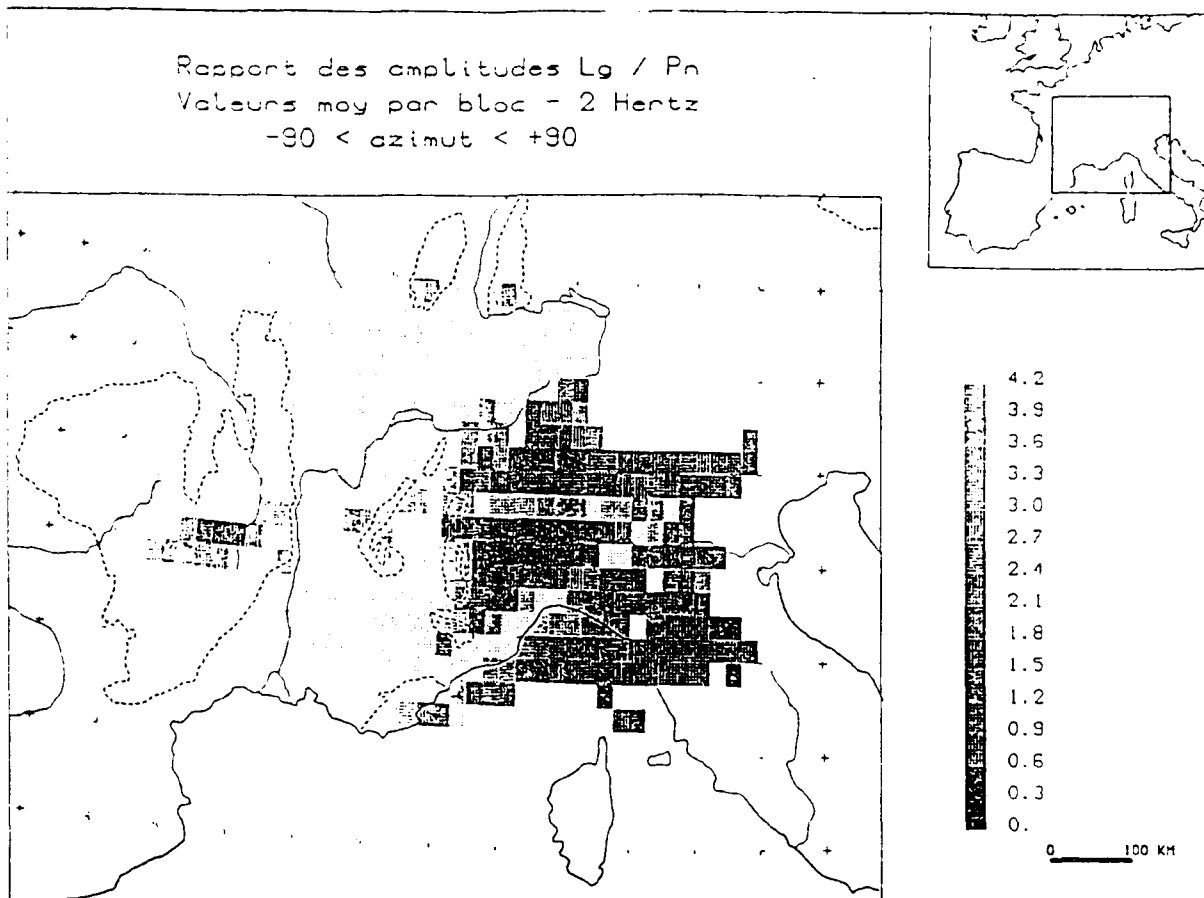
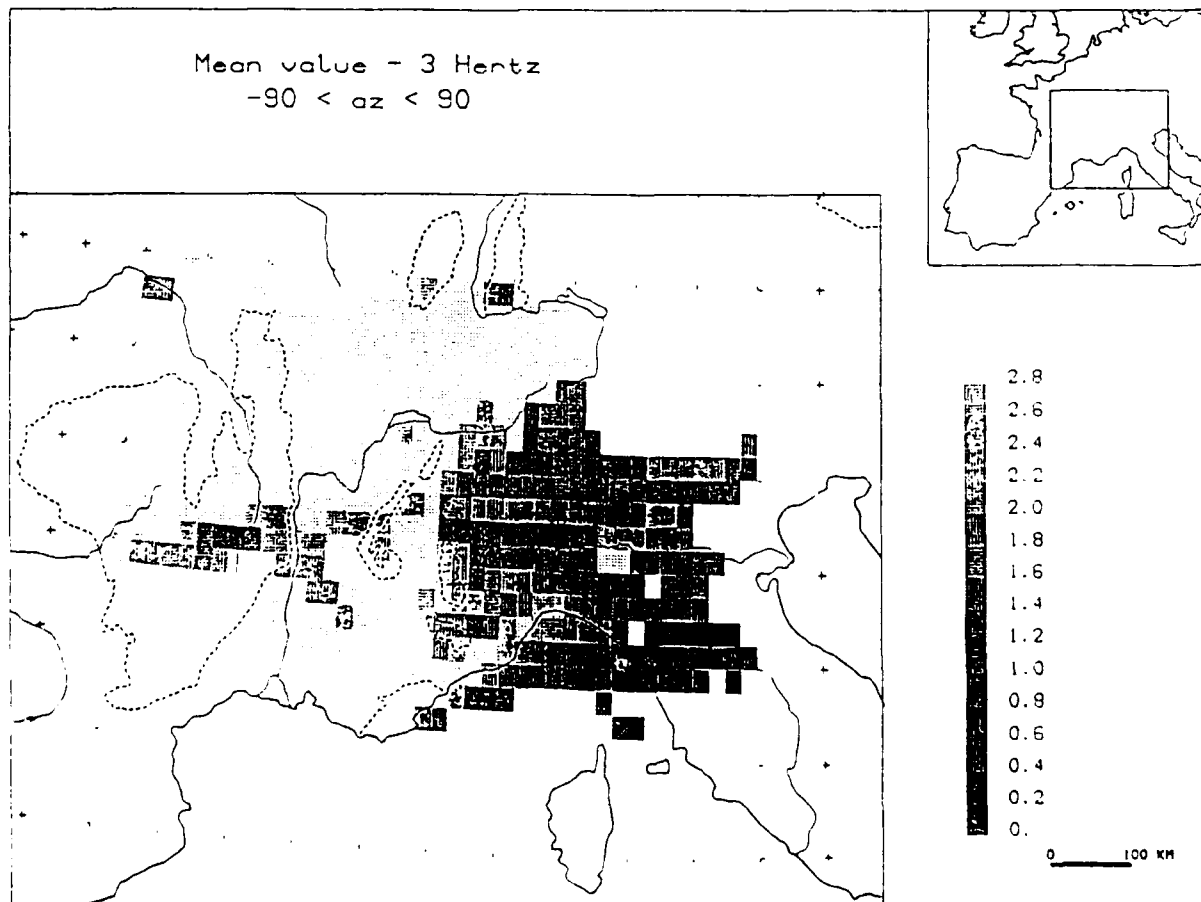
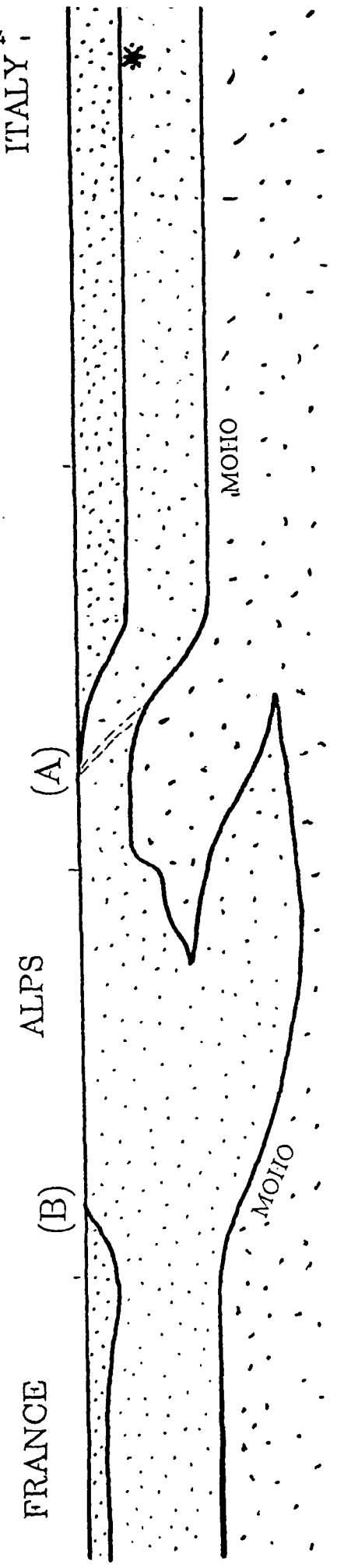
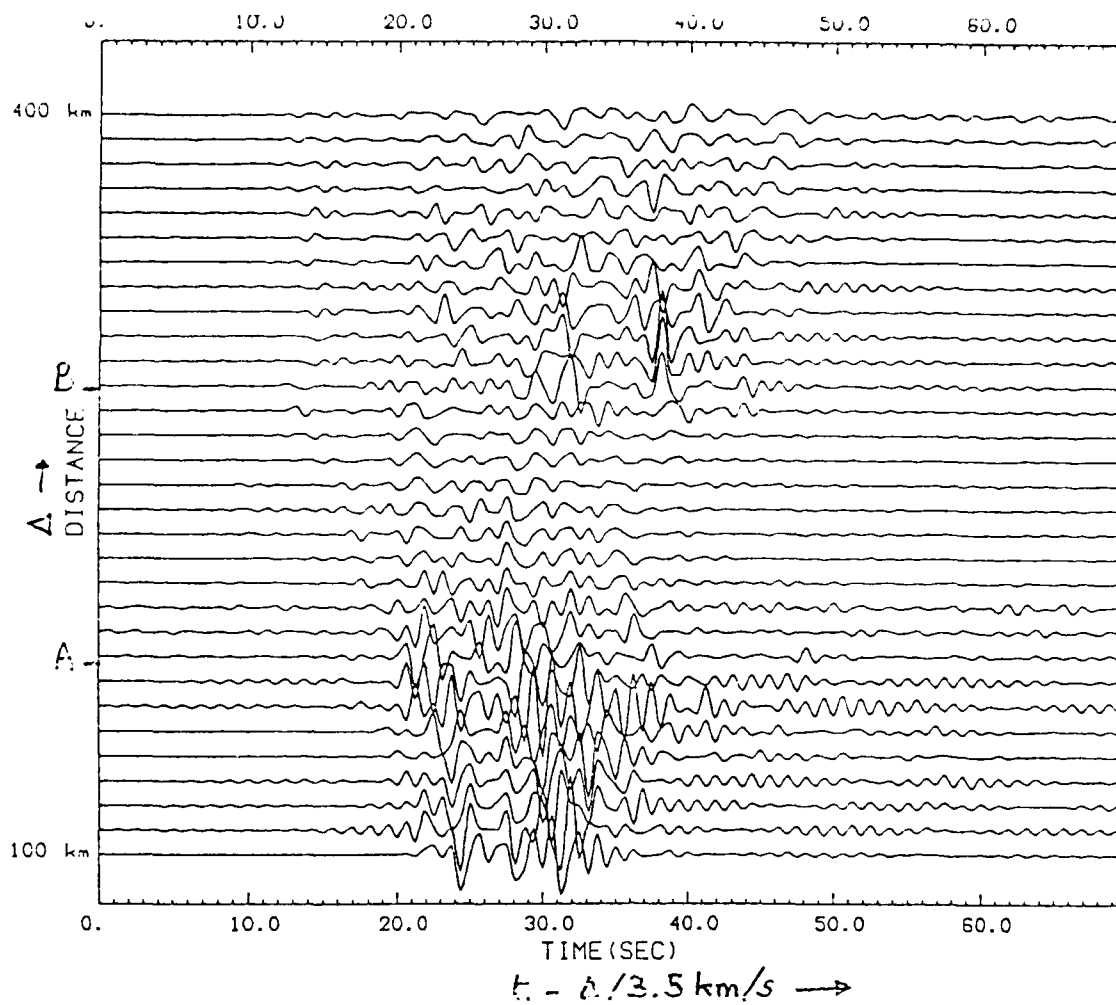


Figure 4a

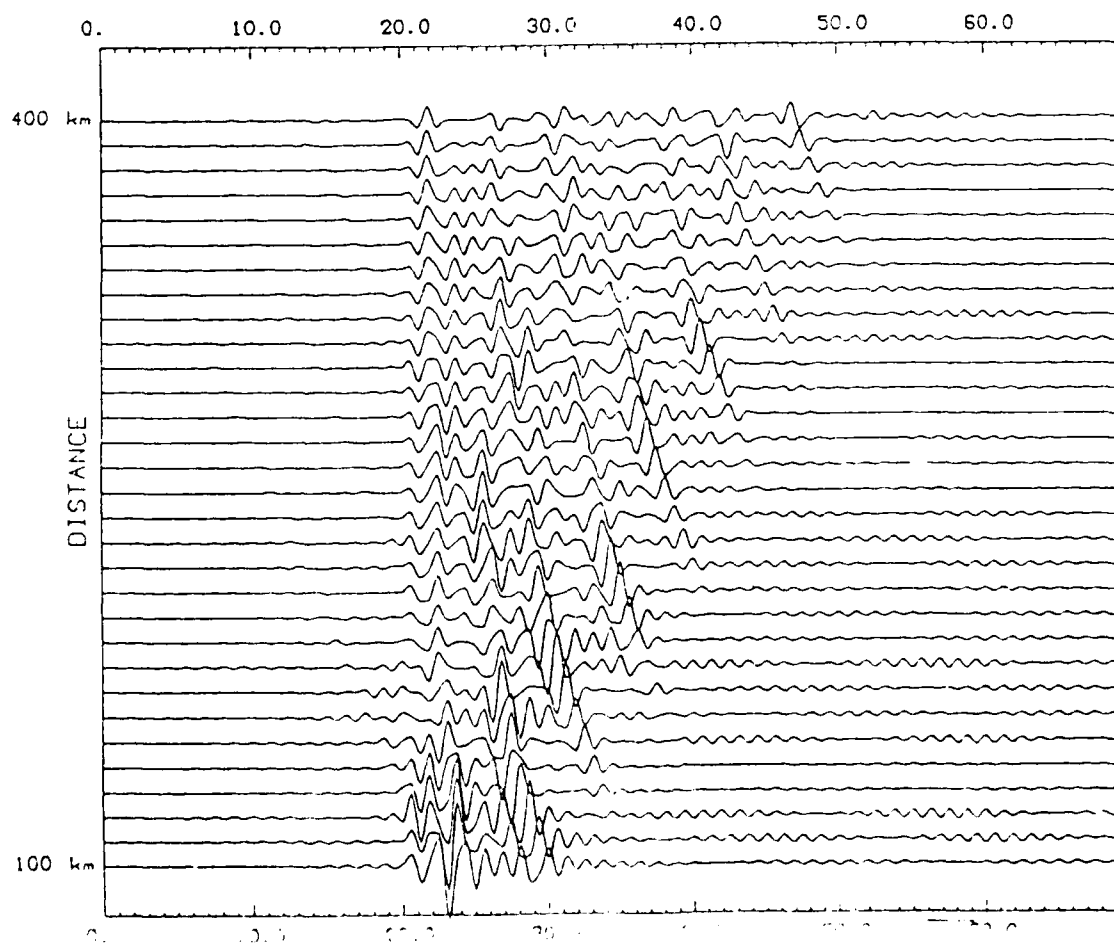




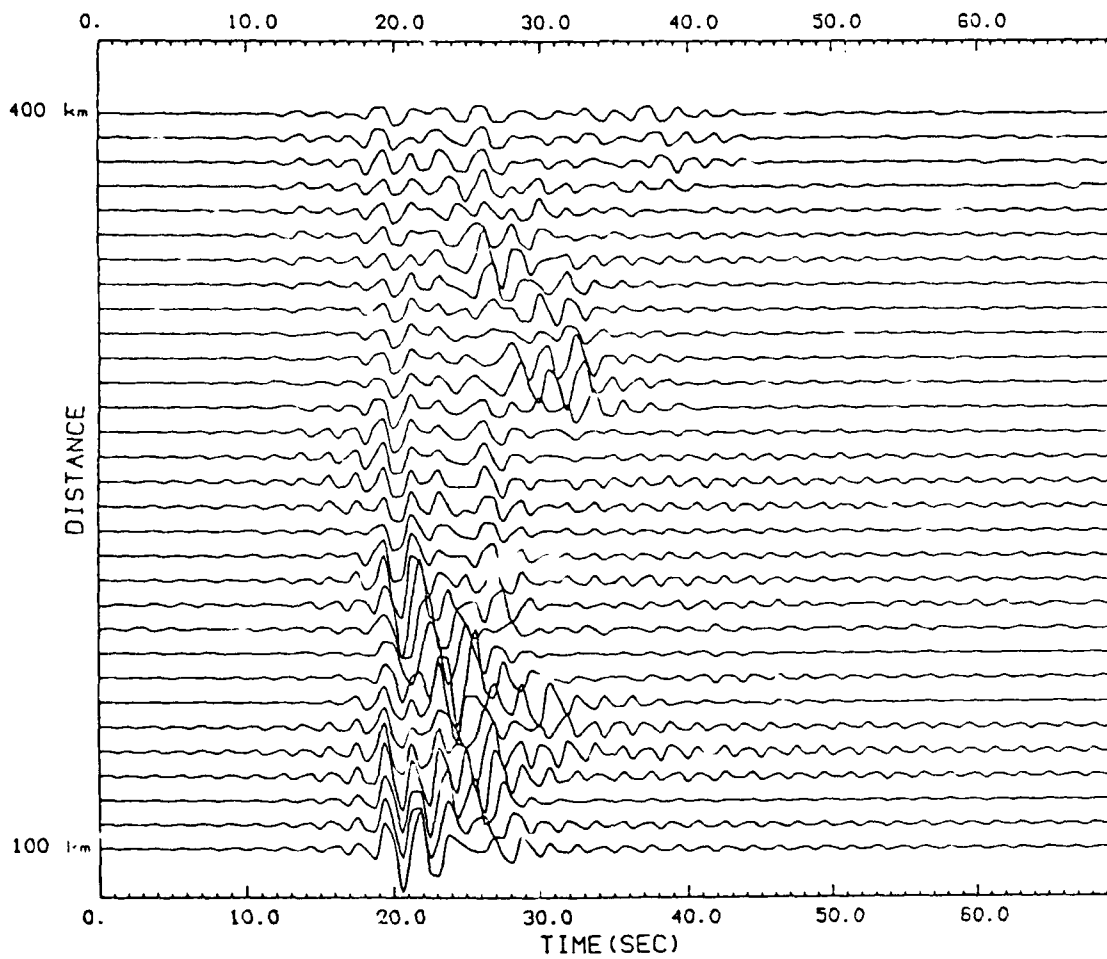
0 100Km



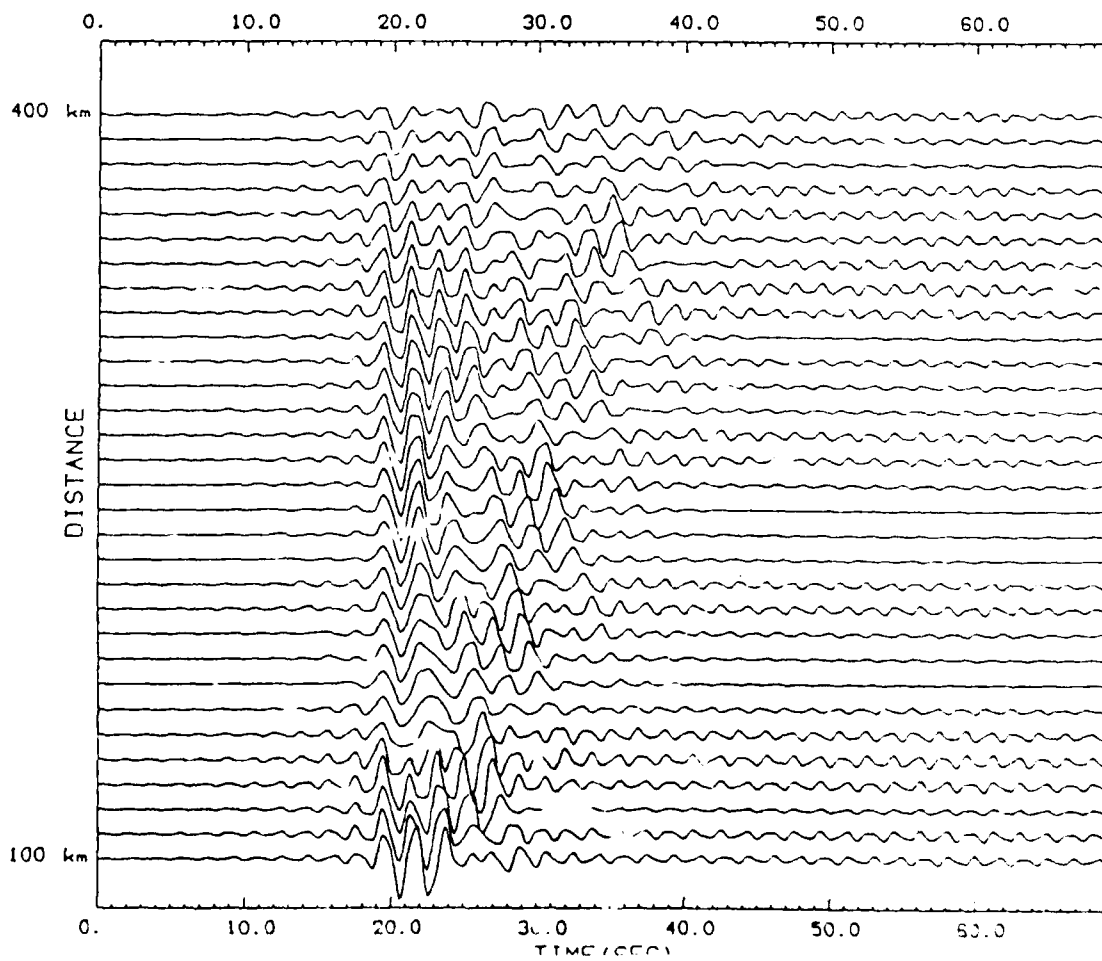
6 a



6 b



7 a



7 b

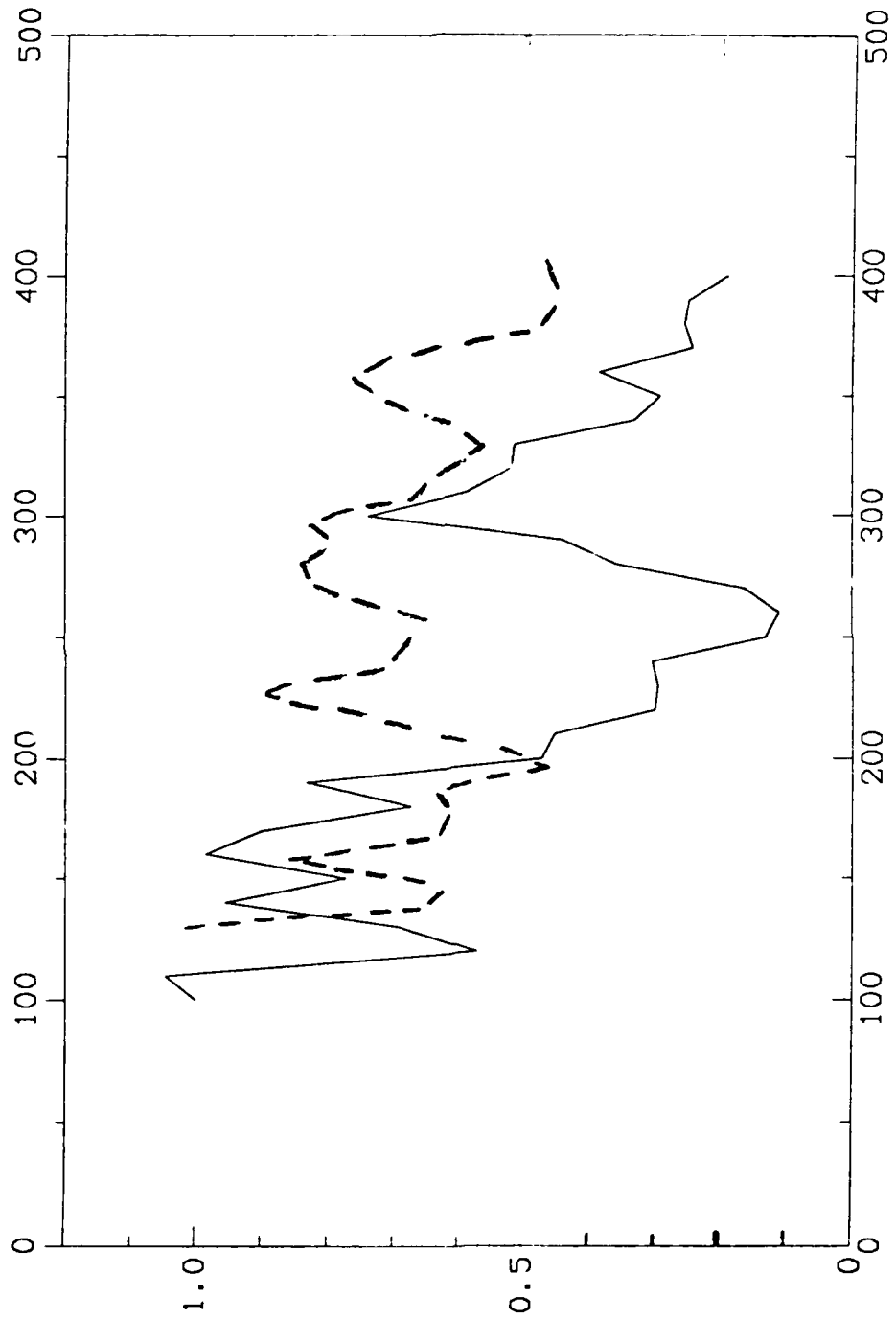


Figure caption

Figure 1

a) Ray paths drawn for Pn waves from the epicenter location (*) to the seismic station (Δ)

b) Ray paths for Lg waves

These two maps allow us to compare grossly the characteristics of propagation in the upper mantle and in the crust.

Figure 2

a) Record obtained at LOR (Central France: H 7°, 16 N 3° 51 E) for an earthquake in the region of Gap in the western part of the Alpine range. The path does not cross the Alps. The Lg wave train is clearly visible and presents a serie of peaks much larger than the coda of earlier arrivals.

b) Record from an earthquake near Genova obtained at BGF in Central France (H 6° 33N 02°50E). In the case the travel path crosses the zone of positive Bouguer anomaly. The Lg wavetrain is no longer visible.

Figure 3

Earthquakes and seismic stations (Δ)

Figure 4

Ratio Lg/Pn amplitudes in each block:

a) at $f = 2$ Hz

b) at $f = 3$ Hz

These images indicate the presence of an anomaly of propagation east of the Alpine range. Notice the existence of a zone of strong weakening of amplitude ratio in the gulf of Genova.

Figure 5

Simplified cross section of the western Alps used in the seismograms modelization with deep sedimentary basins on both sides of the range. We assume the source (*) located 15 km beneath the Po basin.

Figure 6

a) Seismograms computed with a "normal propagation" in a flat layered medium.

b) Seismograms computed with the "Alps model" showing a spectacular decrease of Lg amplitude in the central part of the mountain range.

Figure 7

Computation using similar model as in Fig.6 where sedimentary layers are replaced with crustal materials. The sismograms indicate that multiply reflected waves continue to exist after the crossing of the range.

Figure 8

Effective decay of amplitude due to the crossing of the Alps models= spectral amplitude at 0,75 Hz as a function of distance.

Far field effects due to complex geological structures in the vicinity of point sources.

S. Gaffet*, M. Bouchon**, and B. Massinon*

* Société Radiomana - 27, rue Claude Bernard - 75005 Paris - France

** I. R. I. G. M. - Université Joseph Fourier - B. P. 53X - 38041 Grenoble Cedex - France

CONTRACT No:

Objectives

The objectives of this work are to further our understanding of the source region geological structure effects on the teleseismic displacement recorded by a thin aperture network. The calculations are carried out using the discrete wavenumber - boundary integral equation formulation linked to the reciprocity theorem.

Research accomplished

We investigate here the source region effects that must be taken into account when analysing the Yucca Flat nuclear detonations recorded at distances of 80° by a seismic network. We try to separate the relative effects of the structure heterogeneities and of the source medium which contribute to these teleseismic ground motions.

The farfield displacement is assumed to result from the convolution of the source function, *i.e.* $s(\tau)$, by the propagation path response, *i.e.* $p(\tau)$, by the receiver and source site functions, *i.e.* $c(\tau)$, and by the recording system response, *i.e.* $a(\tau)$. Thus

$$r(t) = s(\tau) * p(\tau) * c(\tau) * a(\tau)$$

Different formulations of the source function $s(\tau)$ have been derivated in term of (i) the reduced displacement potential by Haskell (1967), von Seggern and Blandford (1972), and Helmberger and Hadley (1981). (ii) Another source formulation has been given by Mueller and Murphy (1971). This model takes into account both the yield and the detonation depth. The model scaling factors depending on the medium of burial have been empirically determined by Murphy (1977) for different source environments or have been computed by Power (1974) using a code that simulates underground nuclear explosions theory for tuff having various porosities and liquid densities.

Different numerical methods have been investigated to study the influences of the near source site heterogeneities on the teleseismic *P*-wave seismograms. If the lateral heterogeneities in the source region have effects at teleseismic distances on the m_b estimates that can be averaged or canceled indeed by a network of stations at multiple azimuths, these source site structures are of great importance for thin aperture observations (McLaughlin *et al.*, 1987, McLaughlin and Jih, 1988). Hasegawa (1971 and 1972) using a composite method connects the recorded seismograms shape to the geological complexity of the source environment. Bouchon (1976) links the Thomson-Haskell method (Thomson, 1950; Haskell, 1953) with the reciprocity theorem and shows the great influence of the source depth and of the medium of burial on the m_b estimates for events in layered media. Aki-Larner (1970) calculations for Yucca Flat explosions (Ferguson, 1988), and other data analysis methods (Taylor, 1983; Lay and Wlec, 1987; Lay, 1987a and 1987b) have been processed and emphasize the near source structure effects on the farfield displacement records.

The near source structure effects are hereafter computed using the discrete wavenumber - boundary integral equation formulation associated to the reciprocity theorem. This

discrete wavenumber method has been previously described and developed in the *P*, *SV*, and *SH* cases to study the effect of laterally varying media onto the field diffracted at a few tens of kilometers out of the source (Bouchon and Aki, 1977; Bouchon *et al.*, 1989; Gaffet and Bouchon 1989 and 1990). We study the farfield source environment influence and therefore ignore the receiver structures for such a problem has been the subject of a great deal of works which give prominence and describe using observed teleseismic recordings the wave diffraction effects that are due to the topography (Key, 1967; Bouchon, 1973; Sánchez-Sesma and Rosenblueth, 1979; Bard, 1982; Kawase and Aki 1988) or to the underground structures (Bard and Bouchon, 1980 and 1985) located near the seismometer.

A profile oriented in the azimuthal direction of France has been inferred from the Paleozoic basement depths obtained by Taylor (1983), Ferguson (1988) and McLaughlin *et al.* (1987) for the Yucca Flat valley. In the aim to determine the influence of the different layers, the basin was firstly made up of a wet tuff rocks filling (say model *a*), and then with a wet tuff volcanic rocks underlying a dry alluvium filling (say model *b*). A third model (say model *c*) should take into account a third level (*i.e.* the dry tuff level) but has not been yet processed for long duration computation. The model *b* and the elastic parameters are depicted figure 1. The crosses indicate the true depths of the two interfaces considered. The horizontal scale gives the distance in kilometer from an arbitrary origin. 11 detonations are studied and described in the table below. The map figure 1 displays their repartition nearly SW-NE along the profile given figure 1.

No	Event names	Date	Time	° N	° W	Depth	m_b
1	PYRAMID	16 Apr 1980	20 00 00.1	37 06 04	116 01 50	579 m	5.3
2	JORNADA	28 Jan 1982	16 00 00.1	37 05 29	116 03 04	640 m	5.9
3	TURQUOISE	14 Apr 1983	19 05 00.1	37 04 22	116 02 45	533 m	5.7
4	MUNDO	01 May 1984	19 05 00.1	37 06 22	116 01 21	567 m	5.3
5	CAPROCK	31 May 1984	13 04 00.1	37 06 11	116 02 53	600 m	5.8
6	BRETON	13 Sep 1984	14 00 00.0	37 05 12	116 04 16	483 m	5.0
7	HERMOSA	02 Apr 1985	20 00 00.1	37 05 41	116 01 56	640 m	5.7
8	GLENCOE	22 Mar 1986	16 15 00.1	37 04 59	116 03 58	600 m	5.1
9	TAJO	05 Jun 1986	15 04 00.1	37 05 54	116 00 56	500 m	5.3
10	GASCON	14 Nov 1986	16 00 00.1	37 06 02	116 02 53	600 m	5.8
11	BULLFROG	30 Aug 1988	18 00 00.1	37 05 09	116 04 07	500 m	5.0

The explosions have been projected onto the profile. The layout shows 4 events at the same horizontal location and different depths (*i.e.* Breton (483 m), Bullfrog (500 m), Turquoise (533 m), and Glencoe (600 m)) and a set of 7 events from west to east (resp. Jornada, Gascon, Caprock, Hermosa, Pyramid, Tajo, and Mundo). The mean observing distances is 80° from Yucca Flat and corresponds to an angle of incidence from the source region of 16.95° (Pho and Behe, 1972). Synthetic seismograms have been computed over a 10 s duration window at a such distance for the simple basin *a* and for the two layered basin *b*. The results are respectively presented on the left and right columns of the figure 2. The farfield basin impulsive response has been convolved with the non frequency dispersive Ricker function at 1 Hz. The time domain maximum

displacement amplitude increases with the depth of burial for both models (See *Breton*, *Bullfrog*, *Turquoise*, and *Glencoe*). The general feature observed is the amplitude increase from west to east up to *Pyramid* in connection with the depth of the Paleozoic basement. This shape effect is magnified by the presence of the alluvium layer for which the maximum displacement location always remains at *Pyramid* location. The seismograms are all the more broadened because the alluvium deposit thickens. *Tajo* and *Mundo* do not show significant variations between the two models for the too thin alluvium coverage above them.

We have computed the seismograms that should be recorded in France for the 11 assumed fully coupled detonations and for yields of 20 kt and 120 kt. The Mueller-Murphy source (1971) is used with the parameters corresponding to the wet tuff-rhyolite medium of burial (Murphy, 1977). The t^* value is 0.7 (Cormier, 1982). The frequency responses are presented figure 3 and the resulting signals (i.e. $s(\tau) * p(\tau) * a(\tau)$) are displayed in the two bottom boxes for an infinite space having the characteristics of the wet tuff layer. The main frequencies are 1 Hz and 0.7 Hz for respectively the 20 kt and the 120 kt shots at 500 m depth. Besides the computed seismograms of *Tajo* and *Mundo* which are scarcely modified in comparison with the half space solution, the common feature is an enlargement of the pP -wave (figure 4). For both yields, the amplitude increases while the depth of the Paleozoic basement decreases, the maximum amplitude being recorded in the camber region in the eastern part of the valley. If the amplitude seems to be correlative to the external shape of Yucca Flat, it appears that the frequency of the maximum amplitude has to be related to the thickness of the alluvium. The figure 5 sums up these results. This display depicts the Δm_b predicted by the synthetic data. The Δm_b values correspond to $\log_{10}(A_{ev. k} / T) - \left[\log_{10}(A_{ev. R} / T) \right]_{max}$, i.e. the difference between the magnitude of each detonation k with a reference event R which predicts the maximum magnitude. The general behaviour of the maximum amplitude is similar for the two yields with a Δm_b variation well correlated to the Paleozoic basement shape and a regular decrease of the period of the maximum amplitude with the thinning of the alluvium. A source effect is clearly shown for the explosions 6 (*Breton*), 11 (*Bullfrog*), 3 (*Turquoise*), and 8 (*Glencoe*) for which the Δm_b behaviour is reversed when the yield increases. Thus for small yields (e.g. around 20 kt) the displacement amplitude decreases with the depth of burial while it increases for big yields (e.g. around 120 kt).

We can apply these synthetic Δm_b variations to estimate the correlative yield miss-estimation. Different formulas may be used to estimate the yield in the Yucca Flat test region, i.e.

$$m_b = 3.79 + 0.85 \log_{10} W \quad (\text{Murphy, 1977}) \quad (1)$$

$$m_b = 3.71 + 0.89 \log_{10} W \quad (\text{Bache, 1982}) \quad (2)$$

These two relations can be summarized by $m_b = a + b \log_{10} W$. Thus on the one hand, if the observed magnitude $m_{b, obs}$ is smaller than the magnitude $m_{b, true}$ corresponding to the true value of the yield W_{true} , the miss-estimated percentage of the yield is

$$|\Delta W| / W_{true} = 1 - 10^{\frac{-|\Delta m_b|}{b}}$$

For instance, with $\Delta m_b = -0.25$ the underestimated yield is half times the true yield. On

the other hand, if the observed magnitude $m_{b, obs}$ is greater than the magnitude $m_{b, true}$, the miss-estimated percentage of the yield is given by

$$|\Delta W| / W_{true} = 10^{\frac{|\Delta m_b|}{b}} - 1$$

Thus with $\Delta m_b = +0.25$, the estimated yield is almost 2 times the true yield. The b values proposed in the relations 1 and 2 are close together so that the predictive yield estimation effects are similar for both magnitude vs. energy relations.

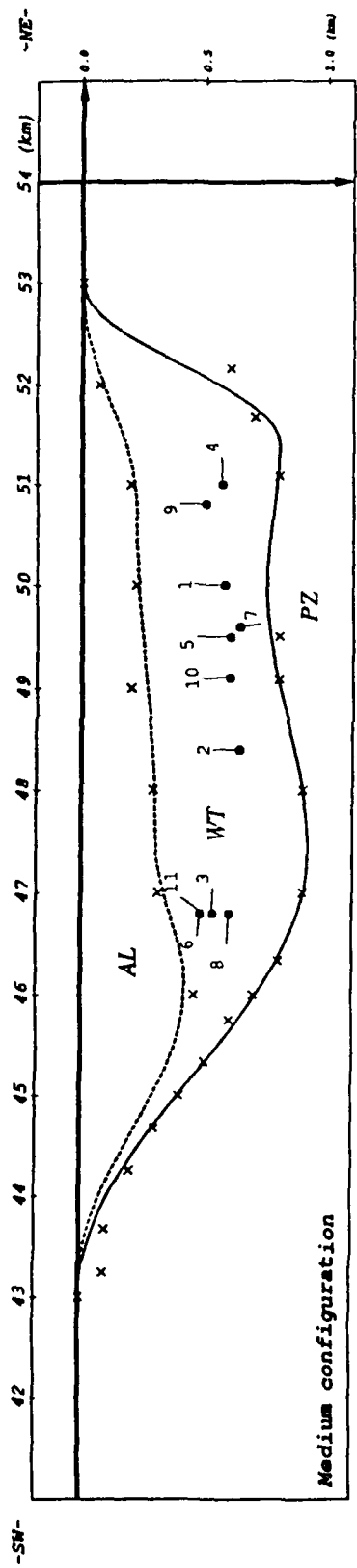
Conclusion

We have implemented the discrete wavenumber - boundary integral equation method to compute the P -wave farfield response of structure heterogeneities in the source region. The computation have been processed using the reciprocity theorem to study 11 underground explosions occurred in the central region of the Yucca Flat valley, Nevada, and recorded in France. We have shown the strong influence of the nature and of the shape of the basin filling. On the one hand, the maximum displacement amplitudes are connected together with the shape of the valley while on the other hand the corresponding frequency is correlative to the thickness of the alluvium deposit. The m_b anomalies determined in this work would be used to reduced the uncertainty in the yield estimations made with data obtained from a thin aperture network. The complete model which has not yet been implemented (*i.e.* the model c) should increase the model b amplitude behaviour and should lengthen the first arrivals recorded for the events that occur in the eastern part of the valley where the dry tuff level is the thickest.

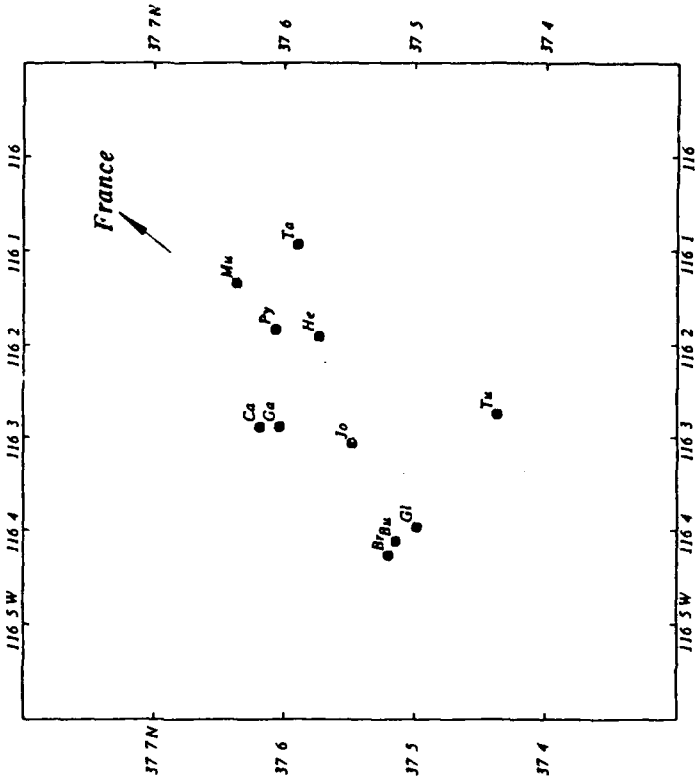
Bibliography

- Aki, K. and K. L. Larner (1970). Surface motion of a layered medium having an irregular interface due to incident plane SH -waves. *J. Geophys. Res.* **75**, 933-954
- Bache, T. C. (1982). Estimating the yield of underground nuclear explosions. *Bull. Seism. Soc. Am.* **72**, S131-S168
- Bard, P.-Y. (1982). Diffracted waves and displacement field over two dimensional elevated topography. *Geophys. J. R. astr. Soc.* **71**, 731-760
- Bard, P.-Y. and M. Bouchon (1980). The seismic response of sediment-filled valleys. Part 1. The case of incident P and SV -waves. *Bull. Seism. Soc. Am.* **70**, 1921-1941
- Bard, P.-Y. and M. Bouchon (1985). The two-dimensional resonance of sediment-filled valleys. *Bull. Seism. Soc. Am.* **75**, 519-541
- Bouchon, M. (1973). Effect of topography on surface motion. *Bull. Seism. Soc. Am.* **63**, 615-632
- Bouchon, M. (1976). Teleseismic body wave radiation from a seismic source in a layered medium. *Geophys. J. R. astr. Soc.* **47**, 515-530
- Bouchon, M. and K. Aki (1977). Discrete wavenumber representation of seismic source wave fields. *Bull. Seism. Soc. Am.* **67**, 259-277
- Bouchon, M., M. Campillo, and S. Gaffet (1989). A boundary integral equation - discrete wavenumber representation method to study wave propagation in multilayered media having irregular interfaces. *Geophysics* **54**, 1134-1140
- Cormier, V. F. (1982). The effect of attenuation on seismic body waves. *Bull. Seism. Soc. Am.* **72**, S169-S200
- Ferguson, J. F. (1988). Body waves magnitude variation at Yucca Flat, Nevada. *Bull. Seism. Soc. Am.* **78**, 863-872
- Futterman, W. I. (1962). Dispersive Body Waves. *J. Geophys. Res.* **67**, 5279-5291
- Gaffet, S. and M. Bouchon (1989). Effects of two-dimensional topographies using the discrete wavenumber - boundary integral equation method in P - SV cases. *J. Acoust. Soc. Am.* **85**, 2277-2283

- Gaffet, S. and M. Bouchon (1990). Source location and boundary shape effects on the *P*-SV near displacement field using a boundary integral equation - discrete wavenumber representation method. *submitted to Geophys. J. Int.*
- Hasegawa, H. S. (1971). Analysis of teleseismic signals from underground nuclear explosions originating in four geological environments. *Geophys. J. R. astr. Soc.* **24**, 365-381
- Hasegawa, H. S. (1972). Analysis of amplitudes spectra of *P*-waves earthquakes and underground explosions. *J. Geophys. Res.* **77**, 3081-3096
- Haskell, N. A. (1953). The dispersion of surface waves in multilayered media. *Bull. Seism. Soc. Am.* **43**, 17-34
- Haskell, N. A. (1967). Analytic approximation for the elastic radiation from a contained underground explosion. *J. Geophys. Res.* **72**, 2583-2587
- Helmberger, D. V. and D. M. Hadley (1981). Seismic source functions and attenuation from local and teleseismic observations of the N.T.S. events JORUM and HANDLEY. *Bull. Seism. Soc. Am.* **71**, 51-67
- Kawase, H. and K. Aki (1988). Time-domain response of a cylindrical canyon for incident SV, *P*, and Rayleigh waves calculated by the discrete wavenumber boundary element method. *Bull. Seism. Soc. Am.* **78**, 1415-1437
- Key, F. A. (1967). Signal generated noise recorded at the Eskdalemuir Seismometer Array station. *Bull. Seism. Soc. Am.* **57**, 27-37
- Lay, T. (1987a). Analysis of near-source contributions to early *P*-wave coda for underground explosions. II. Frequency dependence. *Bull. Seism. Soc. Am.* **77**, 1252-1273
- Lay, T. (1987b). Analysis of near-source contributions to early *P*-wave coda for underground explosions. III. Inversion for isotropic scatterers. *Bull. Seism. Soc. Am.* **77**, 1767-1783
- Lay, T. and J. L. Welc (1987). Analysis of near-source contributions to early *P*-wave coda for underground explosions. I. Waveform complexity. *Bull. Seism. Soc. Am.* **77**, 1017-1040
- McLaughlin, K. L., L. M. Anderson, and A. C. Lees (1987). Effects of local geologic structures on Yucca Flat, Nevada Test Site, explosion waveforms: two dimensional linear finite difference simulations. *Bull. Seism. Soc. Am.* **77**, 1211-1222
- McLaughlin, K. L. and E.-S. Jih (1988). Scattering from near source topography: teleseismic observations and numerical simulations. *Bull. Seism. Soc. Am.* **78**, 1399-1414
- Mueller, R. A. and J. R. Murphy (1971). Seismic characteristics of underground nuclear detonations Part I: seismic spectrum scaling. *Bull. Seism. Soc. Am.* **61**, 1675-1692
- Murphy, J. R. (1972). Calculated compressional-wave arrivals from underground nuclear detonations. *Bull. Seism. Soc. Am.* **62**, 991-1016
- Murphy, J. R. (1977). Seismic source functions and magnitude determinations for underground detonations. *Bull. Seism. Soc. Am.* **67**, 135-158
- Murphy, J. R. and R. A. Mueller (1971). Seismic characteristics of underground nuclear detonations Part II: elastic energy and magnitude determinations. *Bull. Seism. Soc. Am.* **61**, 1693-1704
- Pho, H.-T. and L. Behe (1972). Extended distances and angles of incidence of *P*-waves. *Bull. Seism. Soc. Am.* **62**, 885-902
- Power, F. W. (1974). Inelastic calculations in tuff and spectrum scaling considerations. *Report NVO-1163-241*, Environmental Research Corporation
- Sánchez-Sesma, F. J. and E. Rosenblueth (1979). Ground motion at canyons of arbitrary shape under incident SH-waves. *Int. J. Earthquake Eng. Struct. Dyn.* **7**, 441-450
- Taylor, S. R. (1983). Three-dimensional crust and upper mantle structure at the Nevada Test Site. *J. Geophys. Res.* **88**, 2220-2232
- Thomson, W. T. (1950). Transmission of elastic waves through the stratified solid medium. *J. Appl. Phys.* **21**, 89-93
- von Seggern, D. H. and R. Blandford (1972). Source time functions and spectra for underground nuclear explosions. *Geophys. J.* **31**, 83-98



Medium	α (km/s)	β (km/s)	ρ (g/cm ³)	v
AL	1.340	0.640	1.800	0.35
WT	3.000	1.600	1.800	0.30
PZ	4.570	2.640	2.500	0.25



Yucca Flat events map

Figure 1 - Geometry of the Yucca Flat valley inferred from the model given by Ferguson *et al.* (1988). The basin *a* is assumed to be filled with a wet tuff layer (WT) overlying a semi infinite space made up of Paleozoic sediments (PZ). The model *b* takes into account the alluvial deposits (AL). The elastic parameters are summed up in the above table. The explosions numbered from 1 to 11 in the text are depicted by the black circles in the tuff level. On the right side is displayed a simplified map of the studied events. The gray ellipse is plotted to emphasize the global distribution of the events roughly turned toward the France.

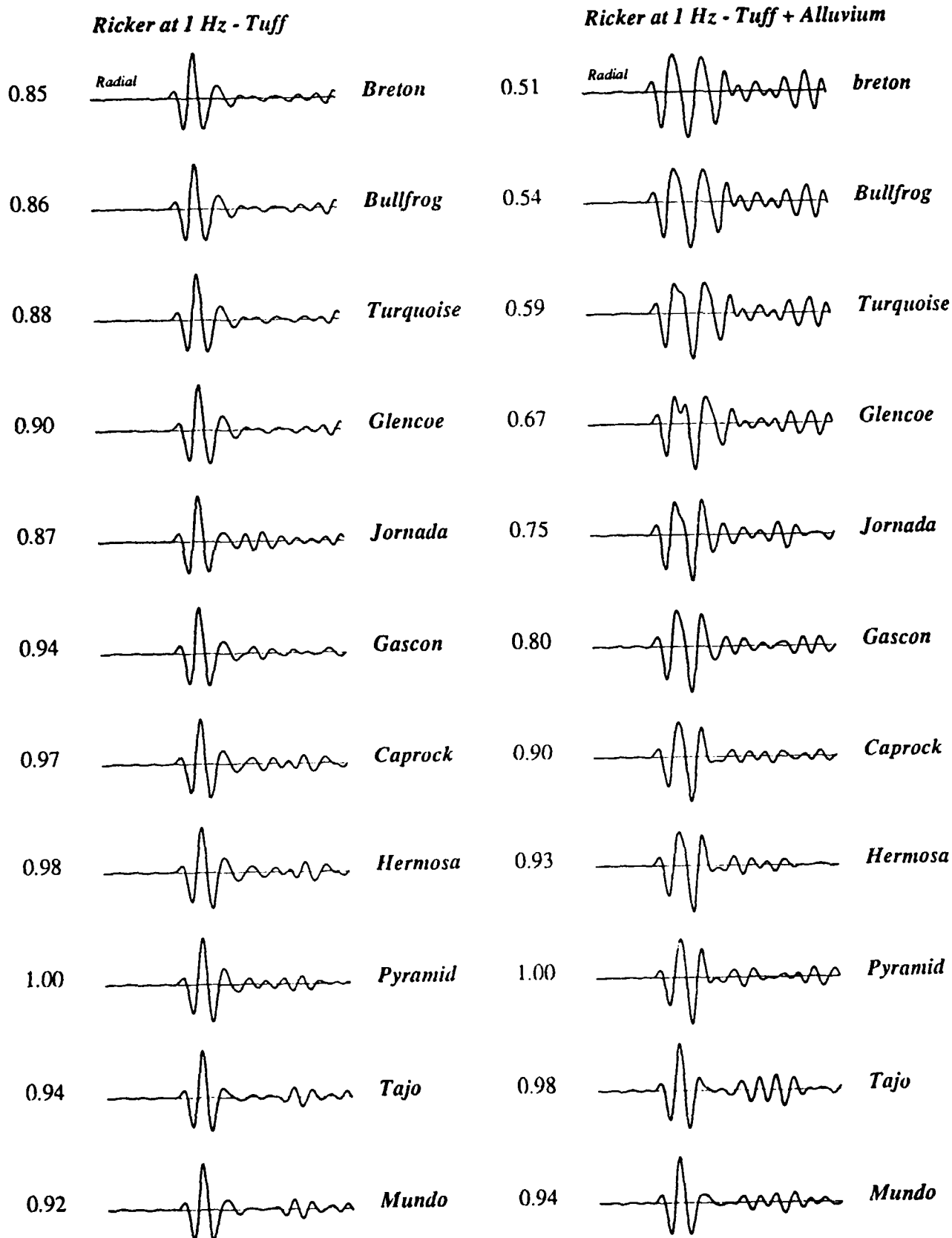


Figure 2 - Displays of the synthetic modellings obtained for the model *a* (left) and *b* (right) for the 11 studied detonations. The source is for both cases a Ricker having a 1 Hz central frequency in displacement. The relative amplitudes are written in the left side of each seismogram.

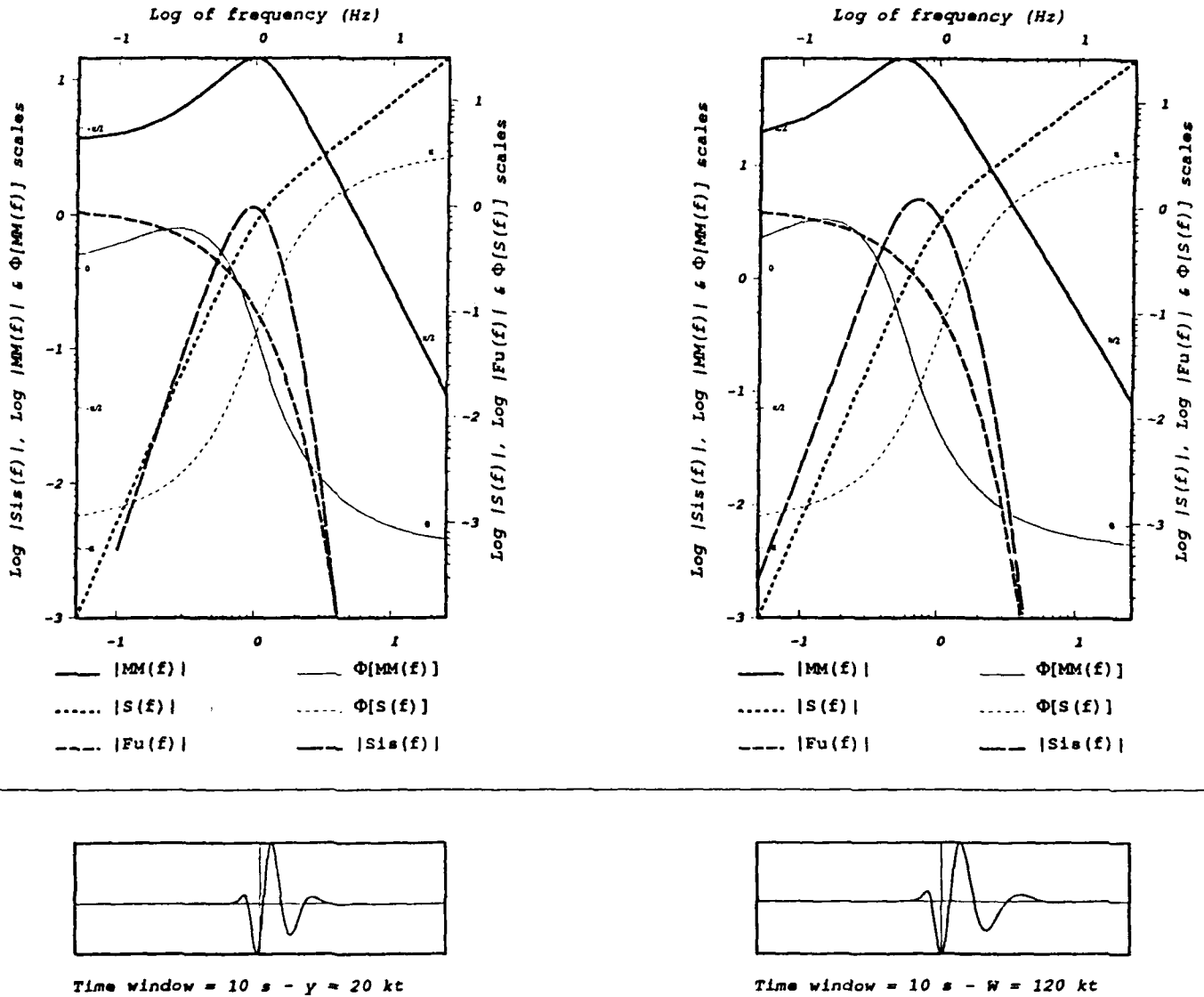


Figure 3 - The shapes of the Mueller-Murphy (1971) source that should be recorded at teleseismic distance in an infinite homogeneous space are given for the yields 20 kt and 120 kt in the two bottom boxes. In these boxes, the middle vertical thin line shows the arrival of the 1 Hz frequency. The transfer functions of the Mueller-Murphy (1971) source function (i.e. modulus $|MM(f)|$, phase $\Phi[MM(f)]$), of the Futterman (1962) mantle attenuation (i.e. modulus $|Fu(f)|$), of the recording system (i.e. modulus $|S(f)|$, phase $\Phi[S(f)]$), and of the far field displacement recording (i.e. modulus $|Sis(f)|$) are depicted in the top part of the display.

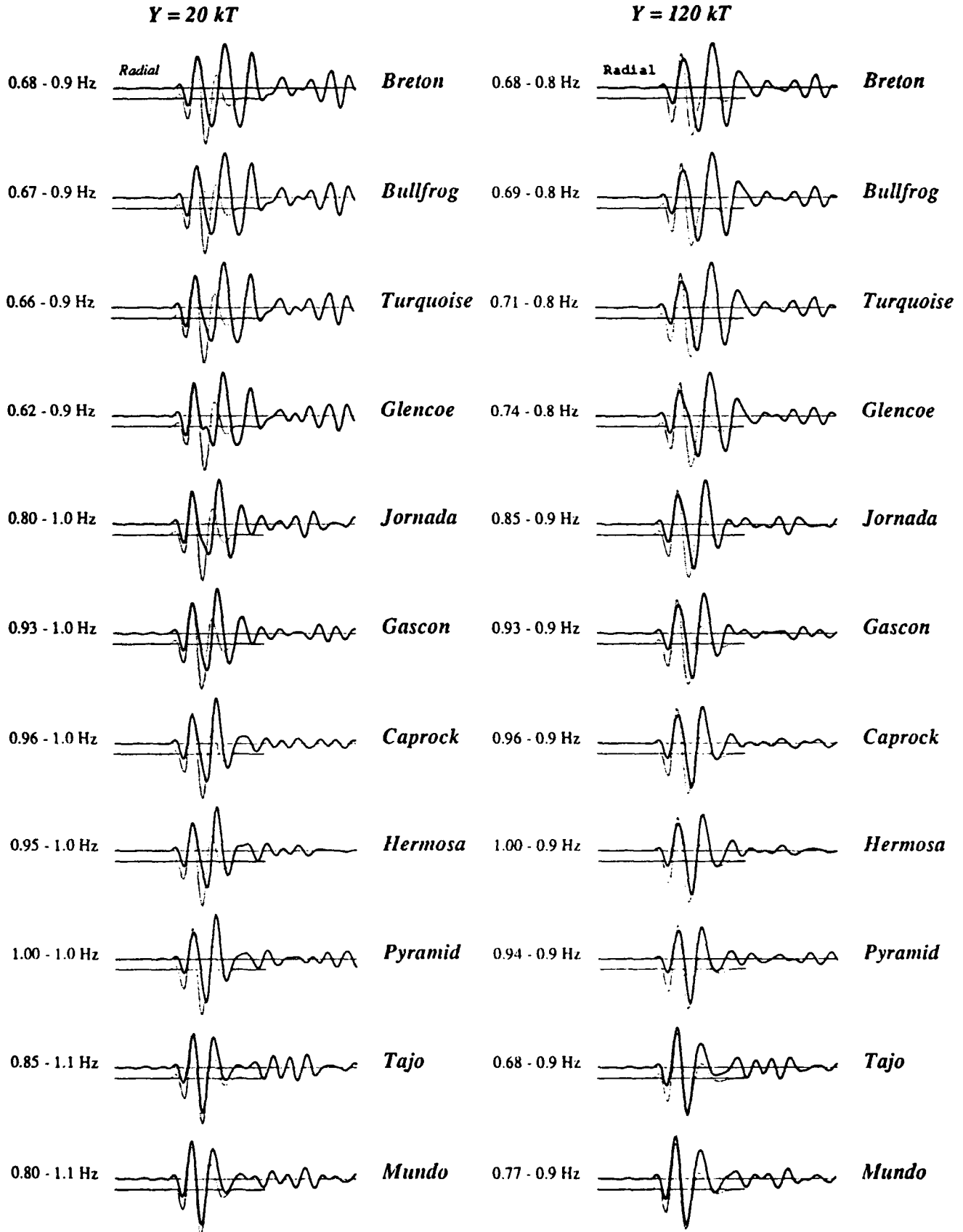


Figure 4 - Seismograms obtained for the Mueller-Murphy source (1971) and for the two yields 20 kt (left) and 120 kt (right). The relative amplitudes and their corresponding frequencies are written at the left of each seismogram. The seismograms are the ones calculated for the model *b*. The solutions obtained in a half space are given in slight superimposed dotted lines.

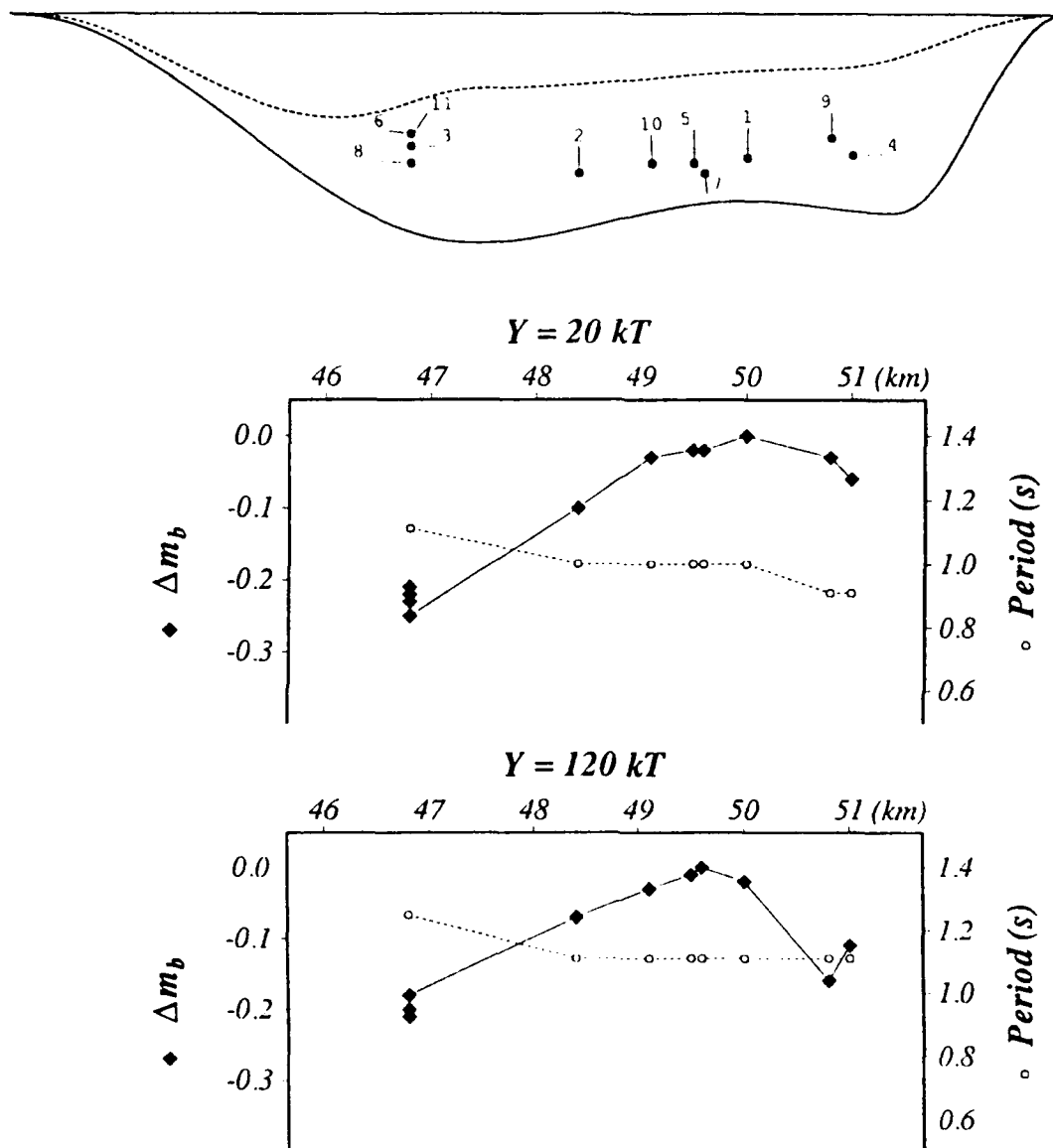


Figure 5 - Representation of the synthetic Δm_b predictions deduced from the calculations presented figure 4. The geometrical configuration is given in the top of the figure. The Δm_b (black squares) and the frequencies (white circles) at which these variations have been computed are plotted for the yields 20 kt and 120 kt.

- STUDY OF SEISMIC SWARM FROM EASTERN KAZAKH

INTRODUCTION

In theory a seismic event can be defined completely by a time function including :

- focal mechanism
- magnitude
- location

The only available information to define these parameters is the recorded signal at a station. This signal is modified along its path, so in addition to the information about the source characteristics, the signal provides information about the earth structure through which it travelled.

In this study, the data are teleseisms from Eastern Kazakh recorded by the french network.

STUDIED DATA

The records studied here were provided by the L.D.G. (Laboratoire de Géophysique). The french seismic network consists of 27 stations with the same features : the velocity response is flat above 1.0 Hz, and the fundamental period of the instrument is 1.0 Hz.

Nineteen events from Eastern Kazakh between 1981 and 1984 were studied. For all of them, we obtained data from both L.D.G. and I.S.C. about the magnitude and the location (see table 1).

The locations from the two networks were somewhat different (see figure 1) ; a systematic bias appeared in the L.D.G. locations, probably due to the limited range of azimuth of the events. The magnitudes also were compared and, with respect to the I.S.C. magnitude, The L.D.G. magnitudes for event magnitudes larger than 6.0 are over-estimated whereas they are under-estimated for smaller magnitudes.

In this study I.S.C. locations and magnitudes were used for reference.

MAGNITUDE ESTIMATION

One of our goals was to provide a way to estimate magnitude based on a more "reliable" method, using only the digital signal records instead of using graphic records. We first supposed that a recorded signal can be represented as the sum of K times an unscaled source function plus noise uncorrelated with the signal and characteristic of the station.

To apply this relation, some assumptions are necessary:

- all the courses have to be the same (same focal mechanism) and in our case we have only underground nuclear explosions coming from the same region;
- the K factor is characteristic for each station;
- the aperture of the network has to be small with respect to the epicentral distance.

Then, the K factor is equivalent to A/T in the theoretical formula for the magnitude and could be defined as the largest eigenvalue of the cross-correlation matrix. Because of the level of noise, we filtered the data between 1.0 and 8.0 Hz. To position the signals on the first arrival, we used a cross-correlation program. A very important feature of the signals is that they are very similar for different events recorded at the same station (see Figure 2) and for this case the cross-correlation program gives good results. But they are very different for the same event recorded at different stations. This result shows the strong influence of the receiver function.

The construction of the cross-correlation matrix requires that the set of signals used in the construction be complete. That is, the set must include one signal for each event-station pair in the set.

Two sets of data were used: one with all the stations (8) having recorded all nineteen events, and a second set having only the events (8) recorded at all 27 stations.

With these calculations, we were able to compute a K factor which was representative of the yield for a given station.

Because we assumed that this factor was equivalent to A/T, we were able to estimate a magnitude for all the events from the relation:

$$mb = a \log(K) + b$$

where 'a' and 'b' were computed by least squares using ISC magnitude for reference.

In the theoretical formula for the magnitude:

$$mb = a \log(A/T) + b$$

'a' is supposed to be equal to 1.0. In our calculation of both values 'a' and 'b' we found that 'a' value varied in a large range (from 0.77 to 1.23). Since we computed the values for all the stations, we were able to map 'a' values as a function of the station location.

As shown on Figure 3, the correlation between the location and 'a' value is strong, for example the stations located in the South of France show the highest values for 'a' (above 1.0) while the stations in Normandie show a value around 0.88. For the stations in Massif Central and Morvan, the relation is less obvious because of the geologic complexity.

Thus, it seems important for accurate computation of magnitude to take into account the fact that the 'a' value could be very different from 1.0 and is strongly influenced by the station environment.

With all this information, we could compute a magnitude for every event, this magnitude being defined as an average value over all the stations. With the aim of comparing our results with ISC magnitudes we computed the $mb(K) - mb(ISC)$ (1) and

also mb(LDG) - mb(ISC) (2).

We reported these differences on a map showing the event locations (see Figure 4). For both cases (1) and (2) the differences are quite similar for each event. One important result shown on the map is the geographic partitioning of those differences. We noticed that for the events located in the middle of Shagan River test site all the differences were zero or greater than 0.1 while the events located in the North-East part of the test site show negative differences. Below we will relate this feature with the structure at the test site.

In conclusion of this first part we were able to say that the 'automatic process' we followed to obtain a magnitude from digital data provides a reliable tool to compute magnitude accounting for the fact that the 'a' value should be used and is characteristic of the station.

The values of magnitudes are all relative since we did not have any reference for the yield.

SPECTRAL ANALYSIS

We were interested in both source-function spectral behavior and receiver function. We followed a method described by different authors and based on the Mueller-Murphy (1971) formula for the theoretical source-function.

We first grouped the stations into six subarrays based on the geological features of the region. For each subarray the region was assumed geologically homogeneous (4 stations were excluded because of their special location far from the other stations). Then, we computed the wave spectrum from the spectral density. We evaluated the noise spectral density from a window 10.24 s. wide ending just before the first arrival and the signal spectral density from a 2.56 s. wide window starting at the onset of the first arrival. We assumed that the signal was the convolution of a source-function, an elastic transfer function and a receiver function.

We first used the Mueller-Murphy reduced displacement potential for an underground nuclear explosion as a source-function to deduce the transfer function for the path. We based this calculation on absorption band model described by Anderson and Given (1982). We computed six different models for our six paths from the source area to the different subarrays.

With these results and the data, we were able to deduce a source-function, in theory. The unknown parameters were the depth and the yield, but the inversion program did not provide a good results because the parameter variations only weakly influence the resulting model.

A great variation in the yield does not imply a great variation in the corner frequency of the source-function. Thus, the inversion was not able to converge to a well-defined and unique value.

TEMPORAL ANALYSIS

With the above work, we can define the limits of spectral analysis by using models. We applied the same method but in the time domain to deduce the transfer function by using the Mueller-Murphy model as a reference and finally a source-function for each event.

The transfer functions computed for all the stations defining a subarray are as consistent in the time domain as in the frequency domain, except for the subarrays located in the Massif Central and Morvan region. We show the results for Vosges region in Figure 5.

From the transfer function, we deduced receiver function, limited in that we only used teleseisms and a narrow azimuthal aperture.

The application of this function should be limited to these particular events.

Using the same convolution relation, we computed source-functions for all the events from the recorded signals and the previously computed transfer functions. We located all the source function on a map. The use of the Mueller-Murphy model to determine the transfer function strongly influenced the shape of the resulting receiver function, but we could notice differences in the shapes of these source-functions. A site effect was indicated in the North-East part of Shagan River test site (see Figure 6). Therefore, we divided the events into two sets, one contained the events located in the North-East part of the site and the other containing the events located on the middle part.

We computed transfer functions again but using only the second set of data to avoid any contamination by the site effect.

The results were not very different in either temporal response or frequency content. We noticed only that the introduction of the first set of data in the computation implied an attenuation in the spectral shape without changing the content.

New source-functions were computed from these "more accurate" transfer functions. That did not change the source-function shape for the events in the central part of the test site, but a second peak was apparent for the other events just after the first peak. In order to confirm the validity of the procedure we computed the "synthetic signal" by convolution of the source-function and transfer function obtained above.

As shown in Figure 7 for two stations, we found a very good agreement between this "synthetic signal" and the actual signal.

Then we tried to locate the anomaly responsible for the site effect using a representation of the ray paths for the P waves from the source to the stations.

We first plotted the ray paths near the stations and we could make two remarks:

- Taking the stations with extremum azimuthal angles we found that all the rays were contained in a beam with a width of less than 100 km at 450 km from the source area which means that the paths in the upper mantle are about the same, especially in depth regardless of the station and source locations.

- The differentiation of the signal for any two stations was already clear very close to the source area.

Then, we plotted the ray paths around the test site. Since the events were very close to each other, we could see some overlappings in the paths from two different events to two different stations. Therefore, we tried to compare pairs of source-functions in order to find any similitude in the shape. This similitude was high when we took a pair of source-functions which overlapped at less than 30 km from the sources as shown on Figure 8. But from 30 km to 100 km we did not find any highly correlated pair of source-functions which means that the anomaly was very close to the source area.

Because the events did not cover a large area of the test site, we were not able to estimate the boundaries for this anomaly but by observing the evolution in the source-function shape in Figure 9, we could give a southern limit located along a Southeast-Northwest trend.

A hypothesis about this anomaly is that the rays are crossing a lens with a very slow velocity generating a 'secondary source.' This hypothesis seems to agree with our observations.

CONCLUSION

We were able to provide a reliable method to compute magnitude from digital records with some assumptions about the data. This method was at least as accurate as the graphic method.

The study of the data in the spectral domain allowed us to determine an attenuation model for six paths from the source area to the subarrays. Then we showed that these paths could be characterized by a transfer function applicable to the event-France part of the path and a receiver function characteristic of each station.

From these transfer functions, we computed experimental source-functions. The result showed a strong site effect at the North-East part of Shagan River test site which appears in the source-function as a secondary arrival probably due to a low velocity region.

REFERENCES

- Anderson, D. L. and J. W. Given (1982) **Absorption Band Q Model for the Earth**, J. Geophys. Res., 87, 3893-3904
- Mueller, R. A. and J. R. Murphy (1971) **Seismic characteristics of Underground Nuclear Detonation, Part I: Seismic Spectrum Scaling, Part II: Elastic Energy and Magnitude Determination**, Bull. Seism. Soc. Am., 61, 1675-1704

FIGURE CAPTIONS

- Table 1: List of events, with LDG and ISC locations
- Figure 1: Map of ISC and LDG locations
- Figure 2: Different events recorded at GRR station
- Figure 3: 'a' values over the LDG seismic network
- Figure 4: Map of mantitude differences:
Left: $m_b(K) - m_b(ISC)$
Right: $m_b(LDG) - m_b(ISC)$
- Figure 5: Station response spectra in Vosges subarray
- Figure 6: Sources determined with two sets of response functions
- Figure 7: Comparison of "synthetic" and actual signals
- Figure 8: Source-functions for different overlapping paths
- Figure 9: Evaluation of source-function shapes

n°	date	LDG location		ISC location	
		latitude	longitude	latitude	longitude
0	27.10.84	50.07 N	79.77 E	49.92 N	78.83 E
1	04.07.82	50.35 N	78.86 E	49.97 N	78.86 E
2	16.12.84	50.39 N	79.45 E	49.88 N	78.82 E
3	13.09.81	50.10 N	79.69 E	49.89 N	78.98 E
4	26.10.83	50.11 N	79.50 E	49.89 N	78.90 E
5	14.07.84	50.18 N	79.64 E	49.85 N	78.92 E
6	26.05.84	50.09 N	80.03 E	49.93 N	79.03 E
7	28.12.84	50.15 N	79.46 E	49.83 N	78.71 E
8	06.10.83	50.20 N	79.46 E	49.91 N	78.83 E
9	25.04.84	50.17 N	79.23 E	49.91 N	78.91 E
10	10.02.85	50.40 N	79.05 E	49.90 N	78.80 E
11	29.03.84	50.33 N	79.29 E	49.87 N	78.97 E
12	02.12.84	49.92 N	80.26 E	49.95 N	79.03 E
13	15.04.84	50.10 N	78.96 E	49.69 N	78.14 E
14	26.12.82	50.47 N	79.89 E	50.06 N	79.05 E
15	07.03.84	50.41 N	79.48 E	50.00 N	78.99 E
16	29.03.81	50.05 N	79.84 E	49.98 N	79.02 E
17	20.11.83	50.28 N	79.79 E	50.06 N	79.02 E
18	31.08.82	50.29 N	79.43 E	49.91 N	78.79 E

Table 1

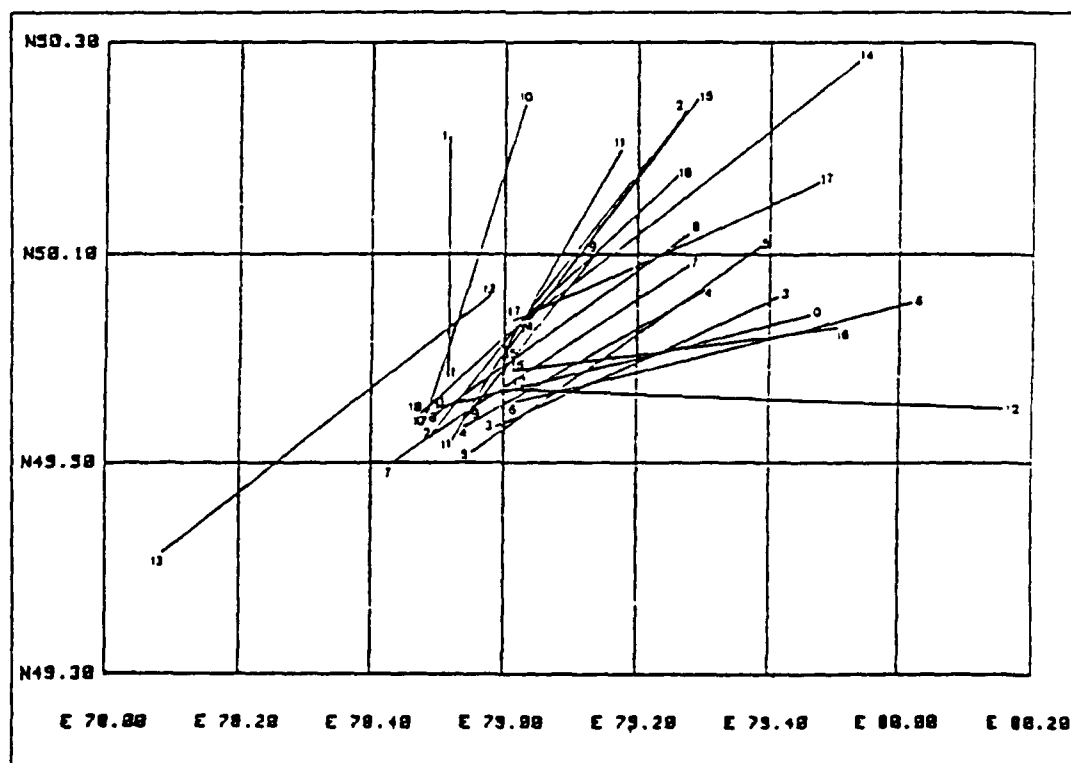


Figure 1

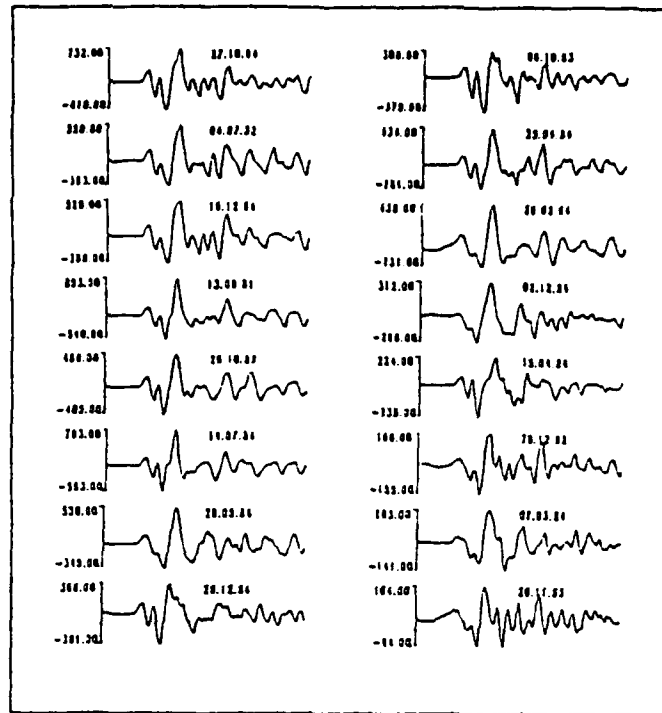


Figure 2

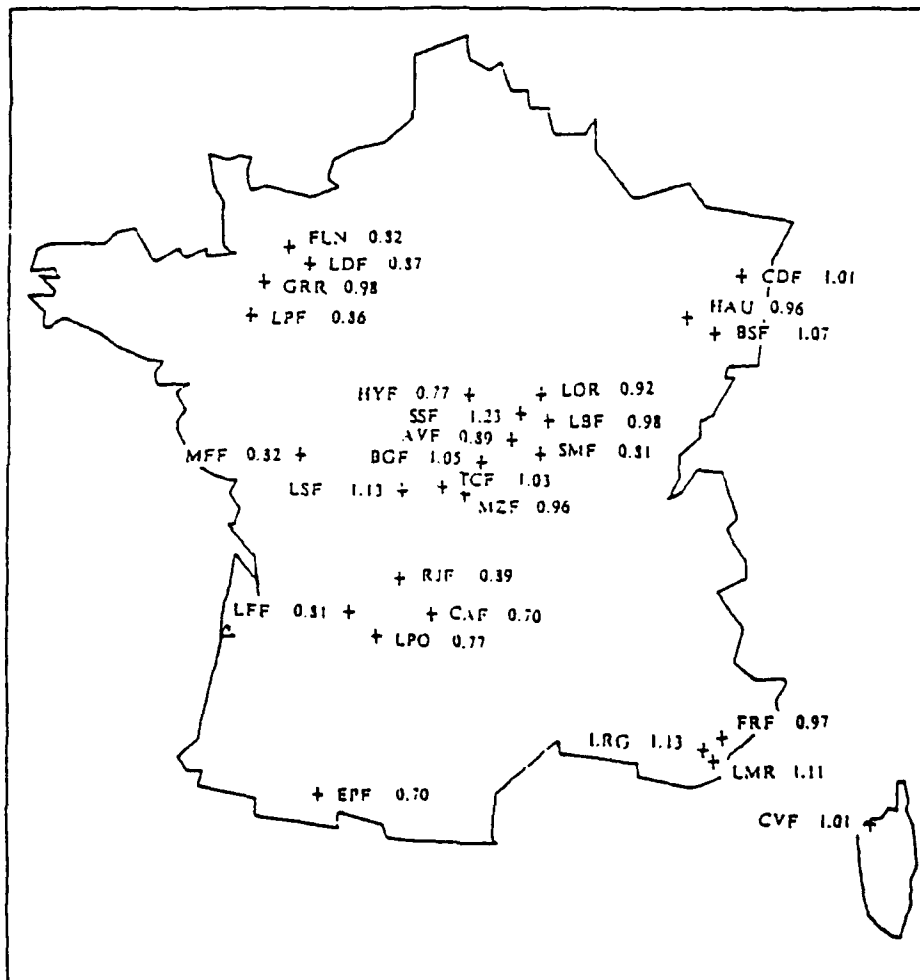


Figure 3

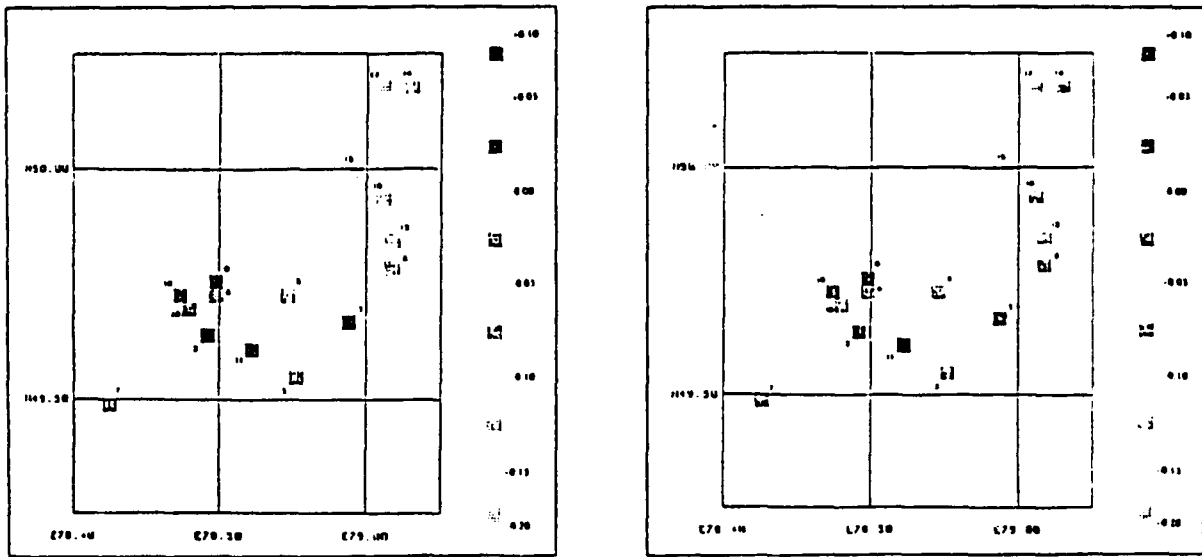


Figure 4

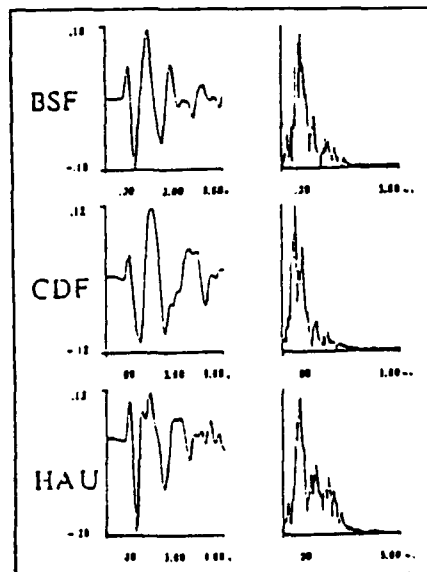


Figure 5

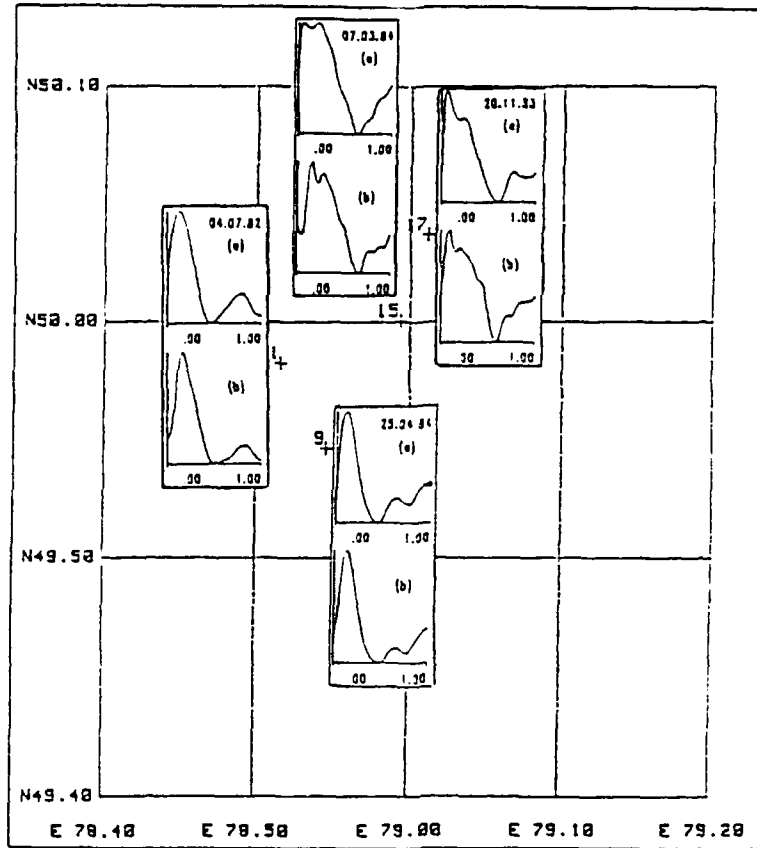


Figure 6

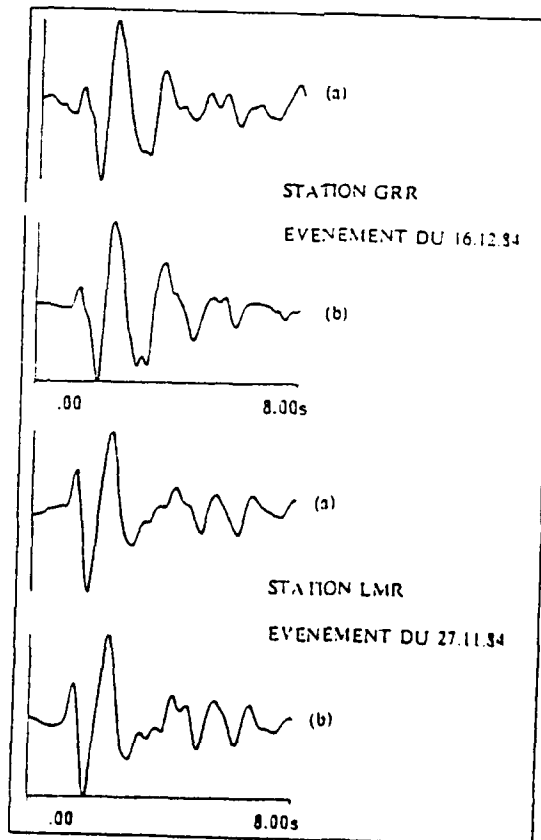


Figure 7

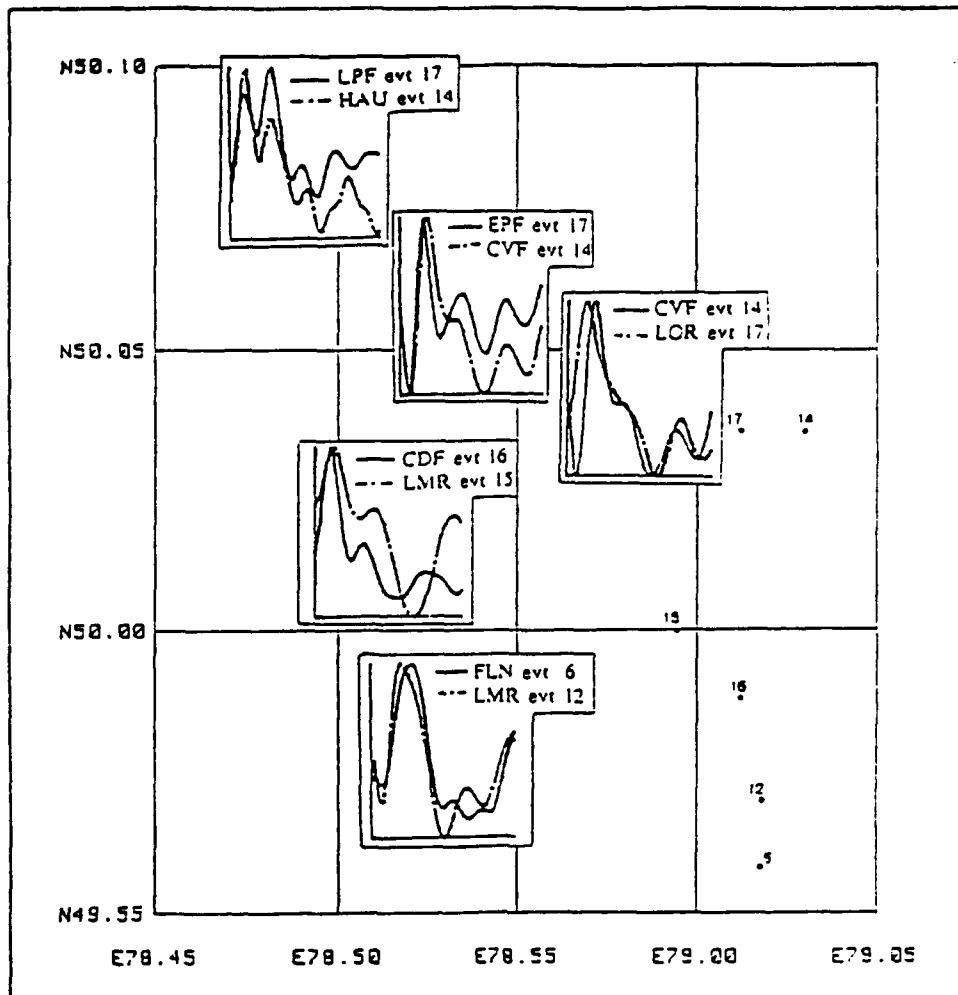


Figure 8

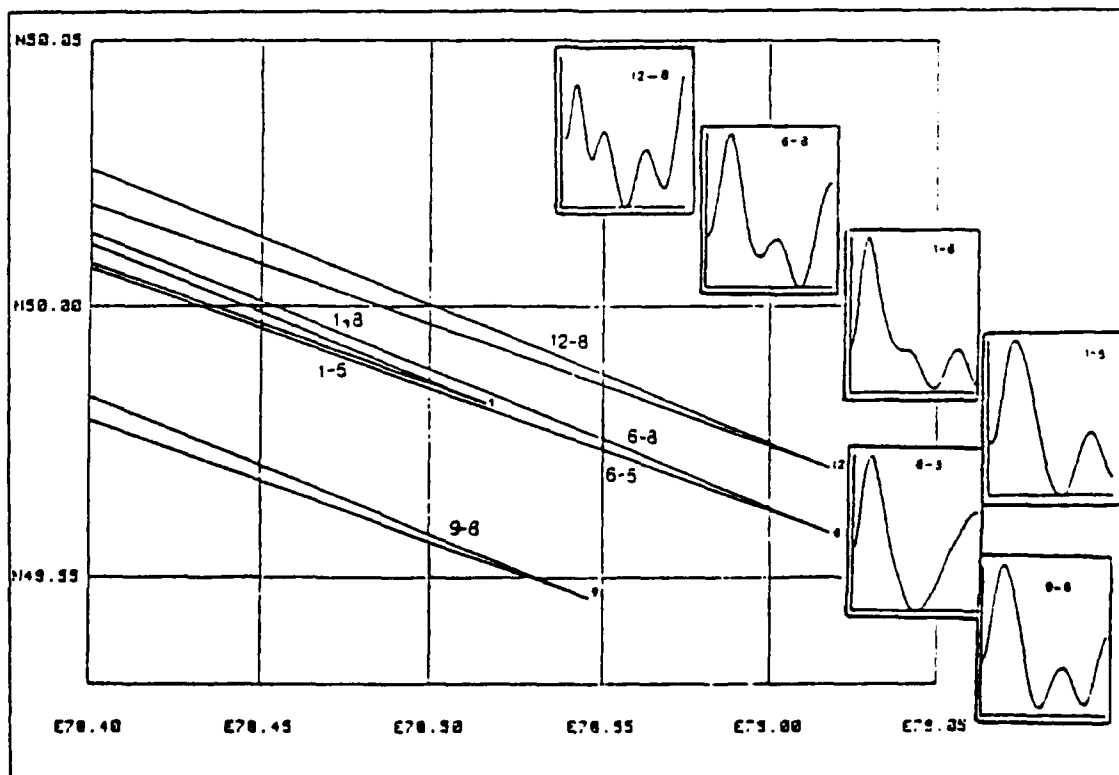


Figure 9

Prof. Thomas Ahrens
Seismological Lab, 252-21
Division of Geological & Planetary Sciences
California Institute of Technology
Pasadena, CA 91125

Prof. Charles B. Archambeau
CIRES
University of Colorado
Boulder, CO 80309

Dr. Thomas C. Bache, Jr.
Science Applications Int'l Corp.
10260 Campus Point Drive
San Diego, CA 92121 (2 copies)

Prof. Muawia Barazangi
Institute for the Study of the Continent
Cornell University
Ithaca, NY 14853

Dr. Jeff Barker
Department of Geological Sciences
State University of New York
at Binghamton
Vestal, NY 13901

Dr. Douglas R. Baumgardt
ENSCO, Inc
5400 Port Royal Road
Springfield, VA 22151-2388

Prof. Jonathan Berger
IGPP, A-025
Scripps Institution of Oceanography
University of California, San Diego
La Jolla, CA 92093

Dr. Gilbert A. Bollinger
Department of Geological Sciences
Virginia Polytechnical Institute
21044 Derring Hall
Blacksburg, VA 24061

Dr. Lawrence J. Burdick
Woodward-Clyde Consultants
566 El Dorado Street
Pasadena, CA 91109-3245

Dr. Jerry Carter
Center for Seismic Studies
1300 North 17th St., Suite 1450
Arlington, VA 22209-2308

Dr. Karl Coyner
New England Research, Inc.
76 Olcott Drive
White River Junction, VT 05001

Prof. Vernon F. Cormier
Department of Geology & Geophysics
U-45, Room 207
The University of Connecticut
Storrs, CT 06268

Professor Anton W. Dainty
Earth Resources Laboratory
Massachusetts Institute of Technology
42 Carleton Street
Cambridge, MA 02142

Prof. Steven Day
Department of Geological Sciences
San Diego State University
San Diego, CA 92182

Dr. Zoltan A. Der
ENSCO, Inc.
5400 Port Royal Road
Springfield, VA 22151-2388

Prof. Lewis M. Duncan
Dept. of Physics & Astronautics
Clemson University
Clemson, SC 29634-1901

Prof. John Ferguson
Center for Lithospheric Studies
The University of Texas at Dallas
P.O. Box 830688
Richardson, TX 75083-0688

Dr. Mark D. Fisk
Mission Research Corporation
735 State Street
P. O. Drawer 719
Santa Barbara, CA 93102

Prof. Stanley Flatte
Applied Sciences Building
University of California
Santa Cruz, CA 95064

Dr. Alexander Florence
SRI International
333 Ravenswood Avenue
Menlo Park, CA 94025-3493

Dr. Holy K. Given
IGPP, A-025
Scripps Institute of Oceanography
University of California, San Diego
La Jolla, CA 92093

Prof. Henry L. Gray
Vice Provost and Dean
Department of Statistical Sciences
Southern Methodist University
Dallas, TX 75275

Dr. Indra Gupta
Teledyne Geotech
314 Montgomery Street
Alexandria, VA 22314

Prof. David G. Harkrider
Seismological Laboratory
Division of Geological & Planetary Sciences
California Institute of Technology
Pasadena, CA 91125

Prof. Danny Harvey
CIRES
University of Colorado
Boulder, CO 80309

Prof. Donald V. Helmberger
Seismological Laboratory
Division of Geological & Planetary Sciences
California Institute of Technology
Pasadena, CA 91125

Prof. Eugene Herrin
Institute for the Study of Earth and Man
Geophysical Laboratory
Southern Methodist University
Dallas, TX 75275

Prof. Bryan Isacks
Cornell University
Department of Geological Sciences
SNEE Hall
Ithaca, NY 14850

Dr. Rong-Song Jih
Teledyne Geotech
314 Montgomery Street
Alexandria, VA 22314

Prof. Lane R. Johnson
Seismographic Station
University of California
Berkeley, CA 94720

Dr. Richard LaCoss
MIT-Lincoln Laboratory
M-200B
P. O. Box 73
Lexington, MA 02173-0073 (3 copies)

Prof Fred K. Lamb
University of Illinois at Urbana-Champaign
Department of Physics
1110 West Green Street
Urbana, IL 61801

Prof. Charles A. Langston
Geosciences Department
403 Deike Building
The Pennsylvania State University
University Park, PA 16802

Prof. Thorne Lay
Institute of Tectonics
Earth Science Board
University of California, Santa Cruz
Santa Cruz, CA 95064

Prof. Arthur Lerner-Lam
Lamont-Doherty Geological Observatory
of Columbia University
Palisades, NY 10964

Dr. Christopher Lynnes
Teledyne Geotech
314 Montgomery Street
Alexandria, VA 22314

Prof. Peter Malin
Department of Geology
Old Chemistry Bldg.
Duke University
Durham, NC 27706

Dr. Randolph Martin, III
New England Research, Inc.
76 Olcott Drive
White River Junction, VT 05001

Prof. Thomas V. McEvilly
Seismographic Station
University of California
Berkeley, CA 94720

Dr. Keith L. McLaughlin
S-CUBED
A Division of Maxwell Laboratory
P.O. Box 1620
La Jolla, CA 92038-1620

Prof. William Menke
Lamont-Doherty Geological Observatory
of Columbia University
Palisades, NY 10964

Stephen Miller
SRI International
333 Ravenswood Avenue
Box AF 116
Menlo Park, CA 94025-3493

Prof. Bernard Minster
IGPP, A-025
Scripps Institute of Oceanography
University of California, San Diego
La Jolla, CA 92093

Prof. Brian J. Mitchell
Department of Earth & Atmospheric Sciences
St. Louis University
St. Louis, MO 63156

Mr. Jack Murphy
S-CUBED, A Division of Maxwell Laboratory
11800 Sunrise Valley Drive
Suite 1212
Reston, VA 22091 (2 copies)

Prof. John A. Orcutt
IGPP, A-025
Scripps Institute of Oceanography
University of California, San Diego
La Jolla, CA 92093

Prof. Keith Priestley
University of Cambridge
Bullard Labs, Dept. of Earth Sciences
Madingley Rise, Madingley Rd.
Cambridge CB3 0EZ, ENGLAND

Dr. Jay J. Pulli
Radix Systems, Inc.
2 Taft Court, Suite 203
Rockville, MD 20850

Prof. Paul G. Richards
Lamont Doherty Geological Observatory
of Columbia University
Palisades, NY 10964

Dr. Wilmer Rivers
Teledyne Geotech
314 Montgomery Street
Alexandria, VA 22314

Prof. Charles G. Sammis
Center for Earth Sciences
University of Southern California
University Park
Los Angeles, CA 90089-0741

Prof. Christopher H. Scholz
Lamont-Doherty Geological Observatory
of Columbia University
Palisades, NY 10964

Thomas J. Sereno, Jr.
Science Application Int'l Corp.
10260 Campus Point Drive
San Diego, CA 92121

Prof. David G. Simpson
Lamont-Doherty Geological Observatory
of Columbia University
Palisades, NY 10964

Dr. Jeffrey Stevens
S-CUBED
A Division of Maxwell Laboratory
P.O. Box 1620
La Jolla, CA 92038-1620

Prof. Brian Stump
Institute for the Study of Earth & Man
Geophysical Laboratory
Southern Methodist University
Dallas, TX 75275

Prof. Jeremiah Sullivan
University of Illinois at Urbana-Champaign
Department of Physics
1110 West Green Street
Urbana, IL 61801

Prof. Clifford Thurber
University of Wisconsin-Madison
Department of Geology & Geophysics
1215 West Dayton Street
Madison, WS 53706

Prof. M. Nafi Toksoz
Earth Resources Lab
Massachusetts Institute of Technology
42 Carleton Street
Cambridge, MA 02142

Prof. John E. Vidale
University of California at Santa Cruz
Seismological Laboratory
Santa Cruz, CA 95064

Prof. Terry C. Wallace
Department of Geosciences
Building #77
University of Arizona
Tucson, AZ 85721

Dr. William Wortman
Mission Research Corporation
8560 Cinderbed Rd.
Suite # 700
Newington, VA 22122

Prof. Francis T. Wu
Department of Geological Sciences
State University of New York
at Binghamton
Vestal, NY 13901

OTHERS (United States)

Dr. Monem Abdel-Gawad
Rockwell International Science Center
1049 Camino Dos Rios
Thousand Oaks, CA 91360

Michael Browne
Teledyne Geotech
3401 Shiloh Road
Garland, TX 75041

Prof. Keiiti Aki
Center for Earth Sciences
University of Southern California
University Park
Los Angeles, CA 90089-0741

Mr. Roy Burger
1221 Serry Road
Schenectady, NY 12309

Prof. Shelton S. Alexander
Geosciences Department
403 Deike Building
The Pennsylvania State University
University Park, PA 16802

Dr. Robert Burrige
Schlumberger-Doll Research Center
Old Quarry Road
Ridgefield, CT 06877

Dr. Kenneth Anderson
BBNSTC
Mail Stop 14/1B
Cambridge, MA 02238

Dr. W. Winston Chan
Teledyne Geotech
314 Montgomery Street
Alexandria, VA 22314-1581

Dr. Ralph Archuleta
Department of Geological Sciences
University of California at Santa Barbara
Santa Barbara, CA 93102

Dr. Theodore Cherry
Science Horizons, Inc.
710 Encinitas Blvd., Suite 200
Encinitas, CA 92024 (2 copies)

Dr. Susan Beck
Department of Geosciences
Bldg. # 77
University of Arizona
Tucson, AZ 85721

Prof. Jon F. Claerbout
Department of Geophysics
Stanford University
Stanford, CA 94305

Dr. T.J. Bennett
S-CUBED
A Division of Maxwell Laboratory
1800 Sunrise Valley Drive, Suite 1212
Reston, VA 22091

Prof. Robert W. Clayton
Seismological Laboratory
Division of Geological & Planetary Sciences
California Institute of Technology
Pasadena, CA 91125

Mr. William J. Best
907 Westwood Drive
Vienna, VA 22180

Prof. F. A. Dahlen
Geological and Geophysical Sciences
Princeton University
Princeton, NJ 08544-0636

Dr. N. Biswas
Geophysical Institute
University of Alaska
Fairbanks, AK 99701

Mr. Charles Doll
Earth Resources Laboratory
Massachusetts Institute of Technology
42 Carleton St.
Cambridge, MA 02142

Dr. Stephen Bratt
Center for Seismic Studies
1300 North 17th Street
Suite 1450
Arlington, VA 22209

Prof. Adam Dziewonski
Hoffman Laboratory, Harvard Univ.
Dept. of Earth Atmos. & Planetary Sciences
20 Oxford St
Cambridge, MA 02138

Prof. John Ebel
Department of Geology & Geophysics
Boston College
Chestnut Hill, MA 02167

Eric Fielding
SNEE Hall
INSTOC
Cornell University
Ithaca, NY 14853

Dr. John Foley
Phillips Laboratory/LWH
Hanscom AFB, MA 01731-5000

Prof. Donald Forsyth
Department of Geological Sciences
Brown University
Providence, RI 02912

Dr. Cliff Frolich
Institute of Geophysics
8701 North Mopac
Austin, TX 78759

Dr. Anthony Gangi
Texas A&M University
Department of Geophysics
College Station, TX 77843

Dr. Freeman Gilbert
IGPP, A-025
Scripps Institute of Oceanography
University of California
La Jolla, CA 92093

Mr. Edward Giller
Pacific Sierra Research Corp.
1401 Wilson Boulevard
Arlington, VA 22209

Dr. Jeffrey W. Given
SAIC
10260 Campus Point Drive
San Diego, CA 92121

Prof. Stephen Grand
University of Texas at Austin
Department of Geological Sciences
Austin, TX 78713-7909

Prof. Roy Greenfield
Geosciences Department
403 Deike Building
The Pennsylvania State University
University Park, PA 16802

Dan N. Hagedorn
Battelle
Pacific Northwest Laboratories
Battelle Boulevard
Richland, WA 99352

Dr. James Hannon
Lawrence Livermore National Laboratory
P. O. Box 808
Livermore, CA 94550

Prof. Robert B. Herrmann
Dept. of Earth & Atmospheric Sciences
St. Louis University
St. Louis, MO 63156

Ms. Heidi Houston
Seismological Laboratory
University of California
Santa Cruz, CA 95064

Kevin Hutchenson
Department of Earth Sciences
St. Louis University
3507 Laclede
St. Louis, MO 63103

Dr. Hans Israelsson
Center for Seismic Studies
1300 N. 17th Street, Suite 1450
Arlington, VA 22209-2308

Prof. Thomas H. Jordan
Department of Earth, Atmospheric
and Planetary Sciences
Massachusetts Institute of Technology
Cambridge, MA 02139

Prof. Alan Kafka
Department of Geology & Geophysics
Boston College
Chestnut Hill, MA 02167

Robert C. Kemerait
ENSCO, Inc.
445 Pineda Court
Melbourne, FL 32940

William Kikendall
Teledyne Geotech
3401 Shiloh Road
Garland, TX 75041

Prof. Leon Knopoff
University of California
Institute of Geophysics & Planetary Physics
Los Angeles, CA 90024

Prof. John Kuo
Aldridge Laboratory of Applied Geophysics
Columbia University
842 Mudd Bldg.
New York, NY 10027

Prof. L. Timothy Long
School of Geophysical Sciences
Georgia Institute of Technology
Atlanta, GA 30332

Dr. Gary McCartor
Department of Physics
Southern Methodist University
Dallas, TX 75275

Prof. Art McGarr
Mail Stop 977
Geological Survey
345 Middlefield Rd.
Menlo Park, CA 94025

Dr. George Mellman
Sierra Geophysics
11255 Kirkland Way
Kirkland, WA 98033

Prof. John Nabelek
College of Oceanography
Oregon State University
Corvallis, OR 97331

Prof. Geza Nagy
University of California, San Diego
Department of Ames, M.S. B-010
La Jolla, CA 92093

Dr. Keith K. Nakaniishi
Lawrence Livermore National Laboratory
L-205
P. O. Box 808
Livermore, CA 94550

Prof. Amos Nur
Department of Geophysics
Stanford University
Stanford, CA 94305

Prof. Jack Oliver
Department of Geology
Cornell University
Ithaca, NY 14850

Dr. Kenneth Olsen
P. O. Box 1273
Linwood, WA 98046-1273

Prof. Jeffrey Park
Department of Geology and Geophysics
Kline Geology Laboratory
P. O. Box 6666
New Haven, CT 06511-8130

Howard J. Patton
Lawrence Livermore National Laboratory
L-205
P. O. Box 808
Livermore, CA 94550

Prof. Robert Phinney
Geological & Geophysical Sciences
Princeton University
Princeton, NJ 08544-0636

Dr. Paul Pomeroy
Rondout Associates
P.O. Box 224
Stone Ridge, NY 12484

Dr. Norton Rimer
S-CUBED
A Division of Maxwell Laboratory
P.O. Box 1620
La Jolla, CA 92038-1620

Prof. Larry J. Ruff
Department of Geological Sciences
1006 C.C. Little Building
University of Michigan
Ann Arbor, MI 48109-1063

Dr. Richard Sailor
TASC Inc.
55 Walkers Brook Drive
Reading, MA 01867

Dr. Susan Schwartz
Institute of Tectonics
1156 High St.
Santa Cruz, CA 95064

John Sherwin
Teledyne Geotech
3401 Shiloh Road
Garland, TX 75041

Dr. Matthew Sibol
Virginia Tech
Seismological Observatory
4044 Derring Hall
Blacksburg, VA 24061-0420

Dr. Albert Smith
Lawrence Livermore National Laboratory
L-205
P. O. Box 808
Livermore, CA 94550

Prof. Robert Smith
Department of Geophysics
University of Utah
1400 East 2nd South
Salt Lake City, UT 84112

Dr. Stewart W. Smith
Geophysics AK-50
University of Washington
Seattle, WA 98195

Donald L. Springer
Lawrence Livermore National Laboratory
L-205
P. O. Box 808
Livermore, CA 94550

Dr. George Sutton
Rondout Associates
P.O. Box 224
Stone Ridge, NY 12484

Prof. L. Sykes
Lamont-Doherty Geological Observatory
of Columbia University
Palisades, NY 10964

Prof. Pradeep Talwani
Department of Geological Sciences
University of South Carolina
Columbia, SC 29208

Dr. David Taylor
ENSCO, Inc.
445 Pineda Court
Melbourne, FL 32940

Dr. Steven R. Taylor
Lawrence Livermore National Laboratory
L-205
P. O. Box 808
Livermore, CA 94550

Professor Ta-Liang Teng
Center for Earth Sciences
University of Southern California
University Park
Los Angeles, CA 90089-0741

Dr. Gregory van der Vink
IRIS, Inc.
1616 North Fort Myer Drive
Suite 1440
Arlington, VA 22209

Professor Daniel Walker
University of Hawaii
Institute of Geophysics
Honolulu, HI 96822

William R. Walter
Seismological Laboratory
University of Nevada
Reno, NV 89557

Dr. Raymond Willeman
Phillips Laboratory - OL-AA/LWH
Hanscom AFB, MA 01731-5000

Dr. Gregory Wojcik
Weidlinger Associates
4410 El Camino Real
Suite 110
Los Altos, CA 94022

Dr. Lorraine Wolf
Phillips Laboratory/LWH
Hanscom AFB, MA 01731-5000

Dr. Gregory B. Young
ENSCO, Inc.
5400 Port Royal Road
Springfield, VA 22151-2388

Dr. Eileen Vergino
Lawrence Livermore National Laboratory
L-205
P. O. Box 808
Livermore, CA 94550

- J. J. Zucca
Lawrence Livermore National Laboratory
P. O. Box 808
- Livermore, CA 94550

GOVERNMENT

Dr. Ralph Alewine III
DARPA/NMRO
1400 Wilson Boulevard
Arlington, VA 22209-2308

Dr. Dale Glover
DIA/DT-1B
Washington, DC 20301

Mr. James C. Battis
Phillips Laboratory/LWH
Hanscom AFB, MA 01731-5000

Dr. T. Hanks
USGS
Nat'l Earthquake Research Center
345 Middlefield Road
Menlo Park, CA 94025

Harley Benz
U.S. Geological Survey, MS-977
345 Middlefield Rd.
Menlo Park, CA 94025

Dr. Roger Hansen
AFTAC/TT
Patrick AFB, FL 32925

Dr. Robert Blandford
AFTAC/TT
Center for Seismic Studies
1300 North 17th St. Suite 1450
Arlington, VA 22209-2308

Paul Johnson
ESS-4, Mail Stop J979
Los Alamos National Laboratory
Los Alamos, NM 87545

Eric Chael
Division 9241
Sandia Laboratory
Albuquerque, NM 87185

Janet Johnston
Phillips Laboratory/LWH
Hanscom AFB, MA 01731-5000

Dr. John J. Cipar
Phillips Laboratory/LWH
Hanscom AFB, MA 01731-5000

Dr. Katharine Kadinsky-Cade
Phillips Laboratory/LWH
Hanscom AFB, MA 01731-5000

Cecil Davis
Group P-15, Mail Stop 7406
P.O. Box 1663
Los Alamos National Laboratory
Los Alamos, NM 87544

Ms. Ann Kerr
IGPP, A-025
Scripps Institute of Oceanography
University of California, San Diego
La Jolla, CA 92093

Mr. Jeff Duncan
Office of Congressman Markey
2133 Rayburn House Bldg.
Washington, DC 20515

Dr. Max Koontz
US Dept of Energy/DP 5
Forrestal Building
1000 Independence Avenue
Washington, DC 20585

Dr. Jack Evernden
USGS - Earthquake Studies
345 Middlefield Road
Menlo Park, CA 94025

Dr. W.H.K. Lee
Office of Earthquakes, Volcanoes,
& Engineering
345 Middlefield Road
Menlo Park, CA 94025

Art Frankel
USGS
922 National Center
Reston, VA 22092

Dr. William Leith
U.S. Geological Survey
Mail Stop 928
Reston, VA 22092

Dr. Richard Lewis
Director, Earthquake Engineering & Geophysics
U.S. Army Corps of Engineers
Box 631
Vicksburg, MS 39180

James F. Lewkowicz
Phillips Laboratory/LWH
Hanscom AFB, MA 01731-5000

Mr. Alfred Lieberman
ACDA/VI-OA State Department Bldg
Room 5726
320 - 21st Street, NW
Washington, DC 20451

Stephen Mangino
Phillips Laboratory/LWH
Hanscom AFB, MA 01731-5000

Dr. Robert Masse
Box 25046, Mail Stop 967
Denver Federal Center
Denver, CO 80225

Art McGarr
U.S. Geological Survey, MS-977
345 Middlefield Road
Menlo Park, CA 94025

Richard Morrow
ACDA/VI, Room 5741
320 21st Street N.W.
Washington, DC 20451

Dr. Carl Newton
Los Alamos National Laboratory
P.O. Box 1663
Mail Stop C335, Group ESS-3
Los Alamos, NM 87545

Dr. Bao Nguyen
AFTAC/TTR
Patrick AFB, FL 32925

Dr. Kenneth H. Olsen
Los Alamos Scientific Laboratory
P. O. Box 1663
Mail Stop D-406
Los Alamos, NM 87545

Mr. Chris Paine
Office of Senator Kennedy
SR 315
United States Senate
Washington, DC 20510

Colonel Jerry J. Perrizo
AFOSR/NP, Building 410
Bolling AFB
Washington, DC 20332-6448

Dr. Frank F. Pilotte
HQ AFTAC/TT
Patrick AFB, FL 32925-6001

Katie Poley
CIA-ACIS/TMC
Room 4X16NHB
Washington, DC 20505

Mr. Jack Rachlin
U.S. Geological Survey
Geology, Rm 3 C136
Mail Stop 928 National Center
Reston, VA 22092

Dr. Robert Reinke
WL/NTESG
Kirtland AFB, NM 87117-6008

Dr. Byron Ristvet
HQ DNA, Nevada Operations Office
Attn: NVCG
P.O. Box 98539
Las Vegas, NV 89193

Dr. George Rothe
HQ AFTAC/TTR
Patrick AFB, FL 32925-6001

Dr. Alan S. Ryall, Jr.
DARPA/NMRO
1400 Wilson Boulevard
Arlington, VA 22209-2308

Dr. Michael Shore
Defense Nuclear Agency/SPSS
6801 Telegraph Road
Alexandria, VA 22310

Mr. Charles L. Taylor
Phillips Laboratory/LWH
Hanscom AFB, MA 01731-5000

Phillips Laboratory
Attn: XO
Hanscom AFB, MA 01731-5000

Dr. Larry Turnbull
CIA-OSWR/NED
Washington, DC 20505

Phillips Laboratory
Attn: LW
Hanscom AFB, MA 01731-5000

Dr. Thomas Weaver
Los Alamos National Laboratory
P.O. Box 1663, Mail Stop C335
Los Alamos, NM 87545

DARPA/PM
1400 Wilson Boulevard
Arlington, VA 22209

Phillips Laboratory
Research Library
ATTN: SULL
Hanscom AFB, MA 01731-5000 (2 copies)

Defense Technical Information Center
Cameron Station
Alexandria, VA 22314 (5 copies)

Phillips Laboratory
ATTN: SUL
Kirtland AFB, NM 87117-6008

Defense Intelligence Agency
Directorate for Scientific & Technical Intelligence
Attn: DT1B
Washington, DC 20340-6158

Secretary of the Air Force
(SAFRD)
Washington, DC 20330

AFTAC/CA
(STINFO)
Patrick AFB, FL 32925-6001

Office of the Secretary Defense
DDR & E
Washington, DC 20330

TACTEC
Battelle Memorial Institute
505 King Avenue
Columbus, OH 43201 (Final Report Only)

HQ DNA
Attn: Technical Library
Washington, DC 20305

DARPA/RMO/RETRIEVAL
1400 Wilson Boulevard
Arlington, VA 22209

DARPA/RMO/Security Office
1400 Wilson Boulevard
Arlington, VA 22209

CONTRACTORS (FOREIGN)

Dr. Ramon Cabre, S.J.
Observatorio San Calixto
Casilla 5939
La Paz, Bolivia

- Prof. Hans-Peter Harjes
Institute for Geophysik
Ruhr University/Bochum
- P.O. Box 102148
4630 Bochum 1, FRG

Prof. Eystein Husebye
NTNF/NORSAR
P.O. Box 51
N-2007 Kjeller, NORWAY

Prof. Brian L.N. Kennett
Research School of Earth Sciences
Institute of Advanced Studies
G.P.O. Box 4
Canberra 2601, AUSTRALIA

Dr. Bernard Massinon
Societe Radiomana
27 rue Claude Bernard
75005 Paris, FRANCE (2 Copies)

Dr. Pierre Mecheler
Societe Radiomana
27 rue Claude Bernard
75005 Paris, FRANCE

Dr. Svein Mykkeltveit
NTNF/NORSAR
P.O. Box 51
N-2007 Kjeller, NORWAY (3 copies)

FOREIGN (OTHERS)

Dr. Peter Basham
Earth Physics Branch
Geological Survey of Canada
1 Observatory Crescent
Ottawa, Ontario, CANADA K1A 0Y3

Dr. Eduard Berg
Institute of Geophysics
University of Hawaii
Honolulu, HI 96822

Dr. Michel Bouchon
I.R.I.G.M.-B.P. 68
38402 St. Martin D'Herès
Cedex, FRANCE

Dr. Hilmar Bungum
NTNF/NORSAR
P.O. Box 51
N-2007 Kjeller, NORWAY

Dr. Michel Campillo
Observatoire de Grenoble
I.R.I.G.M.-B.P. 53
38041 Grenoble, FRANCE

Dr. Kin Yip Chun
Geophysics Division
Physics Department
University of Toronto
Ontario, CANADA M5S 1A7

Dr. Alan Douglas
Ministry of Defense
Blacknest, Brimpton
Reading RG7-4RS, UNITED KINGDOM

Dr. Manfred Henger
Federal Institute for Geosciences & Nat'l Res.
Postfach 510153
D-3000 Hanover 51, FRG

Ms. Eva Johannisson
Senior Research Officer
National Defense Research Inst.
P.O. Box 27322
S-102 54 Stockholm, SWEDEN

Dr. Fekadu Kebede
Geophysical Observatory, Science Faculty
Addis Ababa University
P. O. Box 1176
Addis Ababa, ETHIOPIA

Dr. Tormod Kvaerna
NTNF/NORSAR
P.O. Box 51
N-2007 Kjeller, NORWAY

Dr. Peter Marshall
Procurement Executive
Ministry of Defense
Blacknest, Brimpton
Reading FG7-4RS, UNITED KINGDOM

Prof. Ari Ben-Menahem
Department of Applied Mathematics
Weizman Institute of Science
Rehovot, ISRAEL 951729

Dr. Robert North
Geophysics Division
Geological Survey of Canada
1 Observatory Crescent
Ottawa, Ontario, CANADA K1A 0Y3

Dr. Frode Ringdal
NTNF/NORSAR
P.O. Box 51
N-2007 Kjeller, NORWAY

Dr. Jorg Schlittenhardt
Federal Institute for Geosciences & Nat'l Res.
Postfach 510153
D-3000 Hannover 51, FEDERAL REPUBLIC OF
GERMANY

Universita Degli Studi Di Trieste
Facolta Di Ingegneria
Istituto Di Miniere E. Geofisica Applicata, Trieste,
ITALY

Dr. John Woodhouse
Oxford University
Dept of Earth Sciences
Parks Road
Oxford OX1 3PR, ENGLAND